



HAL
open science

Unusual LREE-rich, peraluminous, monazite- or allanite-bearing pegmatitic granite in the central Grenville Province, Québec

François Turlin, Anne-Sylvie André-Mayer, Abdelali Moukhsil, Olivier Vanderhaeghe, Félix Gervais, Fabien Solgadi, Pierre-Arthur Groulier, Marc Pujol

► To cite this version:

François Turlin, Anne-Sylvie André-Mayer, Abdelali Moukhsil, Olivier Vanderhaeghe, Félix Gervais, et al.. Unusual LREE-rich, peraluminous, monazite- or allanite-bearing pegmatitic granite in the central Grenville Province, Québec. *Ore Geology Reviews*, 2017, 89, pp.627-667. 10.1016/j.oregeorev.2017.04.019 . insu-01524603

HAL Id: insu-01524603

<https://insu.hal.science/insu-01524603v1>

Submitted on 18 May 2017

HAL is a multi-disciplinary open access archive for the deposit and dissemination of scientific research documents, whether they are published or not. The documents may come from teaching and research institutions in France or abroad, or from public or private research centers.

L'archive ouverte pluridisciplinaire **HAL**, est destinée au dépôt et à la diffusion de documents scientifiques de niveau recherche, publiés ou non, émanant des établissements d'enseignement et de recherche français ou étrangers, des laboratoires publics ou privés.

Accepted Manuscript

Unusual LREE-rich, peraluminous, monazite- or allanite-bearing pegmatitic granite in the central Grenville Province, Québec

François Turlin, Anne-Sylvie André-Mayer, Abdelali Moukhsil, Olivier Vanderhaeghe, Félix Gervais, Fabien Solgadi, Pierre-Arthur Groulier, Marc Poujol

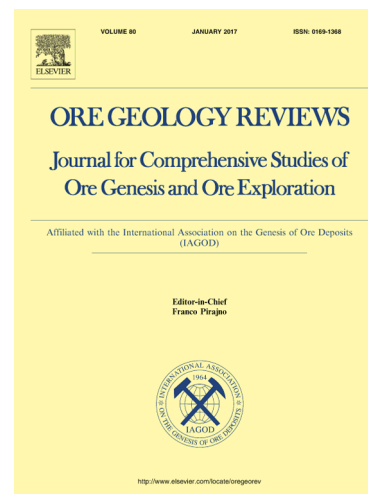
PII: S0169-1368(17)30057-4
DOI: <http://dx.doi.org/10.1016/j.oregeorev.2017.04.019>
Reference: OREGEO 2186

To appear in: *Ore Geology Reviews*

Received Date: 23 January 2017
Revised Date: 19 April 2017
Accepted Date: 24 April 2017

Please cite this article as: F. Turlin, A-S. André-Mayer, A. Moukhsil, O. Vanderhaeghe, F. Gervais, F. Solgadi, P-A. Groulier, M. Poujol, Unusual LREE-rich, peraluminous, monazite- or allanite-bearing pegmatitic granite in the central Grenville Province, Québec, *Ore Geology Reviews* (2017), doi: <http://dx.doi.org/10.1016/j.oregeorev.2017.04.019>

This is a PDF file of an unedited manuscript that has been accepted for publication. As a service to our customers we are providing this early version of the manuscript. The manuscript will undergo copyediting, typesetting, and review of the resulting proof before it is published in its final form. Please note that during the production process errors may be discovered which could affect the content, and all legal disclaimers that apply to the journal pertain.



1 **Unusual LREE-rich, peraluminous, monazite- or allanite-bearing**
2 **pegmatitic granite in the central Grenville Province, Québec**

3 **François Turlin^{a,*}, Anne-Sylvie André-Mayer^a, Abdelali Moukhsil^b, Olivier**
4 **Vanderhaeghe^c, Félix Gervais^d, Fabien Solgadi^e, Pierre-Arthur Groulier^f, Marc Poujol^g**

5 ^a *GeoRessources lab., UMR 7359, Université de Lorraine, CNRS, CREGU, Faculté des*
6 *Sciences et Technologies, Vandœuvre-lès-Nancy, F-54506, France*

7 ^b *Ministère de l'Énergie et des Ressources naturelles, Direction du Bureau de la*
8 *connaissance géoscientifique du Québec, 5700, 4^e Avenue Ouest, Québec (Québec), G1H 6R1*

9 ^c *Géosciences Environnement Toulouse, GET, Université de Toulouse, CNRS, IRD, UPS,*
10 *CNES (Toulouse), France*

11 ^d *Département des génies civil, géologiques et des mines, Ecole Polytechnique de Montréal,*
12 *Canada*

13 ^e *Ministère de l'Énergie et des Ressources naturelles, Direction du Bureau de la connaissance*
14 *géoscientifique du Québec, 400, boulevard Lamaque, Val-d'Or (Québec), J9P 3L4*

15 ^f *Earth Sciences Department, Memorial University, St. John's, NL A1B 3X5, Canada*

16 ^g *Géosciences Rennes, UMR 6118, OSUR, Université de Rennes 1, 35042 Rennes Cedex,*
17 *France*

18 * Corresponding author: François Turlin

19 Université de Lorraine, CNRS, CREGU, GeoRessources lab.

20 Campus Aiguillettes, Faculté des Sciences et Technologies

21 rue Jacques Callot

22 Vandœuvre-lès-Nancy, F-54506, France.

23 Mail: francois.turlin@univ-lorraine.fr

24 Phone: +33 3 83 68 47 67

25 **Abstract**

26 This contribution presents an original study combining detailed mapping, petrography,
27 whole-rock geochemistry and geochronological constraints on the recently identified LREE
28 (Light Rare Earth Elements) occurrences associated with pegmatitic granite dykes (PGD)
29 from the central Grenville (Lac Okaopéo region). These PGD intrude paragneisses or meta-
30 igneous complexes with a REE mineralization hosted either in monazite-(Ce) or in allanite-
31 (Ce) respectively. The investigated samples display peraluminous signatures and are
32 dominated by a quartz+K-feldspar+plagioclase+biotite+monazite/allanite assemblage. Field
33 relationships and the magmatic textures of the dykes combined with U-Pb dating of magmatic
34 monazite grains at 1005.4 ± 4.4 Ma and 996.7 ± 5.3 Ma (concordant igneous ages) imply that
35 the LREE-rich PGD were emplaced in a post-tectonic setting. Allanite-(Ce) and monazite-
36 (Ce)-bearing PGD have Σ REE contents up to 9242 ppm and 7048 ppm, respectively. The
37 allanite-rich assemblage is consistent with the petrographic assemblage of LREE-enriched
38 PGD identified in the southwestern Grenville Province and elsewhere in the world, but this
39 study constitutes the first evidence for a sole presence of monazite as LREE-bearing phase in
40 strongly peraluminous PGD from the Grenville Province.

41 **Keywords:** Grenville Province; Peraluminous; Pegmatitic Granite; LREE; Whole-rock
42 geochemistry; Allanite/Monazite

43 **1. Introduction**

44 Granitic pegmatites host numerous metallic occurrences, mostly rare-metals such as
45 U-Th, Nb-Ta, Y, Rare Earth Elements (REE), Ti, Zr, Be, Li, Cs, Mo, Rb, B, P, Pb, F. Due to
46 their small sizes, REE-rich granitic pegmatites are generally not considered as good economic
47 target when compared to their plutonic counterparts, and have thus not received the same
48 attention (e.g. Ercit, 2005; Goodenough et al., 2016; London, 2016). However, the worldwide
49 overwhelming occurrences of REE-bearing granitic pegmatites may potentially represent
50 important sources of REE and are to be included in the further global investigations of the
51 REE metallogenic system. The lack of detailed field descriptions, whole-rock and
52 mineralogical compositions, as well as structural data for the pegmatitic bodies and their host
53 and country rocks prevent a good understanding of the source, the formation and the
54 concentration of REE-bearing pegmatites (Dill, 2015; Ercit, 2005). Classification schemes,
55 such as the NYF (Nb-Y-F) classes of Černý et al. (2012) or the “chessboard” scheme of Dill
56 (2010), generally depict REE-rich granitic pegmatites as being derived from an alkaline melt
57 fractionation (Dill, 2010, 2015). However, in some cases (e.g. in the Grenville Province)
58 where the lack of coeval granitic pluton is not necessarily due to a lack of outcrops, a
59 derivation of REE-rich granitic pegmatites from partial melting of a crustal/sub-crustal
60 component is generally inferred, but not clearly demonstrated (Ercit, 2005 and references
61 therein).

62 With this in mind, the Proterozoic Grenville Province, mainly exposed in Quebec and
63 Ontario (Canada, Fig. 1), offers the possibility to study numerous magmatic REE occurrences,
64 mainly late- to post-Grenvillian in age, and associated with a large spectrum of magmatic
65 environments including nepheline-syenite (e.g. Saint-Honoré, Crevier, Bergeron, 1980;
66 Gauthier and Chartrand, 2005; Groulier, 2013; Sangster et al., 1992), carbonatite (e.g. Niobec,
67 Crevier, Bergeron, 1980; Groulier, 2013), as well as numerous granitic pegmatites (e.g. Ayres

68 and Černý, 1982; Černý, 1990; Ercit, 2005; Ford, 1982; Lentz, 1996; Masson and Gordon,
69 1981; Moukhsil et al., 2014). Other “non-magmatic” REE occurrences are described in this
70 province such as the metasomatic mineralization of Kipawa or the Kwyjibo IOCG-type
71 deposit, with a REE mineralization dated at ca. 1030 Ma (Saucier et al., 2013; van Breemen
72 and Currie, 2004) and ca. 985-970 Ma (Gauthier et al., 2004; Perreault and Lafrance, 2015
73 and references therein), respectively.

74 During the past few decades, several studies investigated the distribution, mineralogy
75 and petrogenesis of granitic pegmatites from the Grenville Province (Ayres and Černý, 1982;
76 Černý, 1990; Fowler and Doig, 1983; Lentz, 1996, 1991; Masson and Gordon, 1981). They
77 typically comprise with U-Th, Nb-Ta, Y, Ti, Zr, REE, Be, Mo, P, Pb, F (Ayres and Černý,
78 1982; Černý, 1990; Fowler and Doig, 1983; Gauthier and Chartrand, 2005; Lentz, 1996;
79 Masson and Gordon, 1981). They are generally interpreted as representing a silicate melt
80 extracted from partially molten rocks between ca. 1.1 to 0.9 Ga during the late stages of major
81 intrusive events coeval with the end of Grenvillian high-grade metamorphism based on (i) the
82 lack of coeval granitic pluton, (ii) their magmatic and undeformed texture, and (iii) their
83 discordant and intrusive nature in brittle zones within competent units (Ayres and Černý,
84 1982; Ercit, 2005; Lentz, 1991; Lumbers, 1964; Masson and Gordon, 1981). Accordingly, the
85 presence of REE-enriched pegmatitic granite dykes (further designated as ‘PGD’) in the
86 Grenville Province raises the question of (i) the source of these magmas and (ii) the
87 geodynamic context that prevailed during their emplacement. Were these granitic magmas
88 produced by partial melting of the thermally relaxed orogenic root composed of reworked
89 Archean and/or Proterozoic pre-existing continental crust, or do they correspond to extremely
90 differentiated mantle melts produced by decompression owing to post-orogenic extension?

91 The previous studies mentioned above have been mainly focused on the western parts
92 of the Grenville Province and, to our knowledge, no REE-rich PGD have been described in

93 the central part of the Grenville Province (Fig. 1). A recent campaign of cartography in the
94 Lac Okaopéo region conducted by Moukhsil et al. (2014) (Figs. 2-3) has led to the
95 identification of seven REE magmatic occurrences associated with discordant PGD intrusive
96 either in migmatitic paragneisses or in metaplutonic complexes (Fig. 3, Table 1, Moukhsil et
97 al., 2014). These PGD have Σ REE contents ranging from 1418 to 9242 ppm (this study, Table
98 2) and represent new REE occurrences in the Grenville Province. The present paper is
99 dedicated (i) to describe the field relationships between the various PGD and their host rocks
100 to constrain their structural framework; (ii) to characterize their petrography and whole-rock
101 geochemistry, allowing to discuss potential sources and processes responsible for their
102 emplacement and concentration; and (iii) to constrain the timing of REE mineralization by
103 LA-ICP-MS U-Pb dating on monazite in order to replace these PGD in the tectonic-
104 metamorphic framework of the Grenvillian Orogeny. Finally, these results will be compared
105 to other LREE-enriched granitic pegmatites reported elsewhere.

106 **2. Geological framework**

107 **2.1. The Grenville Orogenic Belt**

108 The study area is located in the central Grenville Province (Fig. 1b), which mainly
109 crops out along the southeastern Canadian Shield (Fig. 1a). It results from a long history of
110 tectonic-magmatic accretion through the Mesoproterozoic and subsequent continent-continent
111 collision designated as the Grenvillian Orogeny *sensu stricto* (e.g. Carr et al., 2000; Dunning
112 and Indares, 2010; Gower and Krogh, 2002; Rivers et al., 2012; Tucker and Gower, 1994).

113 **FIGURE 1**

114 The two main tectonometamorphic domains of the Grenville Province, namely the
115 Allochthonous and the Parautochthonous belts recorded the Grenvillian Orogeny as two
116 distinct phases. The Allochthonous Belt (Fig. 1b) is made of terranes that originated outboard

117 of, and were accreted to Laurentia during the Mesoproterozoic (Rivers et al., 2012). The
118 underlying Parautochthonous Belt (Fig. 1b) corresponds to rocks of the Superior Province and
119 its cover sequence or to previously accreted arc that were reworked during the Grenvillian
120 Orogeny (Rivers et al., 1989, 2012). The Allochthonous and the Parautochthonous belts are
121 separated by the southeast-dipping and orogen-scale high-grade shear zone designated as the
122 Allochthon Boundary Thrust (ABT, Figs. 1b, 2). The “Ottawan” crustal thickening phase is
123 first of the Grenvillian Orogeny, and was characterized by the development of a hot ductile
124 crust underneath an orogenic plateau (“Orogenic Lid”, Fig. 1b) with a lower limit inferred to
125 be the ABT, between ca. 1090 and 1020 Ma in the Allochthonous Belt (e.g. Carr et al., 2000;
126 Dunning and Indares, 2010; Indares et al., 2000; Rivers, 2008, 1997; Rivers et al., 2012). This
127 plateau is inferred to have collapsed on itself after the Ottawan phase resulting in the
128 formation of several normal-sense shear zones commonly associated with the emplacement of
129 PGD, and assisted by the intrusion of AMCG suites that resulted in weakening and lubricating
130 of the shear zones (Ketchum et al., 1998; Rivers, 2012; Rivers and Schwerdtner, 2015; Soucy
131 La Roche et al., 2015). Renewed convergence during the relatively short-lived Rigolet phase
132 (1005-960 Ma, Rivers, 2009) resulted in foreland-ward propagation of Grenvillian thrusting
133 and high-grade metamorphism, the northwest limit of which is the Grenville Front (Fig. 1), an
134 orogen-scale, southeast-dipping shear zone that was active during the Rigolet orogenic phase
135 (Krogh, 1994; Rivers et al., 1989; Rivers, 2008, 2009). Synkinematic PGD and sills were
136 intruded at upper and lower structural levels of the Parautochthonous and Allochthonous
137 belts, respectively, between 993 and 961 Ma during this later phase on the south shore of the
138 Manicouagan Reservoir (Fig. 2, Jannin et al., In press).

139 North of Manicouagan Reservoir, the Ottawan tectonic phase reached a metamorphic
140 peak at ca. 1450 MPa and 860-900°C between ca. 1080-1040 Ma (Indares et al., 1998; Indares
141 and Dunning, 2001; Lasalle et al., 2013; Lasalle and Indares, 2014; Rivers et al., 2002) in

142 kyanite-bearing rocks from the Manicouagan Imbricate Zone (MIZ, central Grenville, Fig. 2),
143 a high-grade nappe of Paleoproterozoic and Mesoproterozoic rocks of the Allochthonous HP
144 Belt (aHP, Fig. 1b). It was followed by the exhumation of the MIZ over a crustal-scale ramp
145 structurally above the Parautochthonous Belt at ca. 1100 MPa and 870°C between ca. 1040-
146 1030 Ma (Indares et al., 1998; Indares and Dunning, 2001; Lasalle et al., 2013; Lasalle and
147 Indares, 2014; Rivers et al., 2002), and by the subsequent pervasive intrusion of mantle-
148 derived magmas in the thickened orogenic crust (e.g. Dunning and Indares, 2010; Hynes et
149 al., 2000; Indares et al., 2000; Indares and Dunning, 2004). South of the Manicouagan
150 reservoir (just north of our study area; Fig. 2), however, peak metamorphic conditions at
151 sillimanite-grade conditions reached ca. 950 MPa and 850°C between ca. 1080 and 1040 Ma
152 (Dunning and Indares, 2010; Lasalle et al., 2014; Lasalle and Indares, 2014). In the
153 Parautochthonous Belt south of the reservoir, granulite-facies peak metamorphic conditions of
154 ca. 1500 MPa and 850°C were reached between ca. 1005-980 Ma (Hynes et al., 2000; Jordan
155 et al., 2006; Rivers, 2009; Rivers et al., 2012; van Gool et al., 2008) in metapelites from the
156 Knob Lake Group Paleoproterozoic sequence of the Gagnon Terrane that unconformably
157 overlie the Laurentian Archean basement (Parautochthonous Belt, Fig. 2, Dunning and
158 Indares, 2010; Hynes et al., 2000; Rivers, 1980; Rivers et al., 1989). A recent study indicated
159 that high-grade deformation continued until at least ca. 986 Ma (but could be as young ca. 961
160 Ma) as rocks of the upper and lower parts of the Parautochthonous and the Allochthonous
161 belts, respectively, were likely flowing as an orogenic channel (Jannin et al., In press).

162 **FIGURE 2**

163 **2.2. The Lac Okaopéo lithotectonic units and structures**

164 The Lac Okaopéo region is located south of the MIZ and of the Daniel-Johnson dam
165 (Manic-5, Fig. 2). The various lithotectonic units identified in this region (Gobeil et al., 2002;

166 Moukhsil et al., 2014, 2013a, 2013b, 2012, 2009, 2007) belong to the Allochthonous MP Belt
167 of the Grenville Province, structurally above the Allochthon Boundary Thrust (ABT, Fig. 2).

168 **FIGURE 3**

169 **2.2.1. PGD host rocks**

170 The PGD investigated in this study are hosted either in paragneisses or in two distinct
171 metaplutonic suites, designated as the Bardoux and the Castoréum. The paragneisses from the
172 Plus-Value Complex mainly crop out in the northwestern part of the region (Fig. 3) and are
173 the oldest protolith in the region with a deposition age between 1765 to 1497 Ma (Augland et
174 al., 2015; Lasalle et al., 2013; Moukhsil et al., 2014, 2013b).

175 The Bardoux plutonic suite (Fig. 3) is a greyish metagranite dominated by a
176 metaluminous I-type to minor peraluminous S-type signature with millimetric garnet and
177 biotite completed with phenocrysts (up to 5 cm) of K-feldspar (microcline) showing locally
178 rapakivi texture, and containing some enclaves of diorite, monzonite and monzodiorite, that
179 represent continental-arc granitoids emplaced into the Laurentian margin (Augland et al.,
180 2015; Moukhsil et al., 2014, 2012). It has been dated at 1487.6 ± 6.8 Ma in the Lac du Milieu
181 region (U-Pb on zircon, Moukhsil et al., 2012), and at 1497 ± 5 Ma in the Lac Okaopéo region
182 (U-Pb on zircon, Augland et al., 2015). The Castoréum Plutonic Suite, which is intrusive in
183 the Plus-Value Complex and in the Bardoux Plutonic Suite (Fig. 3), is dominated by a facies
184 of homogeneous porphyric to porphyroclastic metagranite with a metamorphic fabric
185 delineated by the preferred orientation of biotite, hornblende and recrystallized or fractured
186 feldspar phenocrysts (Moukhsil et al., 2014, 2013b). It is associated with minor charnockite,
187 mangerite, granitic gneisses, and metatonalite (Moukhsil et al., 2014, 2013b). It has been
188 dated at 1393 ± 8 Ma (U-Pb on zircon) and emplaced in an arc-setting (Augland et al., 2015).

189 **2.2.2. Other lithotectonic units exposed in the Lac Okaopéo region**

190 The Lac Okaopéo region displays other lithotectonic units besides the ones intruded by
191 the PGD (Fig. 3). All are younger than the Plus-Value Complex paragneisses and the Bardoux
192 Plutonic Suite but their emplacement ages spread over the pre-Grenvillian and Grenvillian
193 history. Pre-Grenvillian units include granitic to dioritic orthogneisses, metamangerite and
194 metagranite. As they were emplaced between 1450 Ma and 1100 Ma (Augland et al., 2015;
195 David et al., 2009; Gobeil et al., 2002; Moukhsil et al., 2007, 2012, 2013a, 2013b, 2014), their
196 emplacement, encompasses most of the Mesoproterozoic evolution of the Province from the
197 late-Pinwarian (ca. 1470-1450 Ma, Ketchum et al., 1994; Tucker and Gower, 1994) to the
198 post-Elzevirian (ca. 1245-1225 Ma, Rivers et al., 2012). Several Grenvillian units are coeval
199 with the Ottawa peak of high-grade metamorphism and include granitic to quartz
200 monzodioritic orthogneisses, monzonitic to granitic slightly deformed plutons, and
201 undeformed mafic rocks (David, 2006; Dunning and Indares, 2010; Moukhsil et al., 2007,
202 2009, 2013b, 2014). Late-Ottawan units include the Berté anorthosite intrusive in the
203 Renwick Mangerite; the weakly deformed metaluminous mangerite and
204 charnockite±leuconorite±granite from the Céline Plutonic Suite (undated), ascribed to the
205 volcanic arc granite domain; the Sabot Mangerite (ca. 1016-1017 Ma); and the high-alkalic
206 mangerite±gabbro±syenite from the Okaopéo Plutonic Suite (1014.6±2.1 Ma) (Gobeil et al.,
207 2002; Moukhsil et al., 2007, 2009, 2013a, 2013b, 2014).

208 **3. Sampling and analytical methods**

209 **3.1. Sampling**

210 The seven PGD sampled for this study are accessible by gravel roads branching from
211 the 389 highway, from Baie-Comeau to the Daniel Johnson dam (Manic-5, Figs. 2-3). They
212 are located in the northwestern part of the studied region (NTS sheets 22K/07 and 22K/10,
213 Figs. 2-3, Table 1), and are aligned along a north to south trend (Fig. 3, Moukhsil et al.,
214 2014). The studied PGD are mainly composed of quartz+K-

215 feldspar+plagioclase+biotite±monazite/allanite (Figs. 4, 6-7, Appendices A-B). Their color
216 and mineralogy are correlated to the nature of the intruded lithologies. Dykes hosted in
217 paragneisses of the Plus-Value Complex are whitish and contain monazite
218 [(Ce,La,Nd,Th)PO₄] as the LREE-bearing phase (outcrops 13-AM-07, -10, -13 and 13-TC-
219 5008, Figs. 6, 8-10), while those hosted in metaplutonic complexes of the Bardoux and
220 Castoréum Plutonic Suites are pinkish (fresh color) and contain allanite
221 [(Ce,Ca)₂(Al,Fe³⁺)₃(SiO₄)₃(OH)] (outcrops 13-TC-5072, 13-FS-1202 and 13-AE-2149, Figs.
222 7, 11-12).

223 3.2. Whole rock geochemistry

224 Whole-rock geochemistry of the most REE enriched facies of the PGD identified on
225 each outcrop was performed by Actlabs (Ancaster, Ontario). Samples were chosen according
226 to the abundance of REE phases, i.e. monazite and allanite, and using a RS125 scintillometer
227 allowing for the identification of LREE-rich and LREE-poor facies as they are hosted in U-
228 Th-bearing phases. Powdered samples were prepared by Li-metaborate or -tetraborate. Major
229 elements were analysed by inductively coupled plasma - atomic emission spectroscopy (ICP-
230 AES), and trace elements by inductively coupled plasma - mass spectrometry (ICP-MS).
231 Results are reported in Table 2. In the present contribution, we report original geochemical
232 data and we include an analysis from Moukhsil et al. (2014) for sample 13-AE-2149 (Tables
233 1-2).

234 3.3. Electron microprobe (EMP)

235 Element composition and chemical maps were obtained by the Electron Microprobe
236 (EMP) method using a Cameca computer-controlled SX-100 (GeoRessources, Nancy)
237 equipped with a wavelength dispersive spectrometer (WDS).

238 For quantitative analyses and chemical mapping of monazite from the 13-AM-13 and
239 the 13-TC-5008 PGD, major and trace elements (Si, P, Ca, Y, La, Ce, Pr, Nd, Sm, Gd, Pb, Th,
240 U) were measured using an accelerating voltage of 20 kV and a beam current of 100 nA. Peak
241 counting time was set to 120 s for Pb, 100 s for U and 20 s for the others elements. Results are
242 reported in Table 3. Chemical mapping were realized at 15 kV and 100 nA, using a stage
243 scanning mode. Dwell time per pixel was adjusted to 30 ms and pixel step range from 0.3 to
244 0.9 μm . The chosen X-ray lines were: $\text{CaK}\alpha$, $\text{ThM}\alpha$, $\text{UM}\beta$, $\text{YL}\alpha$ and $\text{CeL}\alpha$. Maps are reported
245 in Fig. 9.

246 For quantitative analyses of allanite from the 13-TC-5072 and the 13-FS-1202 PGD,
247 major and trace elements (F, Mg, Al, Si, P, K, Ca, Ti, Mn, Fe, Sr, Y, La, Ce, Pr, Nd, Sm, Gd,
248 Pb, Th, U) were measured using an accelerating voltage of 20 kV and a beam current of 100
249 nA. Peak counting time was set to 120 s for Pb, 100 s for U and 20 s for the others elements.
250 Results are reported in Table 4.

251 **3.4. U-Pb dating on monazite using Laser Ablation-Inductively Coupled Plasma-Mass** 252 **Spectrometry (LA-ICP-MS)**

253 U-Pb geochronology of monazite grains from two PGD (13-AM-13 and 13-TC-5008)
254 was conducted directly on thin sections at Géosciences Rennes (France) by in-situ laser
255 ablation inductively coupled plasma mass spectrometry (LA-ICP-MS) using a ESI
256 NWR193UC Excimer laser coupled to a quadripole Agilent 7700x ICP-MS.

257 The signals of $^{204}(\text{Pb}+\text{Hg})$, ^{206}Pb , ^{207}Pb , ^{208}Pb and ^{238}U masses have been acquired
258 during the course of the analyses. The ^{235}U signal is calculated from ^{238}U on the basis of the
259 ratio $^{238}\text{U}/^{235}\text{U} = 137.88$. Single analyses consisted of 20 s of background integration followed
260 by 60 s integration with the laser firing followed by a 10 s delay to wash out the previous
261 sample. Spot diameters of 10 μm associated with repetition rates of 2 Hz and a laser fluency

262 of 6.5 J.cm^{-2} were used during the present study. For more information on the settings of the
263 instrument, see Ballouard et al. (2015) and the Appendix D for details and operating
264 conditions of the LA-ICP-MS measurements. Data reduction was carried out with the
265 GLITTER® software package developed by the Macquarie Research Ltd (Van Achterbergh et
266 al., 2001). Raw data were corrected for Pb/U laser-induced elemental fractionation and for
267 instrumental mass discrimination by standard bracketing with repeated measurements of the
268 Moacir monazite standard (Gasquet et al., 2010). To control the reproducibility and accuracy
269 of the corrections, repeated analyses of the Manangoutry monazite standard ($554.8 \pm 4.2 \text{ Ma}$;
270 $\text{MSWD} = 0.94$, $n = 8$ for the 13-AM-13 sample; $554.4 \pm 3.4 \text{ Ma}$; $\text{MSWD} = 0.94$, $n = 8$ for the
271 13-TC-5008 sample; TIMS age $555 \pm 2 \text{ Ma}$; Paquette and Tiepolo, 2007) were treated as
272 unknown. No common Pb correction was applied. Concordia diagrams were generated using
273 Isoplot/Ex (Ludwig, 2001). All errors given in Table 5 are listed at 1 sigma.

274 **4. Outcrop description and detailed mapping**

275 **4.1. Monazite-bearing PGD (paragneisses-hosted)**

276 Four of the REE occurrences associated with PGD identified by Moukhsil et al. (2014)
277 intrude migmatitic paragneisses of the Plus-Value Complex (Fig. 3). An example of detailed
278 mapping of a monazite-bearing PGD (13-AM-13 outcrop) is provided in Fig. 4, and detailed
279 description and mapping for each of the monazite-bearing outcrops are provided in Appendix
280 A. Structural measurements of the dykes' walls and of the foliation of the host rocks are
281 indicated for each outcrop in Appendix C.

282 **FIGURE 4**

283 To the north of the studied area, PGD are exposed within small (a few square meters
284 in surface) and flat lying outcrops (Fig. 6a) or steep-dipping outcrop along a gravel road. They
285 are made of decimeter- to decameter-sized single dyke bodies with steeply dipping to

286 subvertical walls trending N/S to locally NW/SE or NE/SW that dominantly plunge towards
287 south, and are strongly (Fig. 6b) to slightly (Fig. 6c) discordant to the foliation of their host
288 (Fig. 5a). Stockscheider-like textures delineate the contact between the 13-AM-07 PGD and
289 the intruded paragneisses (Fig. 6b). All contacts are slightly (over a few millimeters, Fig. 6b)
290 to locally diffuse (outcrop 13-TC-5008, Fig. 6c) and do not correspond to fractures
291 crosscutting the host-rock minerals (Fig. 6c). These PGD display various facies that are (i)
292 fine grained (1 mm to over 1 cm, Fig. 6b and d) with garnet and sub-euhedral monazite (Figs.
293 6e, f), (ii) intermediate, (iii) coarse-grained (sometimes over 3 cm, Fig. 6d) dominated by
294 quartz and feldspar with minor biotite, and (iv) pegmatitic dominated by
295 quartz+feldspar±biotite (Fig. 6g) with very few accessory phases, no garnet and few monazite
296 crystals. The transition between the fine- and coarse-grained facies is diffuse but is locally
297 underlined by biotite aggregates (Fig. 6d). Locally, skeletal biotite (up to 15 cm crystals) are
298 arranged as an arborescent texture (Fig. 6h). Up to ca. 20 cm centimeters wide quartz
299 aggregates are expressed with no identifiable link with any of the previous facies (Fig. 4).

300 **FIGURE 5**

301 **FIGURE 6**

302 These PGD with monazite as the REE-hosting mineral, will further be referred as
303 '*monazite-bearing*' (or '*Mnz-bearing*') PGD.

304 **4.2. Allanite-bearing PGD (metaplutonic complexes-hosted)**

305 Three of the REE occurrences associated with PGD identified by Moukhsil et al.
306 (2014) intrude the metaplutonic complexes of the Bardoux or the Castoréum Plutonic Suite
307 (Fig. 3). Detailed mapping and description for each of the allanite-bearing outcrops are
308 provided in Appendix B and structural measurements of the dykes' walls and of the foliation
309 of the host rocks are indicated for each outcrop in Appendix C.

310 Outcrops 13-TC-5072, 13-FS-1202 and 13-AE-2149 are either dome shaped (Fig. 7a),
311 flat lying or large steep-dipping (Fig. 7e). Two of these outcrops (13-TC-5072 and 13-FS-
312 1202) are made of decimeter- to meter-sized dyke swarms with steeply dipping to subvertical
313 walls trending NW/SE to locally N/S or NE/SW that plunge variably towards north and south,
314 and are slightly to strongly discordant to the foliation of their host metamonzogranite and
315 quartz metamonzodiorite (Fig. 5b), respectively. The contacts of these two dykes with their
316 host is slightly diffuse (over a few millimeters, Fig. 7c). One outcrop (13-AE-2149), is made
317 of a main shallow dipping dyke oriented NE/SW that plunges towards the north, in textural
318 continuity to granitic veins concordant/discordant to the foliation of the host metamangerite
319 (Figs. 5b, 7e-f). This dyke is slightly discordant to locally sub-concordant to the foliation of
320 its host rock (Fig. 5b) and locally show a very diffuse contact with its host rock at its lower
321 contact (Fig. 7g). None of the contacts of the allanite-bearing PGD correspond to fractures
322 crosscutting the host-rock minerals (Figs. 7c and g).

323 The metamonzogranite-hosted PGD (13-TC-5072) typically display a fine-grained
324 quartz+feldspar±biotite facies at the contact, with northern boundaries usually marked by K-
325 feldspar phenocrysts (Fig. 7c), and an increasing grain size towards the allanite-rich
326 pegmatitic core that are delineated by biotite aggregates (southern boundary for the dyke
327 represented in Fig. 7c). Allanite from this outcrop may reach several centimeters (Figs. 7c-d).
328 When zoned, the quartz metamonzodiorite-hosted PGD (13-FS-1202) display an internal
329 layering marked by coarse (over 3 cm) allanite-rich and barren facies alternating with fine-
330 grained (0.1-3 cm) allanite-rich facies (Fig. 7b). The metamangerite-hosted PGD (13-AE-
331 2149) is a ca. 1 m wide dyke (Fig. 7e), which displays diffuse contacts with its host rock, the
332 lower being more diffuse than the upper (Fig. 7g). Upper and lower contacts are marked by
333 ca. 20 cm and ca. 45 cm wide pegmatitic facies (some grains being over 10 cm in size)
334 respectively, composed of quartz+feldspar±disseminated allanite phenocrysts. The latter are

335 oriented with their long axis perpendicular to the contact (Fig. 7g). The core of the dyke is a
336 layered fine-grained facies with ca. 30 cm long quartz+K-feldspar-rich lenses that alternate
337 with quartz-plagioclase-rich lenses (Fig. 7g).

338 **FIGURE 7**

339 These PGD with allanite as the REE-hosting mineral, will further be referred as
340 '*allanite-bearing*' (or '*Aln-bearing*') PGD.

341 **5. Detailed petrography of the monazite- and allanite-bearing PGD**

342 **5.1. Petrography of the monazite-bearing PGD (paragneisses-hosted)**

343 All monazite-bearing PGD are dominated by a quartz+K-feldspar+plagioclase±biotite
344 assemblage (Fig. 8a), with a grain size spreading from millimeter to several centimeters (up to
345 5 cm in some facies). It is completed with minor garnet, zircon and monazite that are more
346 abundant in the finest grained facies, and accessory rare pyrite and Ti-oxides. All facies show
347 a magmatic texture and lack evidence for solid-state deformation (Fig. 8a).

348 **FIGURE 8**

349 The monazite crystals from paragneisses-hosted PGD have been investigated in two
350 PGD (the 13-AM-13 and the 13-TC-5008, Figs. 8a-c, 9). In both cases, monazite is expressed
351 as pristine sub-millimetric to several millimeters wide crystals that do not show any signs of
352 corrosion/dissolution. A main difference between monazite crystals from these two samples
353 lies in their inner textures and composition (Figs. 9-10, Table 3).

354 **FIGURE 9**

355 Monazite grains from the 13-AM-13 PGD show oscillatory zoning with a *LREE(Ce)*-
356 *rich* core surrounded by several overgrowths with a composition grading toward a *Th-Si-rich*
357 pole (Figs. 9a-c). These zones display monazite-(Ce) compositions that shift towards

358 monazite-(La) compositions with increasing proportion of Th and Si (Fig. 10a) that is
 359 consistent with the concurrent increase in huttonite end-member (from 3.78 % to 12.27 %,
 360 Fig. 10b, Table 3), where $\text{Th or U} + \text{Si} = \text{REE} + \text{P}$ (Spear and Pyle, 2002). The proportion of
 361 brabantite (from 8.66 % to 9.62 %) remains quite stable (Fig. 10b, Table 3).

362 Monazite grains from the 13-TC-5008 PGD are rather homogeneous or weakly zoned
 363 as expressed in SEM and X-ray maps. Chemical zoning consists of three zones that grade
 364 from a *LREE(Ce)-rich* to a *Th-Si-rich* composition toward the grain boundaries as identified
 365 in X-ray maps (Figs. 9d-f, Table 3). The compositions of all the grains are clustered into the
 366 monazite-(Ce) field (Fig. 10c) as marked by the quite stable P_2O_5 , and REE oxides contents
 367 (Table 3) from *LREE(Ce)-rich* zones to *Th-Si-rich* overgrowths. A slight increase in SiO_2 and
 368 ThO_2 is consistent with the increase in huttonite end-member (from 4.02 % to 5.39 %, Fig.
 369 10d). The proportion of brabantite (from 2.77 % to 3.37 %) remains quite stable (Fig. 10d,
 370 Table 3). Plotted in a Th+U+Si vs REE+Y+P diagram, the three investigated zones cluster
 371 and spread along a narrow range of the huttonite substitution curve (Fig. 10d).

372 **FIGURE 10**

373 Monazite-bearing PGD also comprise sub-euhedral zircon grains (up to 1-1.5 mm, Fig.
 374 8b) that may represent up to ca. 1% of the whole assemblage, mainly in fine grained to
 375 intermediate facies. Late-magmatic Th-U(\pm REE) silicates (Fig. 8c) are present as interstitial
 376 few micrometers wide bands in the vicinity of or as filling fractures of monazite crystals.
 377 Finally, sericite is expressed as an alteration product of feldspar (K-feldspar and plagioclase,
 378 Fig. 8d).

379 **5.2. Petrography of the allanite-bearing PGD (metaplutonic complexes-hosted)**

380 All allanite-bearing PGD are dominated by a quartz+K-feldspar+plagioclase \pm biotite
 381 (Figs. 11a-c) assemblage with a grain size ranging from millimeter to several centimeters

382 (over 10 cm in some pegmatitic facies, outcrop 13-AE-2149). This assemblage is completed
383 with zircon and allanite, and rare apatite (some grains are present in the pegmatitic facies of
384 the 13-AE-2149 outcrop). The abundance of accessory minerals is not correlated with the
385 grain size. All facies display a magmatic texture and lack evidence for solid-state deformation
386 (Figs. 11a-c).

387 **FIGURE 11**

388 The textural characteristics of allanite from metaplutonic complexes-hosted PGD
389 depend on the host granite. Allanite crystals were investigated in the 13-TC-5072 and the 13-
390 FS-1202 samples and in both cases are sub-euhedral and sub-millimetric to several
391 millimeters wide (Figs. 6b-d, g, 11b-c).

392 Allanite grains from the 13-TC-5072 PGD show an oscillatory zoned core, further
393 designated as ' Aln_1 ', corroded and crosscut by an overgrowth of a second generation of
394 intermediate composition allanite, further designated as ' Aln_2 ' (Fig. 11b), that forms the sub-
395 euhedral shape of allanite phenocrysts. It is surrounded by an alteration rim (Fig. 11b). These
396 three zones cluster as typical allanite compositions plotted in the REE vs Al diagram (Fig.
397 12a) of Petrák et al. (1995) and display quite similar compositions, except for the decrease in
398 FeO (from 11.11 to 9.76 wt.%) content from the Aln_1 cores to the alteration rims (Table 4).

399 Allanite grains from the 13-FS-1202 PGD display internal patchy zoning between
400 '*LREE(Ce)-rich*' and '*Fe-Ca-LREE(Ce)-rich*' zones (Fig. 11d). They are surrounded by an
401 alteration rim (Figs. 11c-f). The three zones plot between the epidote and allanite composition
402 in the REE vs Al diagram (Fig. 12b) of Petrák et al. (1995). The Fe-Ca-LREE(Ce)-rich zone
403 displays the most allanite-like composition, whereas the alteration rim is marked by a shift
404 towards the epidote composition (Fig. 12b) associated with an increase in SiO_2 and a decrease
405 in LREE (Table 4).

406 **FIGURE 12**

407 Allantite-bearing PGD also contain sub-euhedral zircon grains (up to 1-1.5 mm, Figs.
 408 11c and d) that may represent up to ca. 1% of the whole assemblage, mainly in fine to coarse
 409 grained facies. Late-magmatic Ca±REE carbonates or silicates are present as interstitial thin
 410 bands (a few micrometers wide) in the vicinity of or in fracture of allantite crystals (Figs. 11e-
 411 f). Finally, sericite is expressed as an alteration product of feldspar (K-feldspar and
 412 plagioclase, Figs. 11a and c).

413 **6. Whole-rock geochemistry of the monazite- and allantite-bearing PGD**414 **6.1. Geochemistry of the monazite-bearing PGD (paragneisses-hosted)**

415 Three of the four monazite-bearing PGD (samples 13-AM-07, 13-AM-10 and 13-TC-
 416 5008) display typical granitic composition with a SiO₂ content of 71.03 wt.%, 70.80 wt.% and
 417 70.79 wt.% respectively (Table 2), and a strong peraluminous character (Fig. 13a) as marked
 418 by their (i) ASI (Aluminum Saturation Index, $ASI = Al / (Ca - 1.67 \times P + Na + K)$ Frost et al.,
 419 2001; Shand, 1943), (ii) A/CNK ($A/CNK = Al / (Na + K + Ca/2)$, Shand, 1943), and (iii) A/NK
 420 ($A/NK = Al / (Na + K)$, Shand, 1943) above 1.19, 1.27 and 1.55 respectively (Table 2). In
 421 contrast, one monazite-bearing PGD (13-AM-13) does not display a typical granitic
 422 composition as its SiO₂ content is down to 60.24 wt.% (Table 2). This low content is
 423 associated with the highest Al₂O₃, CaO and Na₂O contents of 18.58 wt.%, 3.10 wt.% and 4.02
 424 wt.% respectively, and a low K₂O content of 4.36 wt.% leading to the highest ASI ratio of the
 425 monazite-bearing serie at 1.36 (Table 2) that corresponds to a strongly peraluminous signature
 426 (Fig. 13a).

427 All the monazite-bearing samples display high Σ REE content ranging from 1418 to
 428 7048 ppm (Table 2). Their REE patterns are strongly fractionated in LREE over HREE (Fig.
 429 13b), as evidenced by the La_N/Yb_N ratios ranging from 784 to 938 (Table 2), and more or less

430 developed Eu negative anomaly (Fig. 13b), which intensity increases with the Σ REE content,
431 as marked by decreasing Eu/Eu* from 0.72 down to 0.14 (Table 2). The Σ REE content is also
432 associated with (i) increasing U and Th contents (up to 19.10 and 1300 ppm respectively, Fig.
433 13c, Table 2) and Nb/Ta ratio (up to 56 with Nb ranging from 5.60 to 21 ppm and Ta ranging
434 from 0.10 to 0.40 ppm, Fig. 13e, Table 2), (ii) increasing Na₂O, CaO and P₂O₅ contents (up to
435 4.02, 3.10, 0.40 wt.% respectively, Figs. 13d and f, Table 2), and (iii) decreasing K₂O content
436 (down to 4.36 wt.%, Fig. 13d, Table 2). The Σ REE content of monazite-bearing PGD is not
437 linked to the Fe₂O₃ (total) nor MgO contents (Fig. 13g, Table 2). The Zr/Hf ratios are quite
438 stable (ranging from 36 to 44, Fig. 13e, Table 2) with Zr ranging from 195 to 1480 ppm and
439 Hf ranging from 4.40 to 41.50 ppm (Fig. 13e, Table 2).

440 **FIGURE 13**

441 **6.2. Geochemistry of the allanite-bearing PGD (metaplutonic complexes-hosted)**

442 Two of the three allanite-bearing PGD (samples 13-TC-5072 and 13-FS-1202) have
443 typical granitic composition with a SiO₂ content of 70.27 wt.% and 70.85 wt.% respectively
444 (Table 2), and a strong peraluminous character (Fig. 13a) as marked by their ASI, A/CNK,
445 and A/NK over 1.18, 1.24 and 1.64 respectively (Table 2). In contrast, one of the PGD
446 (sample 13-AE-2149) does not display a typical granitic composition as its SiO₂ content is
447 down to 55.84 wt.% (Table 2). This low content is associated with the highest Al₂O₃, CaO,
448 Na₂O contents of 15.05 wt.%, 5.54 wt.%, 4.28 wt.% respectively, and a low K₂O content of
449 1.93 wt.%, leading to the lowest ASI and A/CNK ratio of the allanite-bearing serie at 1.08 and
450 0.87 (Table 2) that corresponds to a weakly peraluminous signature (Fig. 13a).

451 All the allanite-bearing samples display high Σ REE content ranging from 2393 to
452 9242 ppm (Table 2). The REE patterns of the 13-TC-5072 and 13-FS-1202 samples are
453 strongly fractionated in LREE over HREE (Fig. 13b), as evidenced by the La_N/Yb_N ratios

454 ranging from 261 to 619 (Table 2). The REE pattern of the low-SiO₂ PGD (13-AE-2149
455 sample) is more enriched in HREE and displays a less fractionated pattern, as marked by its
456 lower La_N/Yb_N ratio of 28 (Table 2). The intensity of the negative Eu anomaly increases with
457 the Σ REE content as shown by decreasing Eu/Eu* from 0.36 down to 0.12 (Table 2). The
458 Σ REE content is also associated with (i) increasing U and Th contents (up to 30.30 and 766
459 ppm respectively, Fig. 13c, Table 2), (ii) increasing Na₂O, CaO, Fe₂O₃ (total) and MgO contents
460 (up to 4.28, 5.54, 12.42 and 0.85 wt.% respectively, Figs. 13d and g, Table 2), and (iii)
461 decreasing K₂O content (down to 1.33 wt.%, Fig. 13d, Table 2) and Nb/Ta ratio (down to 41
462 with Nb ranging from 7.50 to 132 ppm and Ta ranging 0.11 to 3.20 ppm, Fig. 13e, Table 2).
463 The Σ REE content of allanite-bearing granite dykes is not linked to the P₂O₅ content (Fig. 13f,
464 Table 2), nor to the Zr/Hf ratios that remain quite stable (ranging from 35 to 39, Fig. 13e,
465 Table 2) with Zr ranging from 290 to 6340 ppm and Hf ranging from 7.40 to 171 ppm (Fig.
466 13e, Table 2).

467 7. U-Pb dating of magmatic monazite

468 Monazite grains from the paragneiss-hosted 13-AM-13 PGD have been investigated
469 through 25 analyses performed directly on thin sections on 7 different grains. Plotted on a
470 concordia diagram, data define a discordia yielding an upper intercept of 1003.9±4.7 Ma
471 (MSWD = 0.43) if the lower intercept is anchored to 0±0 Ma (Fig. 14a, Table 5). Eleven of
472 these 25 analyses are concordant and define a concordia age (as of Ludwig, 1998) of
473 996.7±5.3 Ma (MSWD = 0.98, Fig. 14b). Even though the monazite grains from this sample
474 are zoned (Figs. 9a-c, 10a-b), these data do not show any signs of inherited cores with
475 distinctly older ages nor isotopic heterogeneity within a grain as all the data spread on the
476 same discordia and point to a single upper intercept date (Fig. 14a).

477 The monazite grains from the paragneisses-hosted 13-TC-5008 PGD have been
478 investigated through 22 analyses performed on 9 different grains. Plotted on a concordia
479 diagram, data plot on the concordia curve, and yield a concordia age of 1005.4 ± 4.4 Ma
480 (MSWD = 1.01; Fig. 14c, Table 5). As for the 13-AM-13 PGD, these data do not point to the
481 presence of inherited cores with an older age nor heterogeneity within a grain as all the data
482 plot on the concordia curve (Fig. 14c). This is consistent with the lack of chemical zoning on
483 the studied monazite grains (Figs. 9d-f, 10c-d).

484 **FIGURE 14**

485 **8. Discussion**

486 **8.1. LREE-rich PGD from the Lac Okapéo region in the frame of the Grenvillian** 487 **Orogeny**

488 The Grenville Province hosts numerous granitic pegmatites (e.g. Ayres and Černý,
489 1982; Černý, 1990; Ercit, 2005; Ford, 1982; Fowler and Doig, 1983; Lentz, 1996, 1991;
490 Lumbers, 1979; Masson and Gordon, 1981), mainly in the Central Gneiss Belt, in the Central
491 Metasedimentary Belt, in the Central Granulite Terrain and in the Eastern Grenville (Fig. 1b).
492 They are discordant and intrusive in brittle zones within competent units, show magmatic and
493 undeformed texture, and geochronological constraints evidence for their late-Grenvillian
494 Orogeny timing of emplacement (Ford, 1982; Fowler and Doig, 1983; Lentz, 1996, 1991,
495 Lumbers, 1979, 1964). These granitic pegmatites are assumed to be either derived (i) from
496 partial melting of paragneiss and/or orthogneiss, consistent with the presence of migmatites
497 and the lack of coeval intrusive granitic plutons (e.g. Ayres and Černý, 1982; Lentz, 1996,
498 1991; Lumbers, 1964; Masson and Gordon, 1981), or (ii) from the differentiation of a melt
499 segregated from a granite at the end of fractional crystallization (Ayres and Černý, 1982;
500 Masson and Gordon, 1981).

501 The main features of the LREE-rich PGD from the Lac Okaopéo region obtained in
502 this study have been summarized in Table 6. They are discordant to the foliation of their host
503 rocks and present magmatic textures with no macroscopic nor microscopic evidence for solid-
504 state deformation (Figs. 5-7, 8a, d, 11a-c). All of these PGD, to the noticeable exception of
505 one (13-AE-2149 PGD), are steep-dipping dykes with limited diffuse contacts and no
506 interconnection with leucosome (Figs. 5-7) suggesting they are intrusive into the
507 Paleoproterozoic to Mesoproterozoic Plus-Value paragneisses and Bardoux and Castoréum
508 metaplutonic suites, in a late- to post-tectonic regime, as other REE-rich Grenvillian granitic
509 pegmatites (Ercit, 2005; Lentz, 1996, 1991).

510 The 13-AE-2149 PGD is a shallow-dipping dyke connected to a network of
511 concordant/discordant veins to the foliation of its host layered mangerite (Figs. 5b, 7e-f)
512 suggesting a distinct and shallower source, and/or a different stress regime. The diffuse
513 contact at its lower contact (Fig. 7g) emphasizes a different petrogenetic process which might
514 have involved syn-crystallization fluid expulsion.

515 Formation of an orogenic plateau between ca. 1080-1050 Ma has been proposed to be
516 related to ductile lateral flow of the orogenic root beneath the ABT at the base of the Orogenic
517 Lid (Fig. 1b, Rivers, 2008). Late-Ottawan gravitational collapse is inferred to have started in
518 the central Grenville Province by ca. 1065 Ma (Rivers and Schwerdtner, 2015; Soucy La
519 Roche et al., 2015) and to have been completed by ca. 1020 Ma in the western part of the
520 Grenville Province, as evidenced by the reworking of the ABT as an extensional shear zone
521 (Ketchum et al., 1998; Rivers, 2008; Rivers et al., 2012). In the central Grenville, normal
522 shear-sense indicators in a 1015 Ma granite (Indares et al., 2000) in the MIZ and the intrusion
523 of mafic to intermediate magmatic rocks, such as the ca. 1015 Ma Okaopéo Plutonic Suite
524 (Fig. 3) that crosscuts the Ottawan metamorphic fabrics, have been attributed to a phase of
525 crustal extension compatible with this model (e.g. Augland et al., 2015; Indares et al., 2000).

526 Following the poor tectonic record from ca. 1020 to 1005-1000 Ma, the Rigolet orogenic
527 phase at ca. 1005-980 Ma, marked by the deformation and metamorphism of the
528 Parautochthonous Belt structurally below the ABT, is interpreted to represent a short-lived
529 crustal thickening event (e.g. Dunning and Indares, 2010; Jordan et al., 2006; Lasalle et al.,
530 2013). U-Pb dating on magmatic monazite grains from two PGD of the Lac Okaopéo region
531 yield dates of 996.7 ± 5.3 Ma (13-AM-13 PGD, Figs. 14a-b, Table 5) and 1005.4 ± 4.4 Ma (13-
532 TC-5008 PGD, Fig. 14c, Table 5) (see section 7 for details) that are comparable within
533 uncertainty. According to the lack of corrosion of the monazite grains, their oscillatory zoning
534 with no recrystallized domains or their unzoned character, these ca. 1005-1000 Ma
535 concordant dates are interpreted as reflecting their igneous crystallization ages (Crowley et
536 al., 2008) and are therefore attributed to post-Ottawan peak of metamorphism corresponding
537 to the initiation of the Rigolet orogenic phase. These emplacement ages are consistent (i) with
538 the discordant contacts of the dykes to the foliation of their hosts (Figs. 5, 6b, 7c, e-f) and (ii)
539 with the magmatic textures with no evidence for a solid-state deformation nor interconnection
540 with leucosomes (Figs. 6-7, 8a, d, 11a-c). These features suggest a post-tectonic and
541 metamorphic intrusion of the PGD relative to the paragneisses and the metaplutonic
542 complexes of the Allochthonous Belt they intrude and which were affected by the Ottawa
543 orogenic phase (Augland et al., 2015; Moukhsil et al., 2014). This timing of emplacement is
544 similar to the late- to post-Grenvillian Orogeny age of pegmatitic bodies in the western
545 Grenville Province (Fowler and Doig, 1983; Lentz, 1996, 1991, Lumbers, 1979, 1964).

546 **8.2. Potential sources of the LREE-rich PGD from the Lac Okaopéo region**

547 In granitic pegmatite fields reported in the literature, e.g. in Cap de Creus
548 (northeastern Spain, Alfonso and Melgarejo, 2008; Druguet et al., 2014; Van Lichtervelde et
549 al., 2016) or in Gatumba (central Rwanda, Hulsbosch et al., 2014; Melcher et al., 2015), the
550 closest bodies from the sources (usually a granite) (i) are the least evolved, and (ii) contain

551 biotite but no muscovite nor rare-element minerals (i.e. Li, B, Be, Rb, Sn, Nb-Ta... e.g.
552 Hulsbosch et al., 2014; London, 2016, 2008) or REE mineralization (e.g. Ercit, 2005). In the
553 case of the PGD from the Lac Okaopéo region, the ubiquitous presence of biotite in all the
554 investigated dykes with no muscovite nor other rare elements minerals than monazite or
555 allanite and zircon suggests that they do not represent the last melts that differentiated from
556 the source.

557 The intrusive contacts of the PGD (Figs. 5, 6b, 7c) and the lack of textural continuity
558 between the PGD and the leucosomes of the host rocks (except for the 13-AE-2149 dyke), are
559 pointing to an origin from a deeper-seated source. This interpretation is corroborated by their
560 emplacement age during the early Rigolet orogenic phase (ca. 1.0 Ga) in host rocks that have
561 recorded deformation and metamorphism during the Ottawa orogenic phase. Furthermore,
562 their pronounced peraluminous signatures (Fig. 13a) are not compatible with a magma
563 derived from the fractionation of the late-Ottawan mafic to intermediate Plutonic Suites of the
564 Lac Okaopéo region, nor of the undated metaluminous volcanic arc granite Céline Plutonic
565 Suite (Augland et al., 2015; Moukhsil et al., 2009, 2013a, 2014).

566 Jannin et al. (In press) documented that partial melting at a lower structural level than
567 our study area was initiated at least from ca. 1002 Ma at high-pressure in the presence of
568 garnet with pegmatite emplacement taking place between 993 down to possibly 961 Ma.
569 These results confirm that the Parautochthonous Belt experienced the Rigolet crustal
570 thickening phase under granulite facies metamorphism (up to ca. 15 kbar and 850°C between
571 ca. 1005-980 Ma, Jordan et al., 2006), i.e. conditions that are favorable for the partial melting
572 of the Parautochthonous Belt and coeval with the emplacement of the PGD. Nb/Ta ratios of
573 the PGD from the Lac Okaopéo region are very high (ranging from 34 to 58, Fig. 13e, Table
574 2) and are associated with low (except for the 13-AE-2149 dyke) Nb and Ta contents (up to
575 21 and 0.40 respectively, Table 2). Such low values are consistent with the lack of Nb-Ta-

576 bearing minerals in the PGD, and associated with high Nb/Ta are consistent with high-
577 temperature partial melting resulting in a total consumption of biotite from the protolith and
578 the formation of Ti-oxides in the residue that are preferential hosts for Nb and Ta and
579 preferentially fractionate the latter (Stepanov et al., 2014). Phase equilibria modeling of
580 metapelite such as those of the Knob Lake Group indicates that a common partial-melting
581 reaction in high-pressure granulite is $Bt + Pl \pm Ky = Liq + Grt + Kfs + Qtz + Rt$ (Gervais and
582 Crowley, 2017). In addition to producing leucosome with zircon depleted in HREE because of
583 their sequestration in garnet, such as those in leucosome of the Parautochthonous Belt (Jannin
584 et al., In press), the growth of peritectic rutile associated with this reaction should produce
585 melt with the Nb-Ta features observed in the investigated PGD.

586 The strongly peraluminous character of these PGD (Fig. 13a, Table 2) contrast with
587 the metaluminous signature of the western Grenvillian REE-rich granitic pegmatites reported
588 by Lentz (1996) (Fig. 13a, Table 2) and is compatible with their derivation by partial melting
589 of a metasedimentary unit (e.g. Chappell and White, 2001; Cuney, 2014; White and Chappell,
590 1977). The high La_N/Yb_N ranging from 784 to 938 (monazite-bearing PGD) and from 261 to
591 619 (13-TC-5072 and 13-FS-1202 allanite-bearing PGD) suggest that these dykes represent
592 melts segregated from a molten crustal component enriched in a HREE-bearing phase, most
593 probably garnet as it is very common in paragneisses especially in those from the Knob Lake
594 Group of the Gagnon Terrane (Bea, 1996; Hönig et al., 2014; Jordan et al., 2006). These
595 features are consistent with the lack of evidence for coeval kilometric scale granitic intrusive
596 body at this stage of the Grenvillian Orogeny and with the results of the great majority of
597 studies dealing with Grenvillian REE-rich granitic pegmatites (e.g. Ercit, 2005; Lentz, 1996,
598 1991). In addition, it brings evidence that REE-rich granitic pegmatites do not necessarily
599 derive from the fractionation of a granitic intrusive body and that they may be metamorphic in
600 origin as it is proposed by default, especially in the Grenville Province, because of the lack of

601 an exposed coeval granitic intrusive body (Ercit, 2005). Even though the timing of
602 emplacement and field relationships of the dykes are in favor of a source belonging to the
603 Parautochthonous Belt, whether the molten paragneisses that led to the formation of these
604 dykes belong to the deep Allochthonous (Plus-Value Complex, Figs. 2-3, Moukhsil et al.,
605 2014, 2012) or to the Parautochthonous Belt (Knob Lake Group of the Gagnon Terrane, Fig.
606 2, e.g. Rivers, 2008) remains an open question.

607 The 13-AE-2149 allanite-bearing PGD displays quite different features when
608 compared to other PGD such as (i) a shallow-dipping and diffuse contact (Figs. 5b, 7g), (ii)
609 higher Nb and Ta contents of 132 and 3.20 ppm respectively (Table 2), (iii) a weakly
610 peraluminous character (ASI of 1.08, Fig. 13a, Table 2), and (iv) a much lower La_N/Yb_N of 28
611 (Fig. 13b, Table 2). These features suggest its possible derivation by differentiation of a late-
612 Ottawa garnet/rutile-poor source (Bea, 1996; Hönig et al., 2014; Stepanov et al., 2014) such
613 as the ca. 1015 Ma Okaopéo Plutonic Suite (high-alkalic mangerite±gabbro±syenite) and
614 Sabot Mangerite (Augland et al., 2015; Moukhsil et al., 2014), combined with late-
615 crystallization fluid release and/or an interaction with its pre-Grenvillian host metamangerite
616 during its intrusion.

617 **8.3. Unusual petrogeochemical characteristics of the LREE-rich PGD from the Lac** 618 **Okapéo region**

619 Previous studies have shown that Grenvillian granitic pegmatites are dominated by
620 quartz+K-feldspar+plagioclase ± a ferromagnesian phase, completed with a variety of other
621 major and minor phases (e.g. pyroxene, amphibole, biotite, titanite, magnetite, sulfides,
622 allanite, zircon, garnet, monazite, pyrochlore-group minerals and U-Th phases, Ercit, 2005;
623 Fowler and Doig, 1983). Grenvillian granitic pegmatites commonly host REE together with
624 other metals such as U-Th, Nb-Ta, Y, Ti, Zr, Be, Mo, P, Pb, F, with no REE-only
625 mineralization described in these occurrences. The mineralogical assemblage of the PGD

626 from the Lac Okaopéo region is dominated by quartz+K-feldspar+plagioclase+biotite, as
627 proposed by Ercit (2005), Ford (1982) and Lentz (1996, 1991), and is completed with zircon
628 and monazite or allanite (Figs. 8-12, Tables 3 and 4). No complementary rare-element
629 minerals have been recognized in the PGD of the Lac Okaopéo region, except for the late but
630 micrometric Th-U(\pm REE) silicates (Fig. 8c) and the Ca \pm REE silicates or carbonates (Fig.
631 11e-f) identified in the monazite- and allanite-bearing PGD, respectively, and that represent a
632 negligible part of the whole rock. The accessory phases assemblages, even if not uncommon
633 in worldwide abyssal class pegmatitic bodies (Ercit, 2005), is less diverse than for the rest of
634 the LREE-enriched Grenvillian PGD (Ford, 1982; Lentz, 1996, 1991). Accordingly, the PGD
635 from the Lac Okaopéo region represent the first evidence of magmatic REE-only
636 mineralization in this region.

637 Monazite and allanite crystals from the PGD investigated in this study are monazite-
638 (Ce) and allanite-(Ce) and generally display a core to rim zoning (Figs. 9, 10a, c, 11b, d,
639 Tables 3-4). Monazite crystals from the two investigated PGD present a dominant substitution
640 expressed by the huttonite end-member that is consistent with the concurrent evolution of Th
641 and Σ REE contents (13-AM-13 and 13-TC-5008, Figs. 10b and d, 13c, e.g. Spear and Pyle,
642 2002). Monazite from the 13-TC-5008 PGD are rather homogeneous (Figs. 9d-f, 10c-d)
643 whereas oscillatory zoned monazite from the 13-AM-13 PGD are characterized by a gradient
644 trending towards monazite-(La) from LREE(Ce)-rich cores to Th-Si-rich rims (Figs. 9a-c,
645 10a-b, Table 3). This suggests an evolution of the melt composition during crystallization
646 from LREE-rich towards Th-Si-rich most probably related to the crystallization of zircon, the
647 only LREE-poor/Th-Si-bearing phase present in the dykes (e.g. Bea, 1996; Hanchar et al.,
648 2001). Its crystallization would generate a LREE-rich/Th-Si-poor residual melt, allowing the
649 preferential incorporation of LREE into the monazite lattice and a relatively LREE-
650 impoverished/Th-Si-enriched residual melt after zircon growth is completed. In contrast,

651 allanite crystals from the 13-TC-5072 and the 13-FS-1202 PGD display distinct textures.
652 Those from the former show oscillatory zoned cores (Aln_1) corroded by overgrowths (Aln_2 ,
653 Fig. 11b) with stable compositions (Fig. 12a, Table 4). This is most probably related to a new
654 magmatic pulse and not to a significant change in the melt composition. Allanite phenocrysts
655 from the latter however show inner patchy and not oscillatory zoning suggesting a random
656 organization between LREE(Ce)-rich and Fe-Ca-LREE(Ce)-rich zones (Fig. 11d, Table 4).
657 This points to more complex petrogenetic processes than successive growths associated with
658 distinct magmatic pulses. However, a compositional change is recorded in the Fe-poor and in
659 the Si-rich/LREE-poor alteration rims that are expressed on every allanite phenocrysts from
660 the 13-TC-5072 (Fig. 11b) and the 13-FS-1202 (Figs. 11d-e) PGD, respectively (Table 4).
661 According to the lack of corrosion of previous zones associated with no changes in the
662 euhedral shape of the grains, its association with the late-sericitization of feldspar (Fig. 11a, c)
663 and formation of late-Ca \pm REE carbonates or silicates veinlets (Fig. 11e-f), this alteration is
664 most likely related to magmatic-hydrothermal transition processes. In summary, monazite
665 crystals would record the fractionation of zircon during the course of melt crystallization of
666 paragneisses-hosted PGD marked by syn-zircon growth LREE-rich/Th-Si-poor monazite
667 cores and post-zircon growth LREE-poor/Th-Si-rich zones. In contrast, allanite phenocrysts
668 do not allow to discuss magmatic fractionation but offer insights on the magmatic-
669 hydrothermal transition associated with the formation of allanite alteration rims coeval with
670 late veinlets of carbonates or silicates and most probably with feldspar sericitization.

671 The empirical relation of monazite in paragneisses-hosted PGD and allanite in
672 metaplutonic-hosted PGD might reflect either (i) an initial geochemical difference between
673 the two granitic series, and/or (ii) interactions of the melt with different rocks during ascent
674 and/or at emplacement level. On the one hand, the former hypothesis is strengthened by (i) the
675 positive correlation between the P_2O_5 , CaO and the Σ REE contents (Fig. 13f) in monazite-

676 bearing PGD, unlike in allanite-bearing, and (ii) the positive correlation between the Fe_2O_3
677 _(total), MgO and the ΣREE contents in allanite-bearing PGD (Fig. 13g). On the other hand, the
678 hypothesis of an interaction between melts and surrounding rocks is supported by the
679 empirical relationship (i) between monazite-bearing PGD and wide outcropping areas of
680 metasediments (3 over 4 PGD hosted in the Plus-Value Complex), and (ii) between allanite-
681 bearing PGD and metaplutonic complexes (2 over 3 PGD hosted in the Bardoux and
682 Castoréum Plutonic Suites) (Figs. 3, 6-7). These suggest that the crystallization of monazite
683 and allanite could be related to interactions of the granitic melt (i) with the more sodic
684 metasedimentary host of the Plus-Value complex for the former, and conversely (ii) with the
685 more calcic igneous rocks of the Bardoux and Castoréum suites for the latter. This hypothesis
686 is consistent with the locally diffuse contact of the 13-TC-5008 monazite-bearing PGD (Fig.
687 6c) and the very diffuse contact at the lower contact of the 13-AE-2149 allanite-bearing PGD
688 (Fig. 7g). Such a model has been proposed for granitic pegmatites from the southwestern
689 Grenville Province and is designated as “hybridization” by Lentz (1996, 1991), who
690 evidenced bi-metasomatic exchange processes leading to Ca, Fe, $\text{Mg}\pm\text{Ti}$ enrichment in the
691 melts and to the crystallization of titanite and allanite. However, (i) the lack of macroscopic
692 mineralogical reaction zone at the contact of most of the dykes with their host rocks, and (ii)
693 the close geographical association of the 13-TC-5008 monazite-bearing and the 13-AE-2149
694 allanite-bearing PGD (Fig. 3), make the hypotheses of a control of the mineralization by deep
695 interaction between the magma and rocks of distinct chemical composition unlikely. In
696 addition, both monazite- and allanite-bearing samples display a similar positive correlation
697 between the Na_2O , the CaO and the ΣREE contents (Fig. 13d) suggesting that the hypothesis
698 of an initial geochemical difference between the two granitic series is most likely. Therefore
699 we propose that the control of the mineralization either as monazite or allanite observed in the
700 PGD from the Lac Okaopéo may not only be correlated with the activities of Na and Ca as

701 proposed in the models of Berger et al. (2009) and Budzyń et al. (2011) but by the initial CaO
702 and P₂O₅ contents, and the Fe₂O₃ (total) and MgO, respectively. Exception is the 13-AE-2149
703 dyke emplaced in an intermediate host metamangerite with a diffuse lower contact, and that
704 displays a weakly peraluminous character (ASI of 1.08, Fig. 13a, Table 2) that is intermediate
705 between the other PGD investigated in this study and those reported by Lentz (1996). This
706 lower peraluminous signature may reflect an interaction of the dyke with its host during its
707 emplacement, as proposed by Lentz (1996) for western Grenvillian granitic pegmatites.

708 The weak to strong peraluminous character associated with P₂O₅ contents of 0.02-0.40
709 wt.% (Fig. 13f, Table 2) of the PGD from the Lac Okaopéo region correspond to the
710 peraluminous intermediate phosphorous serie defined by Linnen and Cuney (2005). It contrast
711 with the metaluminous Grenvillian LREE-enriched granitic pegmatites of Lentz (1996) (Fig.
712 13a) and with REE-enriched granitic pegmatites reported elsewhere that are ascribed to
713 alkaline intrusive (Dill, 2010, 2015; Ercit, 2005; London, 2016). Allanite is a major LREE
714 carrier in granitoids with ASI below 1.2 (Bea, 1996) and in LREE-enriched granitic
715 pegmatites from the abyssal class, usually ascribed to metaluminous to subaluminous
716 compositions (Ercit, 2005; Ford, 1982; Lentz, 1996, 1991), i.e. not in strongly peraluminous
717 melt. In the PGD from the Lac Okaopéo region, allanite is hosted in three metaplutonic hosted
718 PGD, two of them displaying ASI ranging from 1.18 to 1.35 (13-TC-5072 and 13-FS-1202
719 PGD respectively, Table 2) that are not compatible with the formation of allanite. In contrast,
720 the presence of monazite in paragneisses-hosted PGD with ASI ranging from 1.19 to 1.36
721 (Table 2) is consistent with its expression as a major and widespread LREE-carrier in a
722 variety of granitoids especially in peraluminous granite and abyssal granitic pegmatites (Bea,
723 1996; Ercit, 2005; Linnen and Cuney, 2005; Montel, 1993; Rapp and Watson, 1986), but its
724 sole presence as LREE-bearing phase in PGD is shown for the first time in the Grenville
725 Province.

726 The monazite- and allanite-bearing PGD from the Lac Okaopéo region are generally
727 more concentrated in REE and more fractionated in LREE over HREE than those of the most
728 enriched samples of Lentz (1996), with Σ REE between 1418 to 7048 ppm (monazite-bearing
729 PGD) and between 2393 to 9242 ppm (13-TC-5072 and 13-FS-1202 allanite-bearing PGD),
730 associated with La_N/Yb_N up to 938 (Fig. 13b, Table 2). The Σ REE content of PGD from the
731 Lac Okaopéo region increases with (i) decreasing Eu/Eu* anomaly from 0.72 down to 0.12
732 (Fig. 13b, Table 2), and (ii) with increasing U and Th contents (Fig. 13c), Th being much
733 more concentrated than U (Th/U ratio between 25 and 74, Table 2). Both features are
734 consistent with the increasing proportion of REE-bearing phases relative to major minerals
735 that represent sinks for Eu (e.g. Bea, 1996; London, 2008). The U and Th contents increase
736 more rapidly with Σ REE in monazite-bearing than in allanite-bearing dykes (Fig. 13c) as
737 marked by the formation of ThO_2 -rich monazite relative to allanite (Tables 3-4).

738 The monazite- and allanite-bearing PGD present unusual and some distinct
739 geochemical trends (Fig. 13). The high Zr/Hf ratio (Fig. 13e) associated with high contents of
740 Zr and Hf (up to 1480 and 41.5 ppm respectively, Table 2) and the very low contents of Nb
741 and Ta of the PGD (Table 2) is characteristic of alkaline melts (Linnen and Cuney, 2005;
742 Linnen and Keppler, 2002; Zraiskiy et al., 2009). The quite stable Zr/Hf with increasing
743 Σ REE is also a characteristic feature of alkaline melts in which the high zircon solubility
744 prevents the fractionation of Zr over Hf associated with zircon growth (Ellison and Hess,
745 1986; Linnen, 1998; Linnen and Cuney, 2005; Linnen and Keppler, 2002; Zraiskiy et al.,
746 2009). The contrasting behavior of the Nb/Ta ratio in monazite- and allanite-bearing PGD,
747 with increasing Nb/Ta ratio and Σ REE content in monazite-bearing and decreasing Nb/Ta
748 ratio with increasing Σ REE content in allanite-bearing PGD (Fig. 13e), suggest either distinct
749 (i) magmatic processes, or (ii) fractionation of Nb over Ta associated with distinct sources or
750 (iii) with the crystallization of monazite over allanite. The former hypothesis is unlikely

751 according to the lack of Nb and Ta minerals in the dykes. Accordingly, the whole-rock
752 geochemistry of the REE-rich PGD from the Lac Okaopéo region display contrasting
753 signatures with (i) major elements characteristics of intermediate phosphorous peraluminous
754 granites (e.g. Linnen and Cuney, 2005), and (ii) trace elements (Zr-Hf-Nb-Ta and the REE)
755 enrichment and fractionation more akin to a peralkaline signature of the melts (e.g. Ellison
756 and Hess, 1986; Linnen, 1998; Linnen and Cuney, 2005; Linnen and Keppler, 2002; Zaraisky
757 et al., 2009).

758 **8.4. LREE-rich PGD from the Lac Okapéo region in the granitic pegmatite** 759 **classification scheme**

760 The PGD from the Lac Okaopéo region display peraluminous signatures (Fig. 13a,
761 Table 1), are LREE enriched (Fig. 13b) and are composed of a quartz+K-
762 feldspar+plagioclase+biotite (for major minerals, Figs. 8a, d, 11a-c) with either monazite or
763 allanite and ubiquitous zircon (Figs. 8a-c, 11b-f). Mineralized granitic pegmatites displaying a
764 peraluminous signature usually belong to the LCT family (Černý et al., 2012; Černý and Ercit,
765 2005; Ercit, 2005; London, 2005, 2008; Martin and De Vito, 2005). Even though the seven
766 PGD described in this paper are peraluminous, they do not share any other characteristic of
767 this family since none of them contain any muscovite, nor Li-, Cs- or Ta-minerals, nor
768 tourmaline or beryl and are not enriched in Rb, Ga or Sn. In addition, their trace elements
769 geochemistry is more akin to alkaline melts (e.g. Linnen and Cuney, 2005; Linnen and
770 Keppler, 2002). In the classical classification scheme, the NYF family contains pegmatitic
771 bodies derived from alkaline intrusive bodies and are enriched in Nb, Y, F, Be, Ti, Sc, Zr with
772 LREE concentrations up to 100 to 800 times chondritic and little depletion in HREE (Černý et
773 al., 2012; Černý and Ercit, 2005; Ercit, 2005; London, 2005, 2008). PGD investigated from
774 the Lac Okaopéo region do not contain any minerals hosting the usual rare-metals of the NYF
775 family, show an LREE enrichment from over 1,000 to almost 10,000 times the chondritic

776 value (Fig. 13b), a strong depletion of HREE and, for six of them (exception is the 13-AE-
777 2149 PGD) are most probably derived by partial melting of a deeper-seated metasedimentary
778 source. Therefore, they are not characteristic of the NYF family neither.

779 Ercit (2005) reviewed the general characteristics of world-wide REE-enriched granitic
780 pegmatites. These are mainly observed in Colorado, Virginia and Northern Carolina (USA),
781 Kola-Karelia and Pribaikal regions, and Aldan Shield (Russia), southern Japan, Antsirabé-
782 Kitsamby and Ankazobe districts (Madagascar), and finally in the SW Grenville Province,
783 that represents one of the major districts of such REE occurrences (e.g. Ford, 1982; Lentz,
784 1996, 1991). Ercit (2005) emphasized that REE-enriched granitic pegmatites do not always
785 fall in fields of the previously described granitic pegmatites families (either LCT or NYF) of
786 Černý (1991). However, in the abyssal class, two main types of REE-enriched granitic
787 pegmatites are common: (i) the LREE-enriched that typically host REE as an allanite-
788 monazite and/or uraninite assemblage, and (ii) the (Y,HREE)-enriched that typically host
789 REE assemblage as more complex rare-element assemblages than the previous one (Ercit,
790 2005). The PGD from the Lac Okaopéo region display Σ LREE contents between 1407 and
791 7435 ppm hosted in either monazite or allanite (Figs. 6f, 7b-d, g, 8a-c, 9-12) and Σ HREE
792 contents between 11 and 485 ppm (Fig. 13b, Table 2) and can therefore be ascribed to the
793 LREE-enriched type of Ercit (2005).

794 According to previous sections of the discussion, the zoned PGD from the Lac
795 Okaopéo region intruded metamorphosed sedimentary units and metagneous complexes in a
796 post-tectonic setting relative to the structure and metamorphism of their host rocks with no
797 link, for six of them (except for the 13-AE-2149 PGD), to a plutonic body (see sections 8.1.
798 and 8.2.) and therefore correspond to the class of 'pseudopegmatites' proposed by Dill (2016)
799 in its CMS (Chemical composition - Mineral assemblage - Structural geology) classification
800 scheme. The 13-AE-2149 PGD however could derive by differentiation of a late-Ottawan

801 plutonic suite and would therefore correspond to the ‘pegmatite’ class of Dill (2016). In
802 addition, according to the same scheme the monazite-bearing PGD are paragneisses-hosted
803 zoned meter-sized (Zr)-LREE quartz-feldspar-biotite pseudopegmatite (monazite), whereas
804 the 13-TC-5072 and the 13-FS-1202 allanite-bearing PGD are metamonzogranite-hosted
805 zoned decimeter- to meter-sized (Zr)-LREE quartz-feldspar-biotite pseudopegmatite (allanite)
806 and quartz metamonzodiorite-hosted zoned decimeter- to meter-sized (Zr)-LREE quartz-
807 feldspar-biotite pseudopegmatite (allanite), respectively. In the same way and according to the
808 its possible derivation from a plutonic source, the 13-AE-2149 allanite-bearing PGD is a
809 metamangerite-hosted zoned centimeter- to meter-sized (Zr)-LREE quartz-feldspar-biotite
810 (pseudo)pegmatite (allanite) according to Dill (2016).

811 **Conclusions**

812 The seven pegmatitic granite dykes (PGD) from the Lac Okaopéo region described in
813 this paper represent new LREE-only occurrences in the central Grenville Province. They
814 intrude paragneisses from the Plus-Value Complex or felsic to intermediate metaplutonic
815 complexes from the Bardoux and Castoréum Plutonic Suites that are part of the
816 Allochthonous Belt of the Grenville Province. These LREE occurrences are undeformed
817 dykes discordant to the foliation of their host rocks with no evidence for interconnection with
818 leucosomes and are thus considered as post-tectonic relative to the structure and
819 metamorphism of their host rocks that recorded the Ottawaan orogenic phase. Their
820 peraluminous signature, high Nb/Ta ratio and high fractionation of LREE over HREE suggest
821 their derivation by partial melting of metasedimentary units, either belonging to the base of
822 the Allochthonous or to the Parautochthonous Belt. U-Pb dating of magmatic monazite from
823 two of the LREE occurrences yield concordant igneous ages at 996.7 ± 5.3 Ma and 1005.4 ± 4.4
824 Ma that correspond to an emplacement at the initiation of the Rigolet orogenic phase
825 considered to represent a short-lived phase of renewed crustal thickening as recorded by

826 deformation and metamorphism of the Parautochthonous Belt between ca. 1005 and 980 Ma.
827 Further isotopic and geochronological investigations are needed to constrain their derivation
828 either from the Allochthonous or the Parautochthonous Belt.

829 Field relationships show that monazite host the LREE-mineralization for PGD hosted
830 by paragneisses of the Plus-Value Complex, and that allanite host the LREE-mineralization
831 for PGD hosted by metagranitoids of the Bardoux and Castoréum Plutonic Suites, in both
832 cases without complementary rare-metals minerals. The geochemistry and rare-metals
833 assemblage do not allow to ascribe these PGD to the classical LCT and NYF family. In
834 addition, even if a peraluminous character is marked by the major elements whole-rock
835 geochemistry, the Zr/Hf ratio associated with high Zr and Hf contents, the very low contents
836 in Nb and Ta and the very high contents in LREE are more akin to a peralkaline series.

837 The peraluminous signature of the mineralized PGD contrasts with the typical
838 metaluminous to subaluminous signature of REE-enriched granitic pegmatites reported
839 elsewhere. This peraluminous composition is consistent with the crystallization of monazite-
840 (Ce) but is at odd with the presence of allanite-(Ce). This contribution constitutes the first
841 evidence in the Grenville Province of such a monazite-only mineralization hosted in PGD.
842 Further investigations are required to identify the factors controlling the crystallization of
843 allanite in some of these PGD.

844 **Acknowledgements**

845 The authors would like to thank the Ministère de l'Énergie et des Ressources naturelles
846 (Québec) for providing technical and financial support for the field work and analyses. This
847 contribution constitutes a Ministère de l'Énergie et des Ressources naturelles du Québec
848 publication n°8449-2016-2017-04. The authors are grateful to Sandrine Mathieu (SEM), Lise
849 Salsi (SEM) and Olivier Rouer (EMP) (GeoRessources, Nancy) for technical support in

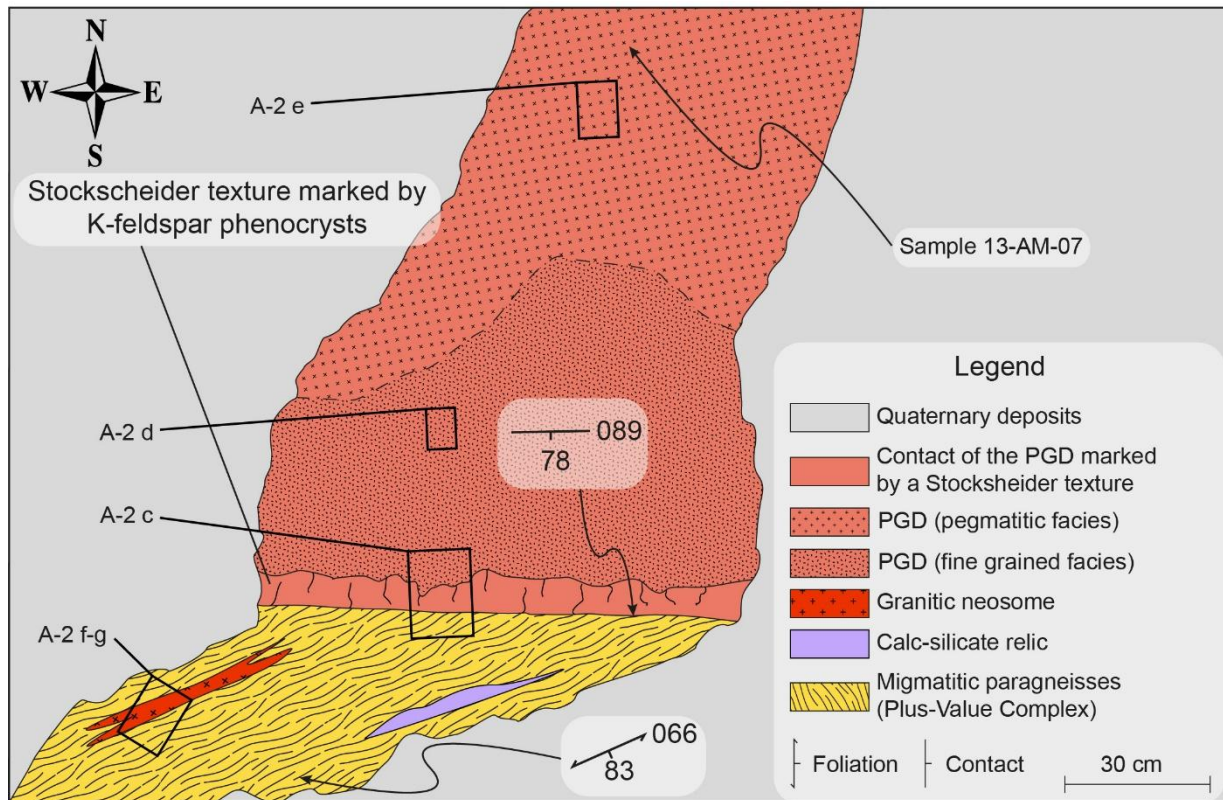
850 providing analytical data on SEM and EMP, to Alexandre Crépon (GeoRessources, Nancy)
851 for their help during field work and to Aurélien Eglinger (GeoRessources, Nancy) for his help
852 in handling geochronological data. The authors also thank Harald G. Dill and an anonymous
853 reviewer for their detailed review that helped to improve the paper, and Franco Pirajno for
854 editorial handling. This work was funded by the Labex Ressources 21 (supported by the
855 French National Research Agency through the national program “Investissements d’avenir”,
856 reference ANR-10-LABX-21–LABEX RESSOURCES 21 and the Region Grand-Est. It
857 benefited from the framework of the DIVEX “Rare earth element” research program.

858

859 **Appendix A: Detailed mapping of the monazite-bearing pegmatitic granite** 860 **outcrops**

861 **9. 13-AM-07 monazite-bearing pegmatitic granite dyke (PGD)**

862 The 13-AM-07 monazite-bearing pegmatitic granite dyke (PGD) and REE occurrence
863 is located in the north of the 22K/10 NTS sheet (Fig. 3) and is exposed as a small (a few
864 square meters in surface) and flat lying outcrop (Fig. A-2a). The detailed map of this outcrop
865 is available in the Fig. A-1.

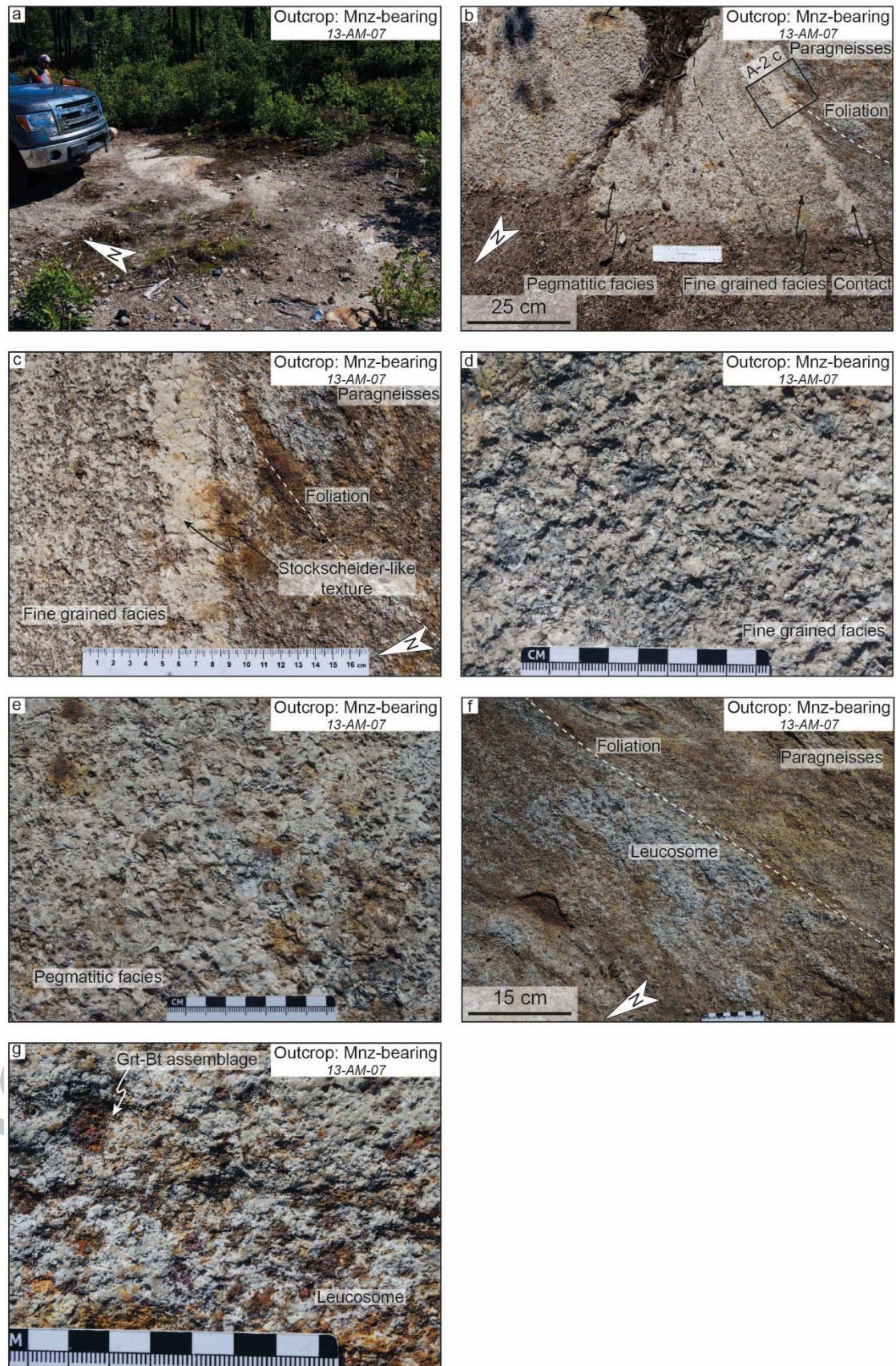


866

867 **Figure A-1:** Detailed map of the 13-AM-07 outcrop made of migmatitic paragneisses from the Plus-Value
 868 Complex intruded by a discordant REE-rich pegmatitic granite dyke. Abbreviation: PGD = pegmatitic granite
 869 dyke.

870 The PGD is steep-dipping and discordant to the foliation of the Plus-Value Complex
 871 migmatitic paragneisses (Figs. A-2b-c, 5a). The dyke is whitish (Figs. A-2b-e) and is layered
 872 parallel to the contact. The discordant contact with the paragneisses is marked by the
 873 development of a Stockscheider texture visible in the development of K-feldspar phenocrysts
 874 reaching a length of up to 5 cm (Fig. A-2c). From the contact and towards the core of the
 875 dyke, these phenocrysts are in contact with a 20 to 50 cm wide fine-grained facies (Figs. A-2b
 876 and d) grading onto a pegmatitic facies (Figs. A-2b and e) with crystals reaching up to ca. 3
 877 cm in the center of the dyke.

878 The host paragneisses from the Plus-Value Complex are migmatitic with
 879 granitic±garnet-biotite leucosomes that can reach several tens of centimeters in width (Figs.
 880 A-2b, f-g).

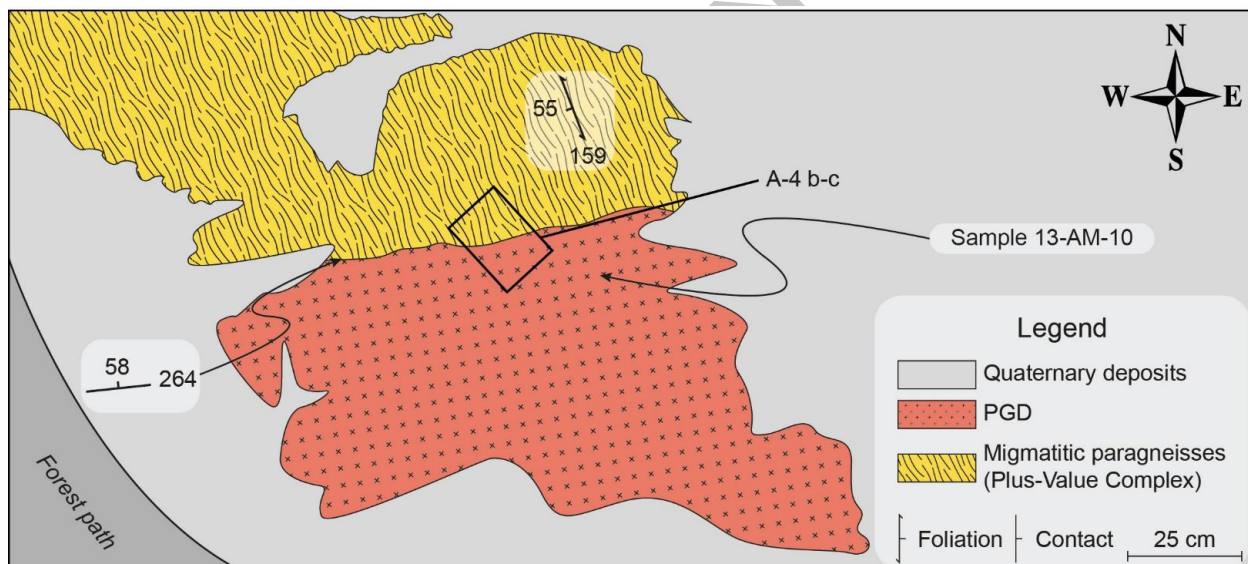


881
 882 **Figure A-2:** Photographs of the 13-AM-07 outcrop from the Lac Okaopéo region. a: general view of the 13-
 883 AM-07 outcrop composed of a pegmatitic granite dyke intruding paragneisses from the Plus-Value Complex;
 884 b: large view of the relationships between the dyke and the paragneisses. Note the discordant contact as
 885 evidenced by the crosscut foliation of the paragneisses by the dyke; c: detailed view of Stockscheider-like
 886 contact between the pegmatitic granite dyke and the intruded paragneisses marked by the crystallization of

887 feldspar from the dyke perpendicular to the contact; d: detailed view of the fine grained facies dominated by
 888 feldspar and quartz; e: detailed view of the pegmatitic facies dominated by feldspar and quartz; f: typical
 889 facies of the Plus-Value Complex paragneisses showing the importance of leucosomes in this facies; g:
 890 mineralogy of the leucosomes from the migmatitic Plus-Value Complex paragneisses. Note the domination of
 891 quartz-feldspar in this granitic leucosome, the abundance of the garnet-biotite assemblage expressed as
 892 several millimeters crystals and the lack of deformation in these leucosomes. Abbreviations: Bt = biotite; Grt
 893 = garnet; Mnz-bearing = monazite-bearing pegmatitic granite dyke.

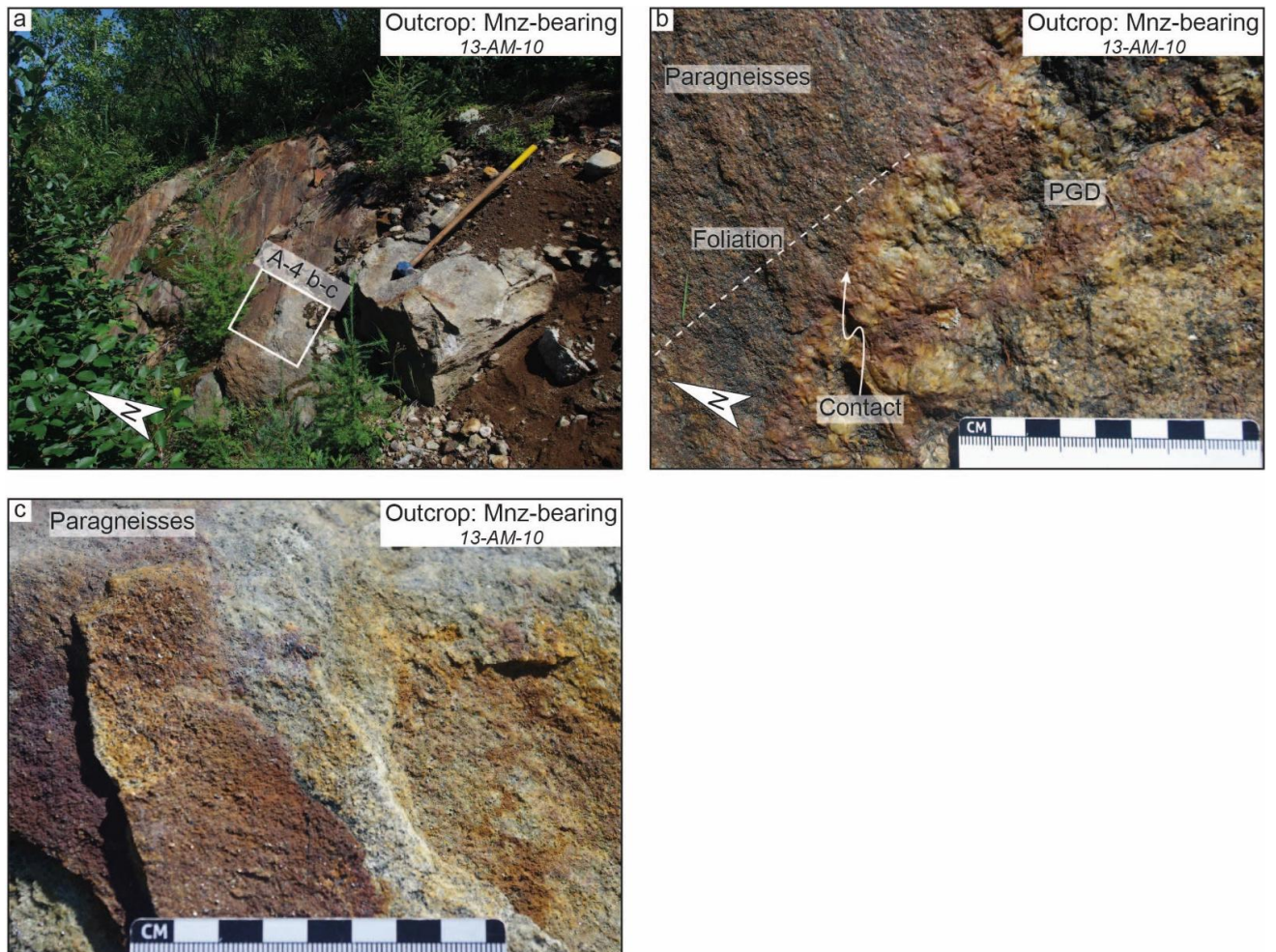
894 10. 13-AM-10 monazite-bearing PGD

895 The 13-AM-10 monazite-bearing PGD and REE occurrence is located at the south of
 896 the 13-AM-07 outcrop, in the north of the 22K/10 NTS sheet (Fig. 3), and is exposed as a
 897 steep-dipping outcrop along a gravel road (Fig. A-4a). The detailed map of this outcrop is
 898 available in Fig. A-3.



899 **Figure A-3:** Detailed map of the 13-AM-10 outcrop made of migmatitic paragneisses from the Plus-Value
 900 Complex intruded by a discordant REE-rich pegmatitic granite dyke. Abbreviation: PGD = pegmatitic granite
 901 dyke.
 902

903 The PGD is steep-dipping and discordant to the rusty Plus-Value Complex migmatitic
 904 paragneisses (Figs. A-4c, 5a). The contact between the dyke and the host paragneiss is straight
 905 but is slightly diffuse (over a few millimeters, Fig. A-4b) and the dyke do not display
 906 noticeable facies variations.



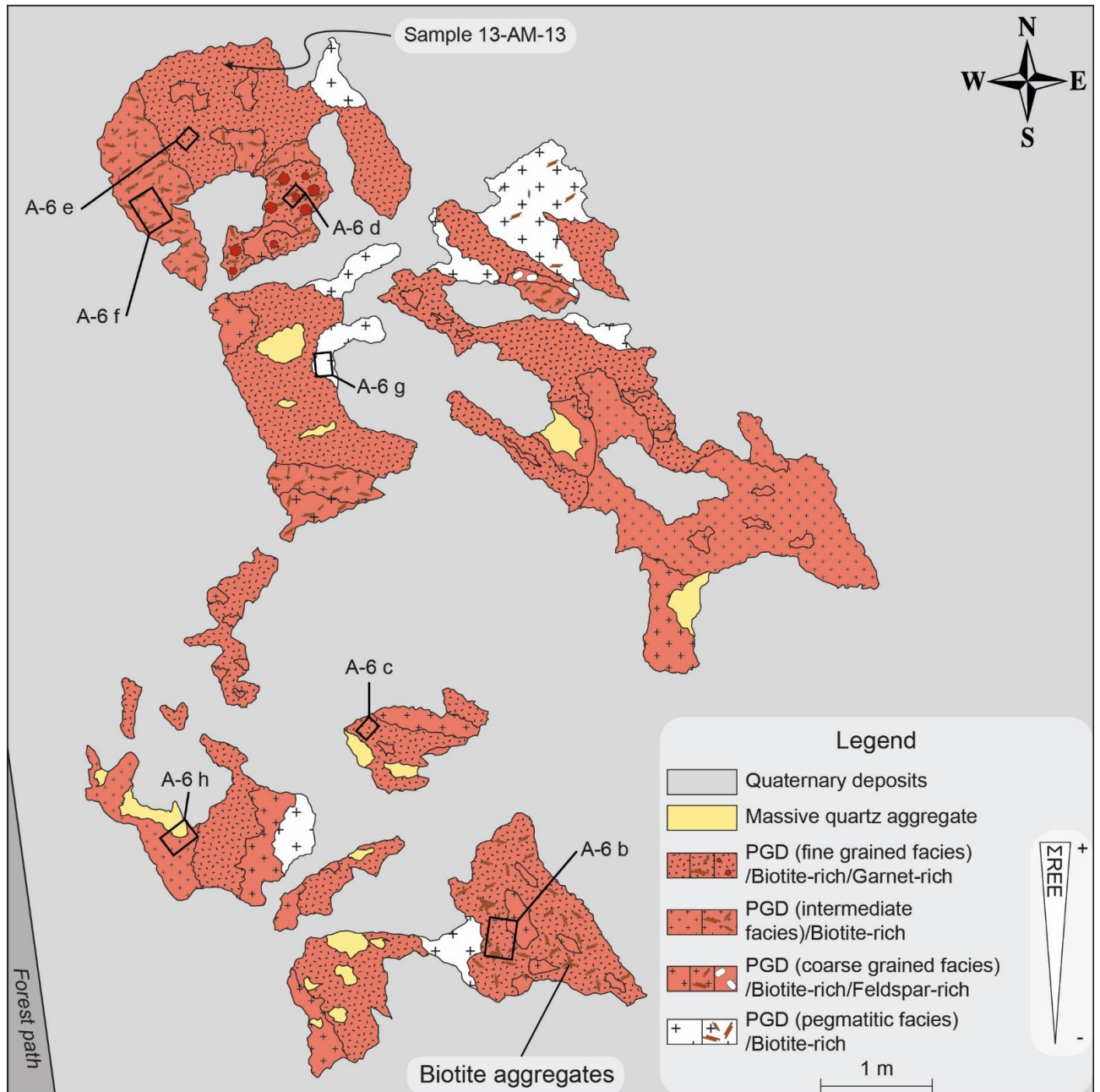
907
 908 **Figure A-4:** Photographs of the 13-AM-10 outcrop from the Lac Okaopéo region. a: general view of the 13-
 909 AM-10 outcrop composed of a pegmatitic granite dyke intruding paragneisses from the Plus-Value Complex.
 910 The hammer is ca. 1.2 m long; b: detailed view of the relationships between the dyke and the paragneisses.
 911 The foliation is not noticeable on this photograph but its general orientation is represented; c: detailed view
 912 of the intruded paragneisses. Abbreviation: Mnz-bearing = monazite-bearing pegmatitic granite dyke; PGD =
 913 pegmatitic granite dyke.

914

915 **11. 13-AM-13 monazite-bearing PGD**

916 The whitish 10 to 20 meters wide 13-AM-13 monazite-bearing PGD and REE
917 occurrence is located to the south of the 13-AM-10 outcrop, in the north of the 22K/10 NTS
918 sheet (Fig. 3), and is exposed as a large flat lying outcrop (Fig. A-6a). The Fig. A-5 proposes
919 the detailed mapping of this outcrop with localization of the samples and of the photographs
920 presented in Fig. A-6.

ACCEPTED MANUSCRIPT

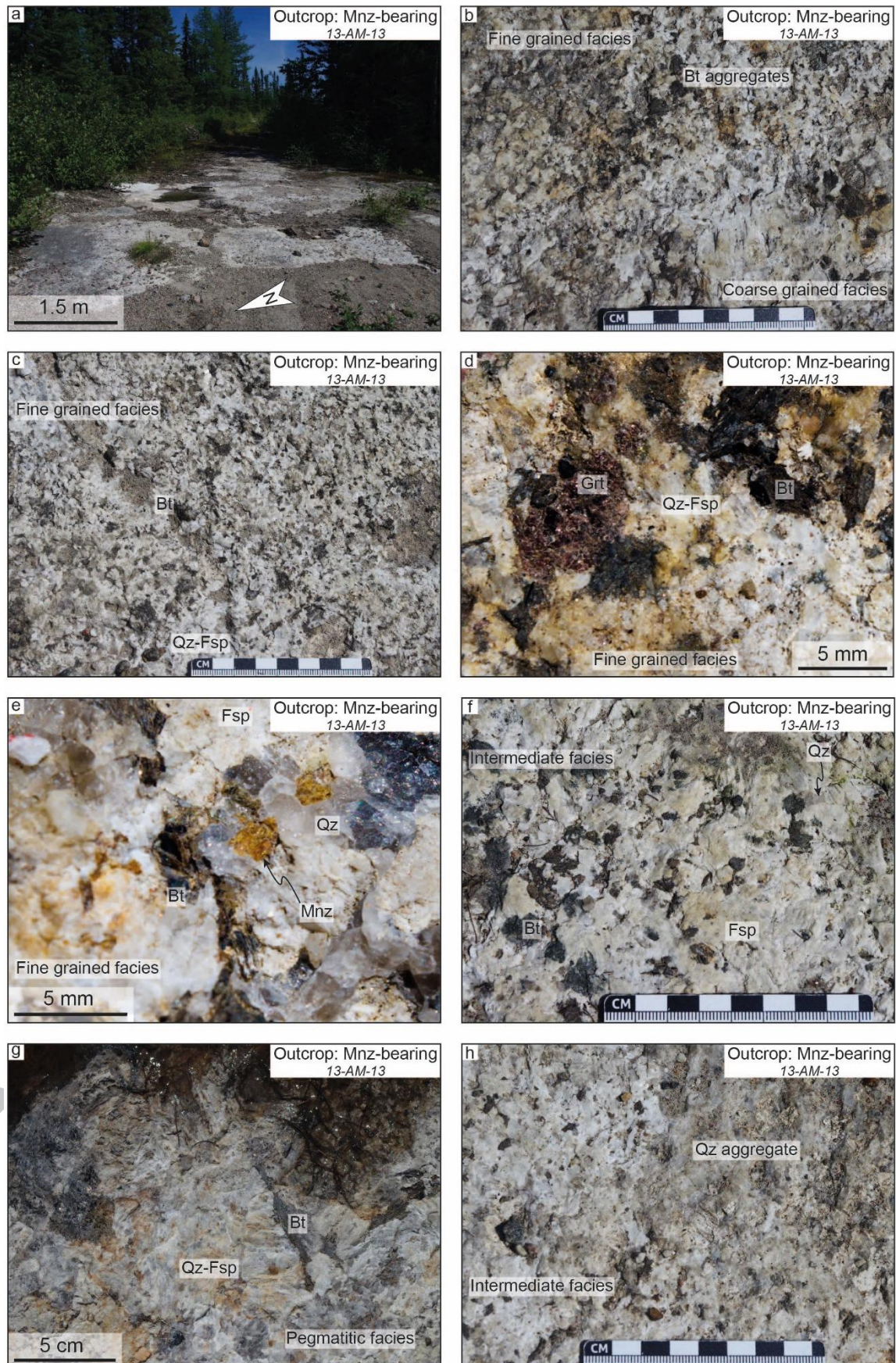


921

922 **Figure A-5:** Detailed map of the 13-AM-13 outcrop made of migmatitic paragneisses from the Plus-Value
 923 Complex intruded by a discordant REE-rich pegmatitic granite dyke. Abbreviation: PGD = pegmatitic granite
 924 dyke.

925 The PGD is steep-dipping and discordant to the foliation of the paragneisses from the
 926 Plus-Value Complex (Fig. 5a). The contact between the PGD and the host paragneisses is
 927 poorly exposed but the distribution of outcrops suggests that the contact is not straight over
 928 several meters.

929 The PGD is dominated by a fine-grained (1 mm to sometimes over 1 cm) quartz and
930 feldspar-rich facies with minor biotite and garnet (Figs. A-5 and 6b-d). This facies is the main
931 host for the mineralization expressed as sub-euhedral monazite grains (Fig. A-6e). The PGD
932 comprises randomly distributed tens of centimeters to 1 m large patchy zones characterized by
933 (i) an intermediate quartz and feldspar-rich±biotite facies (Figs. A-5, A-6f), (ii) a coarse-
934 grained quartz and feldspar-rich facies with more or less abundant biotite and phenocrysts of
935 feldspar (Fig. A-6b), and (iii) a pegmatitic quartz and feldspar-rich±biotite facies (some grains
936 over 5 cm, Fig. A-6g). Locally, up to ca. 20 cm centimeters wide quartz aggregates are also
937 noticeable but do not seem associated with any of the previous facies (Figs. A-5 and 6h). The
938 transition between two facies is mostly diffuse and difficult to delineate, but it may also be
939 underlined by biotite aggregates (Fig. A-6b).



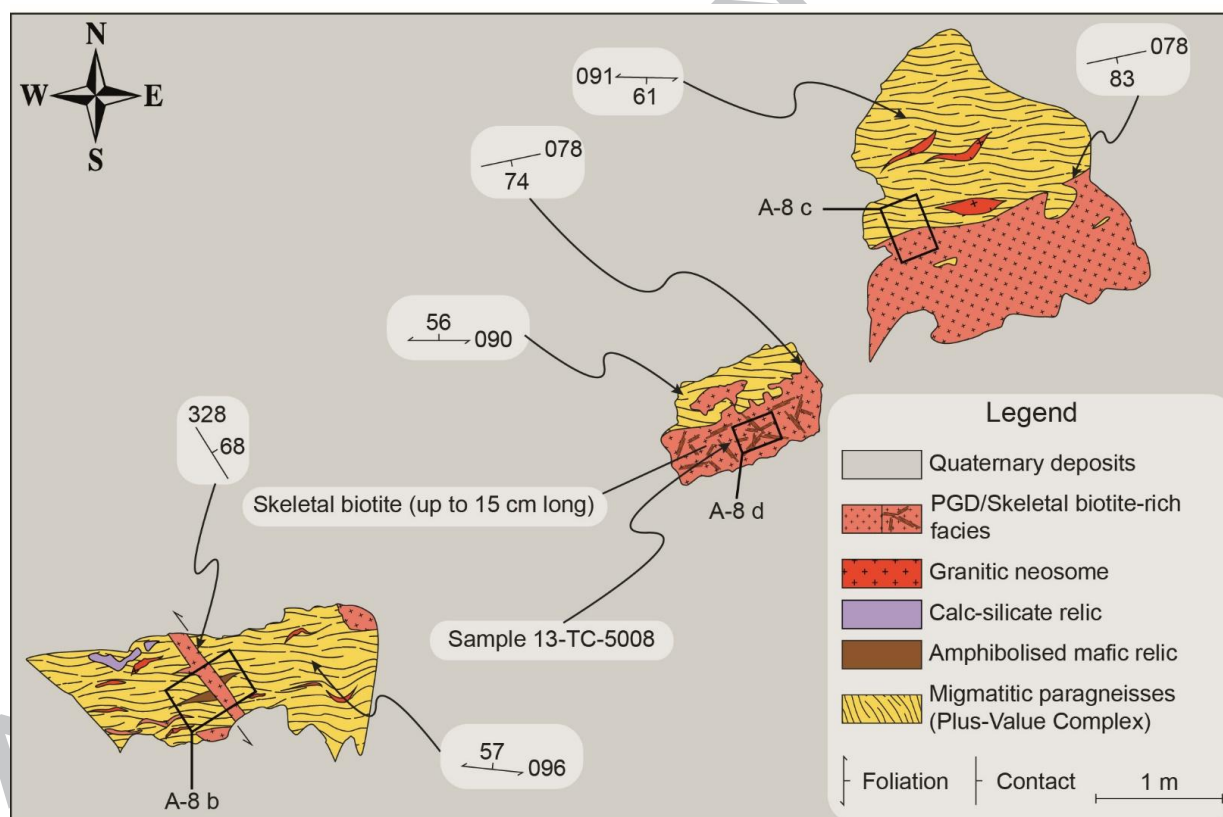
940
941
942
943

Figure A-6: Photographs of the 13-AM-13 outcrop from the Lac Okaopéo region. a: general view of the 13-AM-13 outcrop composed of a pegmatitic granite intruding paragneisses from the Plus-Value Complex; b: typical transition between the fine and coarse grained facies underlined by biotite aggregates. Note that the

944 abundance of biotite in the fine grained facies on this photograph is related to the vicinity of the coarse
 945 grained facies; c: typical fine grained facies dominated by a quartz+feldspar±biotite assemblage; d: detailed
 946 view of a garnet phenocryst in the fine grained facies; e: monazite crystals from the fine grained facies; f:
 947 typical intermediate facies composed of a quartz-feldspar-biotite assemblage; g: typical pegmatitic facies
 948 essentially composed of a quartz-feldspar-biotite assemblage in which feldspar and biotite crystals can reach
 949 over 5 cm; h: quartz aggregates in the intermediate facies. Abbreviations: Bt = biotite; Fsp = feldspar; Grt =
 950 garnet; Mnz = monazite; Mnz-bearing = monazite-bearing pegmatitic granite dyke; Qz = quartz.

951 12. 13-TC-5008 monazite-bearing PGD

952 The 13-TC-5008 monazite-bearing PGD and REE occurrence is located in the north of
 953 the 22K/07 NTS sheet (Fig. 3) and is exposed as a large flat lying outcrop (Fig. A-8a). The
 954 Fig. A-7 proposes the detailed mapping of this outcrop with localization of the samples and of
 955 the photographs presented in Fig. A-8.

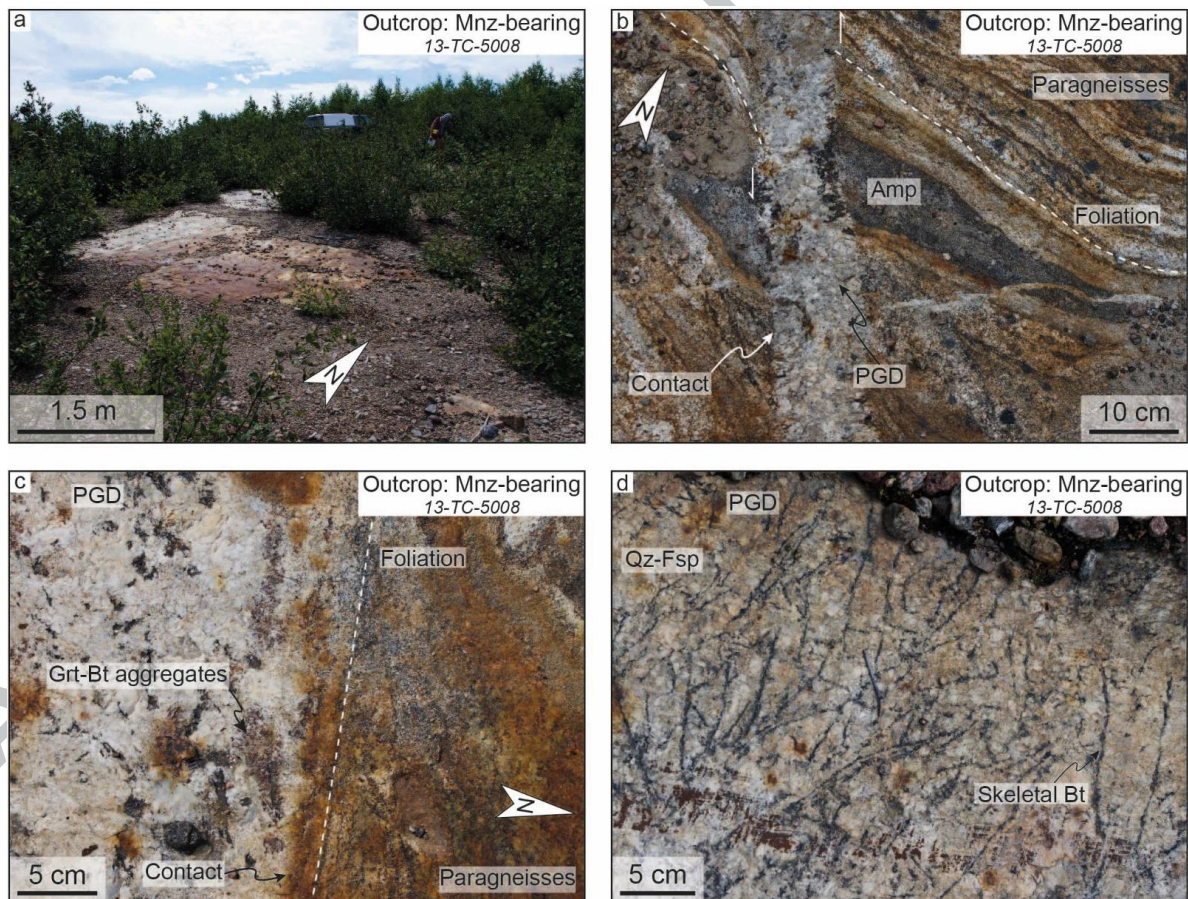


956
 957 **Figure A-7:** Detailed map of the 13-TC-5008 outcrop made of migmatitic paragneisses from the Plus-Value
 958 Complex intruded by a discordant REE-rich pegmatitic granite dyke. Abbreviation: PGD = pegmatitic granite
 959 dyke.

960 The 13-TC-5008 outcrop displays several showings of a few square meters large area
 961 (Figs. A-7, A-8a) made of large or thin (ca. 10 cm wide, Fig. A-8b) steep-dipping PGD
 962 discordant to the foliation of the migmatitic paragneisses of the Plus-Value Complex (Figs. A-

963 8b, 5a). The contact is locally diffuse (over a few millimeters) and is either straight or wavy
 964 (Figs. A-8b-c). It seems to represent a zone of reactions between the granitic melt and the
 965 intruded metasediments as it may be underlined in the PGD by garnet-biotite aggregates (Fig.
 966 A-8c).

967 The few square meters PGD showings and the thin whitish PG dyke do not display
 968 any zoning from the contact to their core. However, some patchy zoning made of facies
 969 enriched in skeletal biotite (cluster as arborescent arrangements of up to 15 cm biotite
 970 crystals, Fig. A-8d) are noticeable and are about a few tens of centimeters wide. The transition
 971 between these patches and the dominant facies is diffuse.



972 **Figure A-8:** Photographs of the 13-TC-5008 outcrop from the Lac Okaopéo region. a: general view of the 13-
 973 TC-5008 outcrop composed of a pegmatitic granite intruding paragneisses from the Plus-Value Complex; b:
 974 intrusion of a pegmatitic granitic dyke favored by a sinistral shearing that affect both the migmatitic
 975 paragneisses from the Plus-Value Complex and the amphibolized mafic relic it contains. The resulting contact
 976 is discordant as evidenced by the crosscut foliation of the intruded paragneisses by the dyke; c: locally diffuse
 977 contact between the dyke and the intruded paragneisses delineated by garnet-biotite aggregates; d:
 978 arborescent textures made by skeletal crystals reaching up to 15 cm long. Abbreviations: Amp = amphibolized
 979

983 **Appendix B: Detailed mapping of the allanite-bearing pegmatitic granite**
984 **outcrops**

985 **13. 13-TC-5072 allanite-bearing pegmatitic granite dyke (PGD)**

986 The 13-TC-5072 allanite-bearing pegmatitic granite dyke (PGD) and REE occurrence
987 is located in the south of the 22K/10 NTS sheet (Fig. 3) and is exposed as a large and dome
988 shaped outcrop (Fig. B-2a). The detailed map of this outcrop is available in the Fig. B-1. It
989 consists in numerous straight pinkish (fresh color) PGD (up to 4 m wide, Figs. B-1 and B-2b-
990 f) intruding a metamonzogranite from the Bardoux Plutonic Suite.

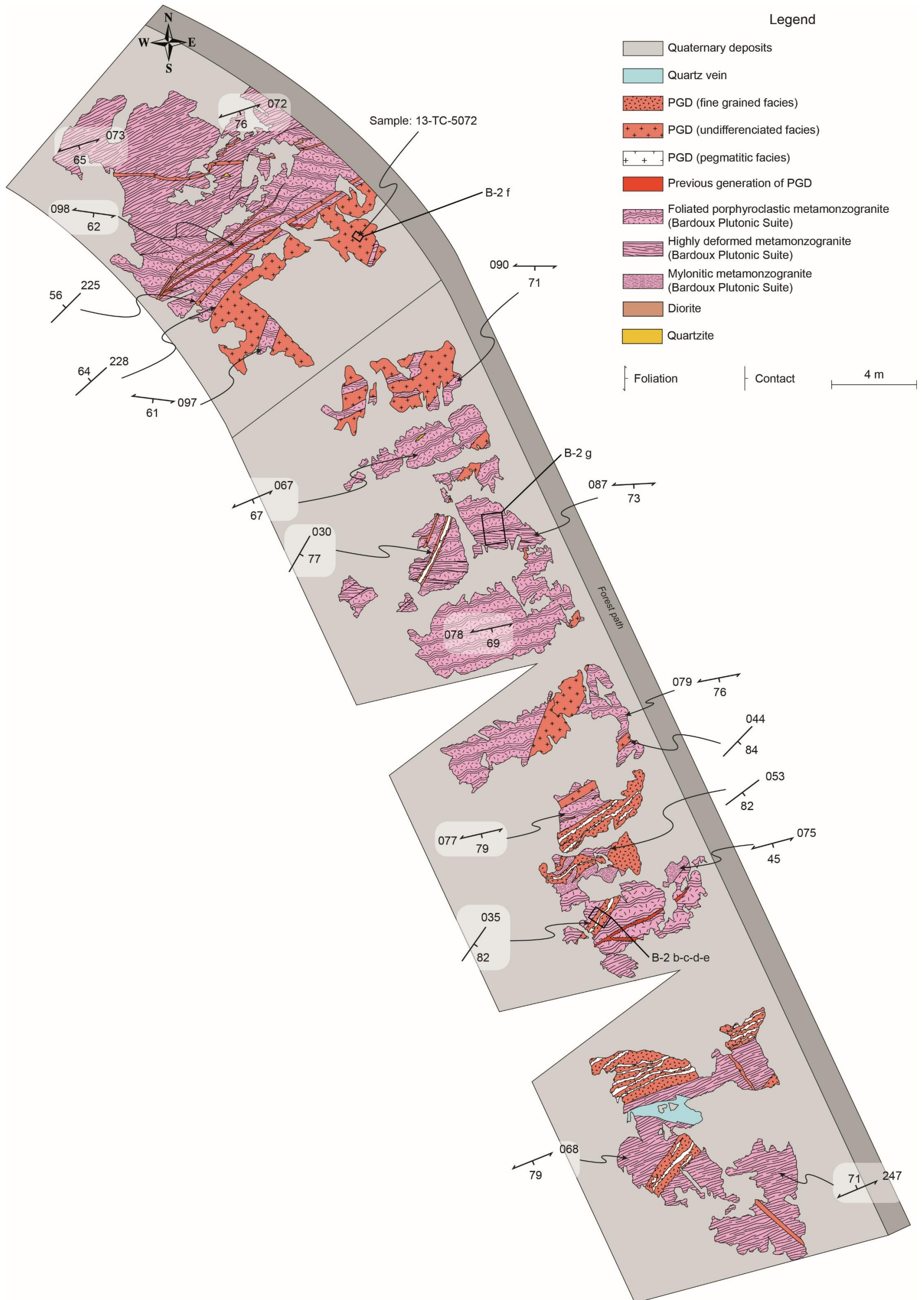


Figure B-1: Detailed map of the 13-TC-5072 outcrop made of a metamonzogranite from the Bardoux Plutonic Suite intruded by discordant REE-rich pegmatitic granite dykes. Abbreviation: PGD = pegmatitic granite dyke.

The dykes are steep-dipping and mostly discordant to the fabric of the host metamonzogranite but are locally sub-concordant (Figs. B-2b-c and e, 5b). Several of these dykes may present internal zoning which typically consists in (i) a thin contact (few millimeter to a centimeter wide, zone 1, Figs. B-2b-c), followed by (ii) a ca. 20 to 30 cm wide fine grained facies (ca. < 1 mm and 2 mm, zone 2, Figs. B-2b-c), and (iii) by a coarser grain size zone (ca. 1 to 5 mm, zone 3, Figs. B-2b and d). The (iv) core of the dykes (zone 4, Figs. B-2b and d) may vary from a few centimeters to tens of centimeters wide and displays a pegmatitic texture. It is followed by (v) another fine grained facies (zone 5, Figs. B-2b, B-2d-e), which transition is quite diffuse from the later one, that ends at the boundary of the dyke by (vi) the growth of K-feldspar phenocrysts perpendicular to the contact (zone 6, Figs. B-2b and e). The whole contact is not marked by these phenocrysts that also developed in the fine grained facies with no relations with the dyke boundary (Fig. B-2e), suggesting that it does not correspond to Stockscheider textures. This kind of internal zoning in the dykes of this outcrop is quite representative as most of them display either this sequence or its repetition, probably related to several magmatic pulses. A few intrusive bodies, mostly wider than the dykes, do not display any evident zoning. Allanite grains (Fig. B-2f) are present in both zoned and unzoned intrusive bodies, and seems mostly associated with fine to medium grained facies.

The intruded metamonzogranite from the Bardoux Plutonic Suite displays various textures related to the degree of deformation it underwent, from a foliated facies with rounded rapakivi K-feldspar porphyroclasts to a mylonitic texture with elongated K-feldspar porphyroclasts (Fig. B-2g).

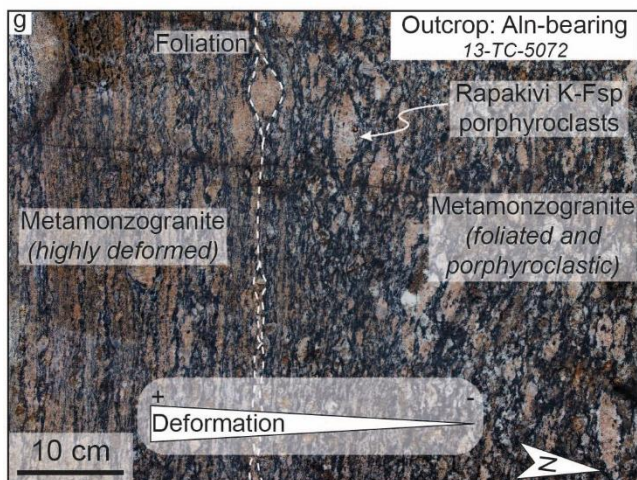
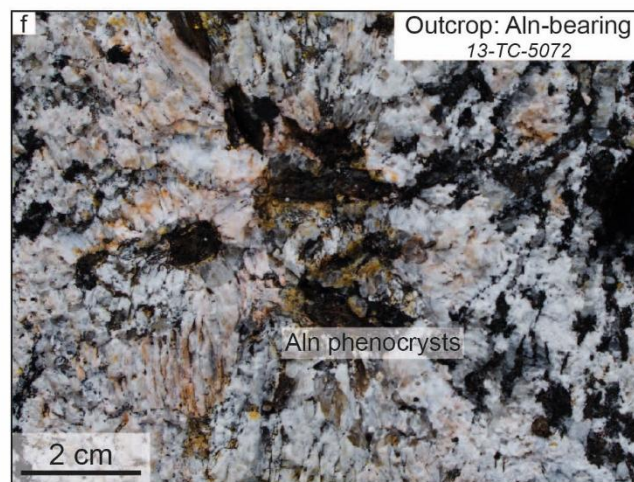
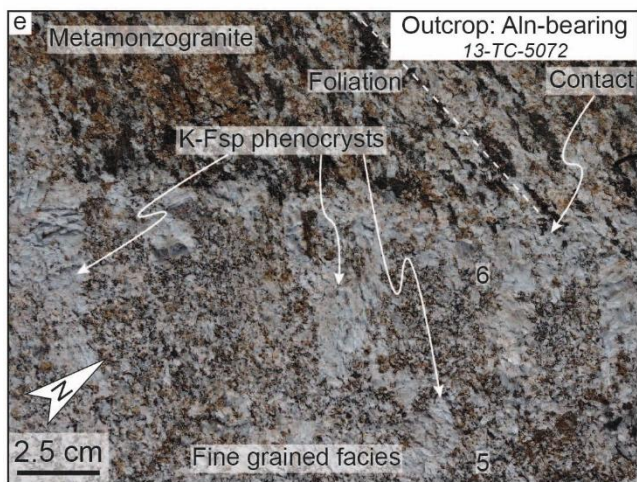
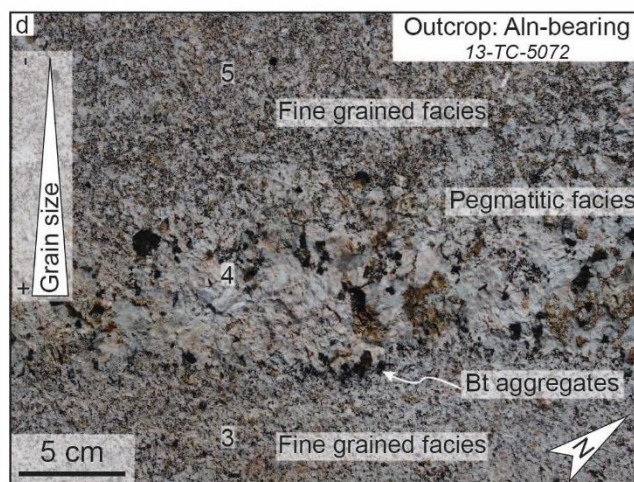
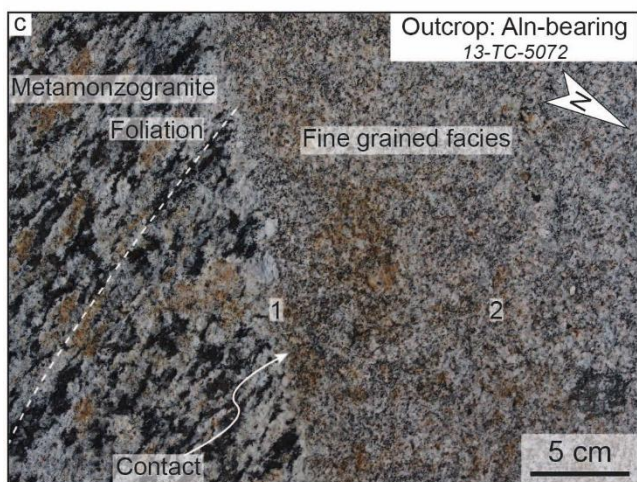
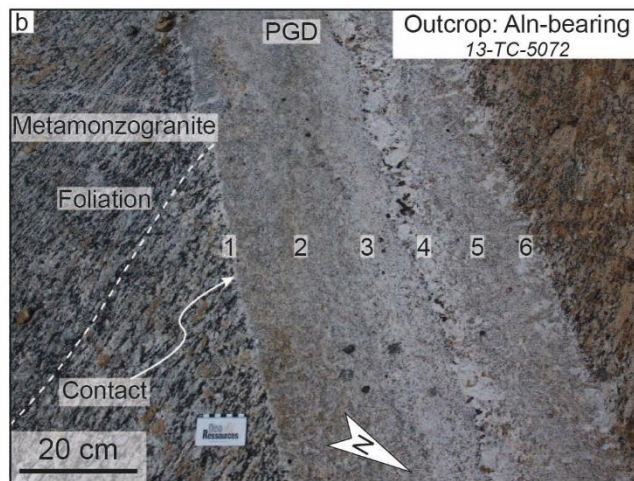


Figure B-2: Photographs of the 13-TC-5072 outcrop from the Lac Okaopéo region. a: general view of the 13-TC-5072 outcrop composed of a pegmatitic granite intruding as a dyke swarm a metamonzogranite from the Bardoux Plutonic Suite; b: typical dyke zonation of the 13-TC-5072 pegmatitic dykes, with a southeastern boundary (1) marked by a thin zone of reaction with the host rock developed over a few millimeters with almost no biotite, followed by a fine grained facies with increasing grain size and proportions of biotite (2, 3) up to a pegmatitic core (4). This core is followed by a progressive fine grained facies with decreasing grain size zone (5). The northern contact (6) is marked by the development of K-feldspar phenocrysts perpendicular to the contact. Note that the dyke is discordant to the foliation of the intruded metamonzogranite; c: detailed view of the southern contact presented in figure b. Numbers refer to the zones identified in figure b; d: detailed view of the pegmatitic core of the dyke presented in figure b. Note the pegmatitic facies is underlined on its southern boundary by biotite aggregates whereas the northern one is opened to a fine grained facies which transition is undulating along the core. Numbers refer to the zones identified in figure b; e: detailed view of the northern contact presented in figure b. Note the diffuse boundary and the crystallization of K-feldspar phenocrysts perpendicular to the contact. Numbers refer to the zones identified in figure b; f: typical allanite phenocrysts in pegmatitic granite dykes intruding the metamonzogranite; g: typical metamonzogranite facies variations from a foliated and porphyroclastic facies where porphyroclasts of rapakivi K-feldspar are wrapped by the foliation (north) to transposed in a highly deformed facies (south). Abbreviations: Aln = allanite; Aln-bearing = allanite-bearing pegmatitic granite dyke; Bt = biotite; K-Fsp = K-feldspar; PGD = pegmatitic granite dyke.

14. 13-FS-1202 allanite-bearing PGD

The 13-FS-1202 allanite-bearing PGD and REE occurrence is located at the south of the 13-TC-5072 PGD, in the south of the 22K/10 NTS sheet (Fig. 3), and is exposed as a large (several tens square meters in surface) and flat lying outcrop (Fig. B-4a). The detailed map of this outcrop is available in the Fig. B-3. It consists in numerous straight pinkish (fresh color) PGD (2-5 m wide, Figs. B-3 and B-4b) intruding a quartz metamonzodiorite from the Castoréum Plutonic Suite.

ACCEPTED MANUSCRIPT

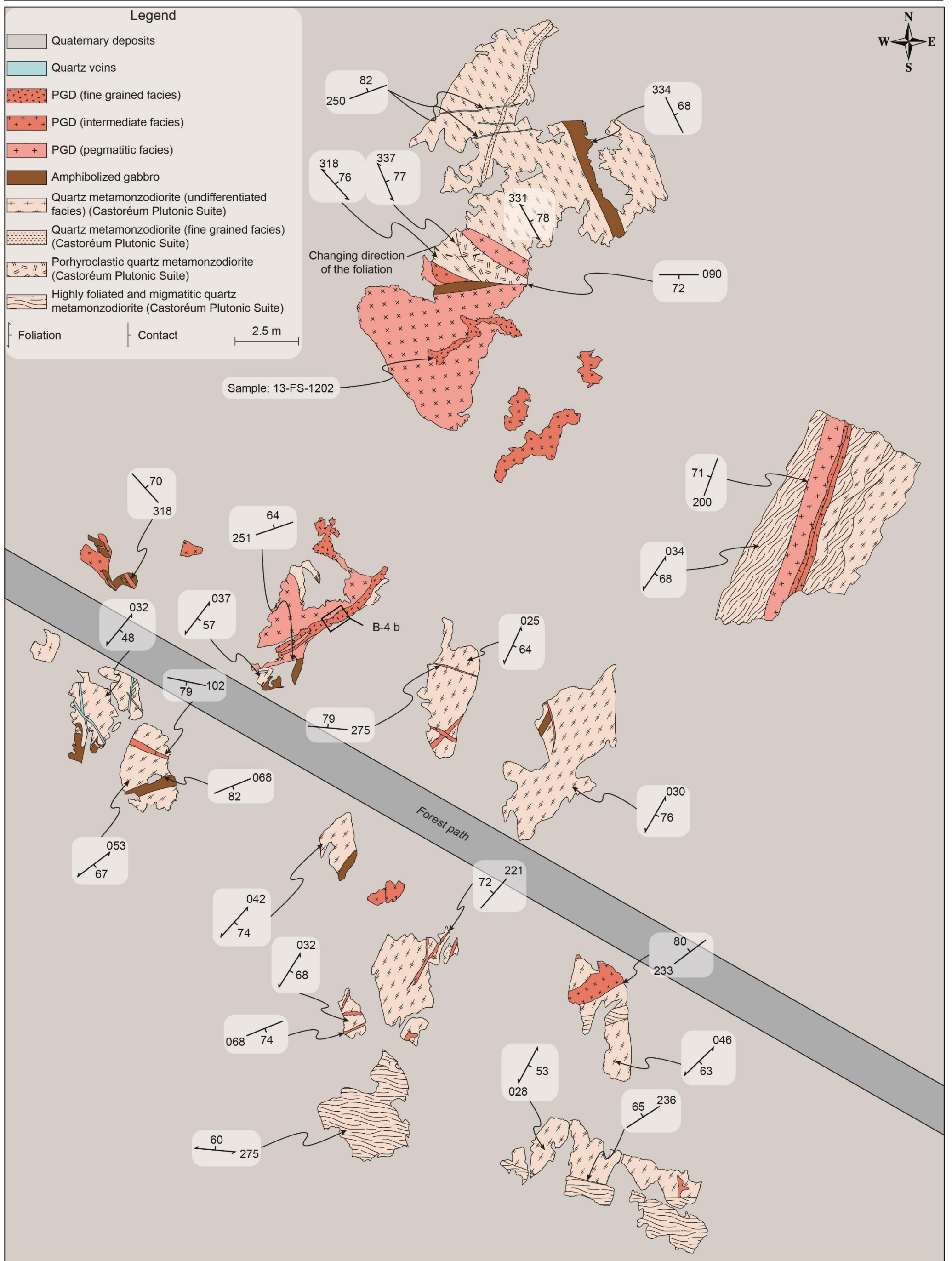
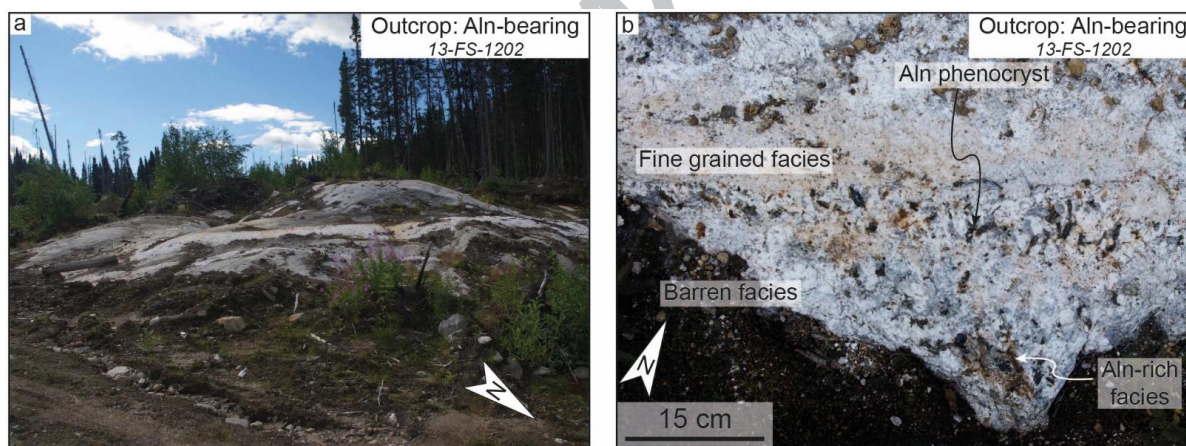


Figure B-3: Detailed map of the 13-FS-1202 outcrop made of a quartz metazonzodiorite from the Castoréum Plutonic Suite intruded by discordant REE-rich pegmatitic granite dykes.

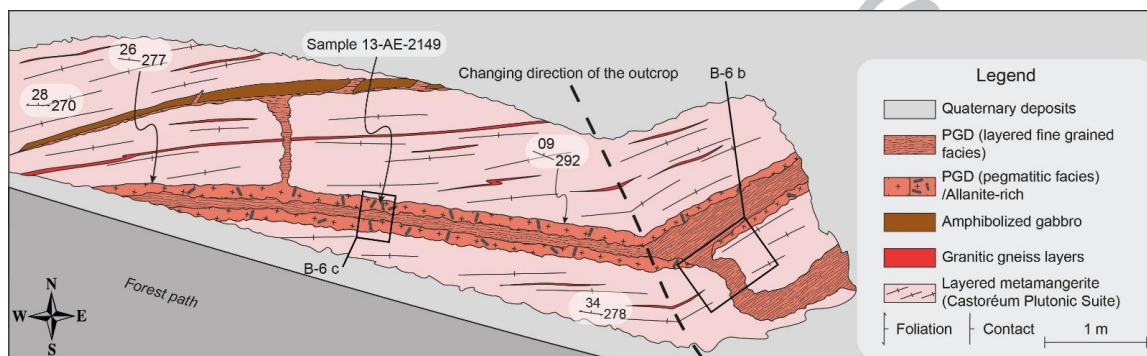
1 The dykes are steep-dipping and slightly to strongly discordant to the fabric of the host
 2 quartz metamazonzodiorite (Fig. 5b). The contacts of the PGD with their hosts are straight or
 3 irregular, and are slightly diffuse (over a few millimeters). This dyke is mainly composed of
 4 quartz, feldspar and biotite and contains large allanite phenocrysts (>1 cm, Fig. B-4b). The
 5 most mineralized zone, i.e. containing the most allanite grains that may reach over 1 cm,
 6 corresponds to an intermediate facies which is layered with a pegmatitic (over 3 cm) barren
 7 facies at the contact and a finer-grained (0.1-3 cm) allanite-rich facies in the center (Fig. B-
 8 4b). The rest of the PGD does not display any sign of organization with random patches
 9 ranging from a medium grained allanite-rich facies to a coarse grained barren facies. Coarse
 10 grained to pegmatitic facies may locally present allanite aggregates.



11
 12 **Figure B-4:** Photographs of the 13-FS-1202 outcrop from the Lac Okaopéo region. a: general view of the 13-FS-
 13 1202 outcrop composed of a pegmatitic granite intruding as a dyke swarm a quartz metamazonzodiorite from
 14 the Castoréum Plutonic Suite; b: detailed view of the typical zoning observed in the pegmatitic granite. Note
 15 that the allanite phenocrysts are associated with an intermediate size grained facies. Abbreviations: Aln =
 16 allanite; Aln-bearing = allanite-bearing pegmatitic granite dyke; Qz = quartz.

17 **15. 13-AE-2149 allanite-bearing PGD**

18 The 13-AE-2149 allanite-bearing PGD and REE occurrence is located in the north of
19 the 22K/07 NTS sheet (Fig. 3) and is exposed as a large and steep-dipping outcrop. The
20 detailed map of this outcrop is available in the Fig. B-5. It consists in a main straight pinkish
21 PGD (up to ca. 1 m wide, Figs. B-5 and B-6a) intruding a layered metamangerite from the
22 Castoréum Plutonic Suite.



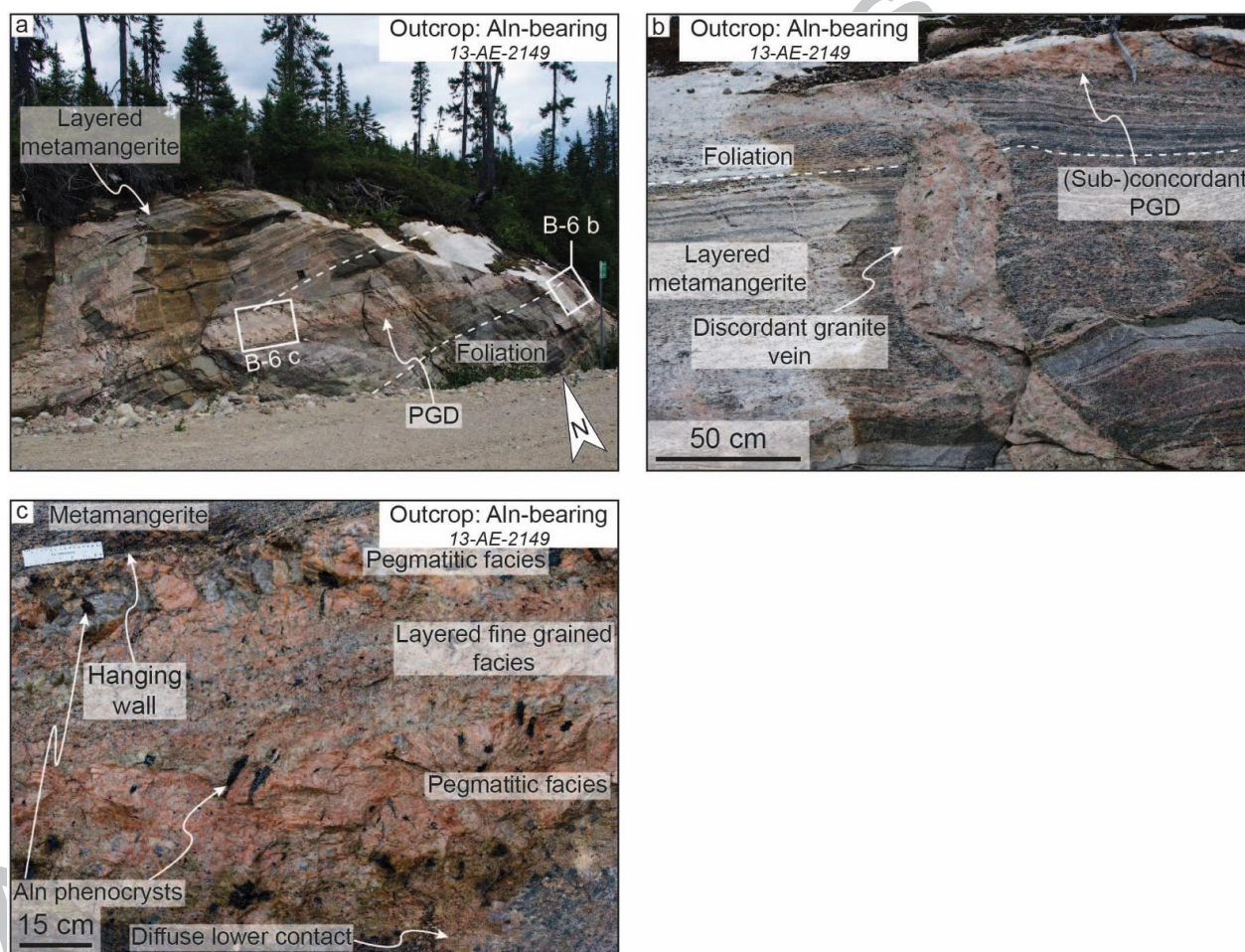
23
24 **Figure B-5:** Detailed map of the 13-AE-2149 outcrop made of a layered metamangerite from the Castoréum
25 Plutonic Suite intruded by a discordant REE-rich pegmatitic granite dyke. Abbreviation: PGD = pegmatitic
26 granite dyke.

27 This PGD is connected to a network of texturally continuous veins concordant and
28 discordant to the foliation of the host layered metamangerite from the Castoréum Plutonic
29 Suite (Fig. B-6b). The main dyke is shallow-dipping (Fig. 5b) and the contact between the
30 PGD and the metamangerite is slightly discordant to locally sub-concordant and may be very
31 diffuse (Figs. B-6c, 5b).

32 The upper contact of the dyke is marked by a ca. 20 cm wide pegmatitic facies with a
33 grain size over 10 cm. A few large allanite phenocrysts are disseminated across this contact,
34 and may reach over 10 cm (Fig. B-6c). The core of the dyke is composed of a layered fine
35 grained facies composed of alternating (i) quartz-K-feldspar-rich lenses, and (ii) quartz-
36 plagioclase-rich lenses that are generally not longer than 30 cm (Fig. B-6c). The lower contact
37 of the dyke is similarly marked by a pegmatitic facies up to ca. 45 cm in width (Fig. B-6c).

38 Allanite phenocrysts are up to ca. 10 cm, with a long axis mainly perpendicular to the walls of
 39 the dyke. The lower contact of the dyke with the layered metamangerite is more diffuse than
 40 at the upper contact and might reflect melt/crystal segregation (Fig. B-6c).

41 A few meters away from the contacts with granitic veins, the host layered
 42 metamangerite displays a homogeneous texture and structure while close to the contacts, the
 43 metamangerite grades into a migmatitic gneiss dominated by K-feldspar and clinopyroxene.



44
 45 **Figure B-6:** Photographs of the 13-AE-2149 outcrop from the Lac Okaopéo region. a: general view of the 13-
 46 AE-2149 outcrop composed of a pegmatitic granite dyke intruding a layered metamangerite from the
 47 Castoréum Plutonic Suite; b: detailed view of one of the pegmatitic granite vein discordant to the foliation of
 48 its host rock and its connection with the main pegmatitic granite dyke expressed on this outcrop, here with a
 49 sub-concordant contact with the layered metamangerite; c: detailed view of the whole dyke zonation from
 50 its upper to its lower contact, both marked by a pegmatitic facies with large allanite phenocrysts, through a
 51 layered fine grained facies. Abbreviation: Aln = allanite; Aln-bearing = allanite-bearing pegmatitic granite
 52 dyke; PGD = pegmatitic granite dyke.

53

54 **References**

- 55 Alfonso, P., Melgarejo, J.C., 2008. Fluid Evolution in the Zoned Rare-Element Pegmatite
56 Field at Cap De Creus, Catalonia, Spain. *Can. Mineral.* 46, 597–617.
57 doi:10.3749/canmin.46.3.597
- 58 Augland, L.E., Moukhsil, A., Solgadi, F., Indares, A., McFarlane, C., 2015. Pinwarian to
59 Grenvillian magmatic evolution in the central Grenville Province: new constraints
60 from ID-TIMS U-Pb ages and coupled Lu-Hf S-MC-ICP-MS data. *Can. J. Earth Sci.*
61 52, 701–721. doi:10.1139/cjes-2014-0232
- 62 Ayres, L.D., Černý, P., 1982. Metallogeny of granitoid rocks in the Canadian Shield. *Can.*
63 *Mineral.* 20, 439–536.
- 64 Ballouard, C., Boulvais, P., Poujol, M., Gapais, D., Yamato, P., Tartèse, R., Cuney, M., 2015.
65 Tectonic record, magmatic history and hydrothermal alteration in the Hercynian
66 Guérande leucogranite, Armorican Massif, France. *Lithos* 220–223, 1–22.
67 doi:10.1016/j.lithos.2015.01.027
- 68 Bea, F., 1996. Residence of REE, Y, Th and U in Granites and Crustal Protoliths;
69 Implications for the Chemistry of Crustal Melts. *J. Petrol.* 37, 521–552.
70 doi:10.1093/petrology/37.3.521
- 71 Berger, A., Rosenberg, C., Schaltegger, U., 2009. Stability and isotopic dating of monazite
72 and allanite in partially molten rocks: examples from the Central Alps. *Swiss J.*
73 *Geosci.* 102, 15–29. doi:10.1007/s00015-009-1310-8
- 74 Bergeron, A., 1980. Petrographie et géochimie du complexe igne alcalin de crevier et de son
75 encaissant metasomatise (Unpublished MSc thesis). Université du Québec à
76 Chicoutimi, Chicoutimi.

- 77 Budzyń, B., Harlov, D.E., Williams, M.L., Jercinovic, M.J., 2011. Experimental
78 determination of stability relations between monazite, fluorapatite, allanite, and REE-
79 epidote as a function of pressure, temperature, and fluid composition. *Am. Mineral.*
80 96, 1547–1567. doi:10.2138/am.2011.3741
- 81 Carr, S.D., Easton, R.M., Jamieson, R.A., Culshaw, N.G., 2000. Geologic transect across the
82 Grenville orogen of Ontario and New York. *Can. J. Earth Sci.* 37, 193–216.
83 doi:10.1139/e99-074
- 84 Černý, P., 1991. Rare-element Granitic Pegmatites. Part I: Anatomy and Internal Evolution of
85 Pegmatitic Deposits. *Geosci. Can.* 18, 49–67.
- 86 Černý, P., 1990. Distribution, affiliation and derivation of rare-element granitic pegmatites in
87 the Canadian Shield. *Geol. Rundsch.* 79, 183–226. doi:10.1007/BF01830621
- 88 Černý, P., Ercit, T.S., 2005. The classification of granitic pegmatites revisited. *Can. Mineral.*
89 43, Part 6, 2005–2026.
- 90 Černý, P., London, D., Novák, M., 2012. Granitic Pegmatites as Reflections of Their Sources.
91 *Elements* 8, 289–294. doi:10.2113/gselements.8.4.289
- 92 Chappell, B.W., White, A.J.R., 2001. Two contrasting granite types: 25 years later. *Aust. J.*
93 *Earth Sci.* 48.
- 94 Crowley, J.L., Brown, R.L., Gervais, F., Gibson, H.D., 2008. Assessing Inheritance of Zircon
95 and Monazite in Granitic Rocks from the Monashee Complex, Canadian Cordillera. *J.*
96 *Petrol.* 49, 1915–1929. doi:10.1093/petrology/egn047
- 97 Cuney, M., 2014. Felsic magmatism and uranium deposits. *B. Soc. Geol. Fr.* 185, 75–92.
98 doi:10.2113/gssgfbull.185.2.75

- 99 David, J., 2006. Géochronologie d'échantillons provenant de Géologie Québec, année 2005-
100 2006 - Rapport final. Ministère de l'Énergie et des Ressources Naturelles, Québec GM
101 63236, 12 p.
- 102 David, J., Moukhsil, A., Clark, T., Hébert, C., Nantel, S., Dion, C., Sappin, A.-A., 2009.
103 Datations U-Pb effectuées dans les provinces de Grenville et de Churchill en 2006-
104 2007. Ministère des Ressources naturelles et de la Faune, Québec, RP2009-03, 32 p.
- 105 Dill, H.G., 2016. The CMS classification scheme (Chemical composition-Mineral
106 assemblage-Structural geology) - linking geology to mineralogy of pegmatitic and
107 aplitic rocks. *N. Jb. Miner. Abh. (J. Min. Geochem.)* 193, 231–263.
- 108 Dill, H.G., 2015. Pegmatites and aplites: Their genetic and applied ore geology. *Ore Geol.*
109 *Rev.* 69, 417–561. doi:10.1016/j.oregeorev.2015.02.022
- 110 Dill, H.G., 2010. The “chessboard” classification scheme of mineral deposits: Mineralogy and
111 geology from aluminum to zirconium. *Earth Sci. Rev.* 100, 1–420.
112 doi:10.1016/j.earscirev.2009.10.011
- 113 Druguet, E., Castro, A., Chichorro, M., Pereira, M.F., Fernández, C., 2014. Zircon
114 geochronology of intrusive rocks from Cap de Creus, Eastern Pyrenees. *Geol. Mag.*
115 151, 1095–1114. doi:10.1017/S0016756814000041
- 116 Dunning, G., Indares, A., 2010. New insights on the 1.7–1.0 Ga crustal evolution of the
117 central Grenville Province from the Manicouagan – Baie Comeau transect.
118 *Precambrian Res.* 180, 204–226. doi:10.1016/j.precamres.2010.04.005
- 119 Ellison, A.J., Hess, P.C., 1986. Solution behavior of +4 cations in high silica melts: petrologic
120 and geochemical implications. *Contr. Mineral. Petrol.* 94, 343–351.
121 doi:10.1007/BF00371443

- 122 Ercit, T.S., 2005. REE-enriched granitic pegmatites. Short Course Notes - Geological
123 Association of Canada 17, 175–199.
- 124 Ford, K.L., 1982. Uraniferous pegmatites of the Sharbot Lake area, Ontario, Uranium in
125 Granites. Geological Survey Canada, Paper 81-23.
- 126 Fowler, A.D., Doig, R., 1983. The significance of europium anomalies in the REE spectra of
127 granites and pegmatites, Mont Laurier, Quebec. *Geochim. Cosmochim. Ac.* 47, 1131–
128 1137. doi:10.1016/0016-7037(83)90243-0
- 129 Frost, B.R., Barnes, C.G., Collins, W.J., Arculus, R.J., Ellis, D.J., Frost, C.D., 2001. A
130 geochemical classification for granitic rocks. *J. Petrol.* 42, 2033–2048.
- 131 Gasquet, D., Bertrand, J.-M., Paquette, J.-L., Lehmann, J., Ratzov, G., Guedes, R.D.A.,
132 Tiepolo, M., Boullier, A.-M., Scaillet, S., Nomade, S., 2010. Miocene to Messinian
133 deformation and hydrothermal activity in a pre-Alpine basement massif of the French
134 western Alps: new U-Th-Pb and argon ages from the Lauzière massif. *B. Soc. Geol.*
135 *Fr.* 181, 227–241. doi:10.2113/gssgfbull.181.3.227
- 136 Gauthier, M., Chartrand, F., 2005. Metallogeny of the Grenville Province revisited. *Can. J.*
137 *Earth Sci.* 42, 1719–1734. doi:10.1139/E05-051
- 138 Gauthier, M., Chartrand, F., Cayer, A., David, J., 2004. The Kwyjibo Cu-REE-U-Au-Mo-F
139 Property, Quebec: A Mesoproterozoic Polymetallic Iron Oxide Deposit in the
140 Northeastern Grenville Province. *Econ. Geol.* 99, 1177–1196.
141 doi:10.2113/gsecongeo.99.6.1177
- 142 Gervais, F., Crowley, J.L., 2017. Prograde and near-peak zircon growth in a migmatitic pelitic
143 schist of the southeastern Canadian Cordillera. *Lithos* 282–283, 65–81.
144 doi:10.1016/j.lithos.2017.02.016

- 145 Gobeil, A., Hébert, C., Clark, T., Beaumier, M., Perreault, S., 2002. Géologie de la région du
146 lac De la Blache (22K/03 et 22K/04). Ministère des Ressources Naturelles, Québec,
147 RG 2002-01, 53 p.
- 148 Goodenough, K.M., Schilling, J., Jonsson, E., Kalvig, P., Charles, N., Tuduri, J., Deady, E.A.,
149 Sadeghi, M., Schiellerup, H., Müller, A., Bertrand, G., Arvanitidis, N., Eliopoulos,
150 D.G., Shaw, R.A., Thrane, K., Keulen, N., 2016. Europe's rare earth element resource
151 potential: An overview of REE metallogenetic provinces and their geodynamic setting.
152 *Ore Geol. Rev.* 72, Part 1, 838–856. doi:10.1016/j.oregeorev.2015.09.019
- 153 Gower, C.F., Krogh, T.E., 2002. A U–Pb geochronological review of the Proterozoic history
154 of the eastern Grenville Province. *Can. J. Earth Sci.* 39, 795–829. doi: 10.1139/E01-
155 090
- 156 Groulier, P.-A., 2013. Étude des minéralisations en Nb-Ta du complexe igné alcalin de
157 Crevier (Québec) (Rapport de Master), Université de Lorraine, 77 p.
- 158 Hanchar, J.M., Finch, R.J., Hoskin, P.W.O., Watson, E.B., Cherniak, D.J., Mariano, A.N.,
159 2001. Rare earth elements in synthetic zircon: Part 1. Synthesis, and rare earth element
160 and phosphorus doping. *Am. Mineral.* 86, 667–680. doi:10.2138/am-2001-5-607
- 161 Hoffman, P.F., 1989. Precambrian geology and tectonic history of North America The
162 geology of North America. *Geol. Soc. Am. : Boulder, CO, United States, United*
163 *States*, pp. 447–512.
- 164 Hönig, S., Čopjaková, R., Škoda, R., Novák, M., Dolejš, D., Leichmann, J., Galiová, M.V.,
165 2014. Garnet as a major carrier of the Y and REE in the granitic rocks: An example
166 from the layered anorogenic granite in the Brno Batholith, Czech Republic. *Am.*
167 *Mineral.* 99, 1922–1941. doi:10.2138/am-2014-4728

- 168 Hulsbosch, N., Hertogen, J., Dewaele, S., André, L., Muchez, P., 2014. Alkali metal and rare
169 earth element evolution of rock-forming minerals from the Gatumba area pegmatites
170 (Rwanda): Quantitative assessment of crystal-melt fractionation in the regional
171 zonation of pegmatite groups. *Geochim. Cosmochim. Ac.* 132, 349–374.
172 doi:10.1016/j.gca.2014.02.006
- 173 Hynes, A., Indares, A., Rivers, T., Gobeil, A., 2000. Lithoprobe line 55: integration of out-of-
174 plane seismic results with surface structure, metamorphism, and geochronology, and
175 the tectonic evolution of the eastern Grenville Province. *Can. J. Earth Sci.* 37, 341–
176 358. doi:10.1139/e99-076
- 177 Indares, A., Dunning, G., 2004. Crustal architecture above the high-pressure belt of the
178 Grenville Province in the Manicouagan area: new structural, petrologic and U–Pb age
179 constraints. *Precambrian Res.* 130, 199–228. doi:10.1016/j.precamres.2003.11.005
- 180 Indares, A., Dunning, G., 2001. Partial Melting of High-P–T Metapelites from the
181 Tshenukutish Terrane (Grenville Province): Petrography and U–Pb Geochronology. *J.*
182 *Petrol.* 42, 1547–1565. doi:10.1093/petrology/42.8.1547
- 183 Indares, A., Dunning, G., Cox, R., 2000. Tectono-thermal evolution of deep crust in a
184 Mesoproterozoic continental collision setting: the Manicouagan example. *Can. J. Earth*
185 *Sci.* 37, 325–340. doi:10.1139/e99-069
- 186 Indares, A., Dunning, G., Cox, R., Gale, D., Connelly, J., 1998. High-pressure, high-
187 temperature rocks from the base of thick continental crust: Geology and age
188 constraints from the Manicouagan Imbricate Zone, eastern Grenville Province.
189 *Tectonics* 17, 426–440. doi:10.1029/98TC00373

- 190 Jannin, S., Gervais, F., Moukhsil, A., Crowley, J.L., Augland, L.E., In press. Datation U/Pb
191 des déformations inverses et normales dans la Province de Grenville central
192 (Manicouagan, Québec): évidence d'un chenal orogénique dans le Parautochtone, in:
193 Géologie et Ressources Minérales de La Partie Centrale de La Province de Grenville;
194 Abdelali Moukhsil Coordonnateur, Ministère de l'Énergie et Des Ressources
195 Naturelles, Québec.
- 196 Jordan, S.L., Indares, A., Dunning, G., 2006. Partial melting of metapelites in the Gagnon
197 terrane below the high-pressure belt in the Manicouagan area (Grenville Province):
198 pressure–temperature (P–T) and U–Pb age constraints and implications. *Can. J. Earth*
199 *Sci.* 43, 1309–1329. doi:10.1139/E06-038
- 200 Ketchum, J.W.F., Heaman, L.M., Krogh, T.E., Culshaw, N.G., Jamieson, R.A., 1998. Timing
201 and thermal influence of late orogenic extension in the lower crust: a U-Pb
202 geochronological study from the southwest Grenville orogen, Canada. *Precambrian*
203 *Res.* 89, 25–45. doi:10.1016/S0301-9268(97)00079-X
- 204 Ketchum, J.W.F., Jamieson, R.A., Heaman, L.M., Culshaw, N.G., Krogh, T.E., 1994. 1.45 Ga
205 granulites in the southwestern Grenville province: Geologic setting, P-T conditions,
206 and U-Pb geochronology. *Geology* 22, 215–218. doi:10.1130/0091-
207 7613(1994)022<0215:GGITSG>2.3.CO;2
- 208 Krogh, T.E., 1994. Precise U-Pb ages for Grenvillian and pre-Grenvillian thrusting of
209 Proterozoic and Archean metamorphic assemblages in the Grenville Front tectonic
210 zone, Canada. *Tectonics* 13, 963–982. doi:10.1029/94TC00801
- 211 Lasalle, S., Dunning, G., Indares, A., 2014. In situ LA–ICP–MS dating of monazite from
212 aluminous gneisses: insights on the tectono-metamorphic history of a granulite-facies

- 213 domain in the central Grenville Province. *Can. J. Earth Sci.* 51, 558–572.
214 doi:10.1139/cjes-2013-0170
- 215 Lasalle, S., Fisher, C.M., Indares, A., Dunning, G., 2013. Contrasting types of Grenvillian
216 granulite facies aluminous gneisses: Insights on protoliths and metamorphic events
217 from zircon morphologies and ages. *Precambrian Res.* 228, 117–130.
218 doi:10.1016/j.precamres.2013.01.014
- 219 Lasalle, S., Indares, A., 2014. Anatectic record and contrasting P-T paths of aluminous
220 gneisses from the central Grenville Province. *J. Metamorph. Geol.* 32, 627–646.
221 doi:10.1111/jmg.12083
- 222 Lentz, D., 1996. U, Mo, and REE mineralization in late-tectonic granitic pegmatites,
223 southwestern Grenville Province, Canada. *Ore Geol. Rev.* 11, 197–227.
224 doi:10.1016/0169-1368(95)00034-8
- 225 Lentz, D.R., 1991. Petrogenesis of uranium-, thorium-, molybdenum-, and rare earth element-
226 bearing pegmatites, skarns, and veins in the central metasedimentary belt of the
227 Grenville Province, Ontario and Quebec. (Unpublished Ph.D. thesis). University of
228 Ottawa (Canada), 491 p.
- 229 Linnen, R.L., 1998. The solubility of Nb-Ta-Zr-Hf-W in granitic melts with Li and Li + F;
230 constraints for mineralization in rare metal granites and pegmatites. *Econ. Geol.* 93,
231 1013–1025. doi:10.2113/gsecongeo.93.7.1013
- 232 Linnen, R.L., Cuney, M., 2005. Granite-related rare-element deposits and experimental
233 constraints on Ta-Nb-W-Sn-Zr-Hf mineralization. *Short Course Notes - Geological*
234 *Association of Canada* 17, 45–68.

- 235 Linnen, R.L., Keppler, H., 2002. Melt composition control of Zr/Hf fractionation in magmatic
236 processes. *Geochim. Cosmochim. Ac.* 66, 3293–3301. doi:10.1016/S0016-
237 7037(02)00924-9
- 238 London, D., 2016. Rare-Element Granitic Pegmatites. *Rev. Econ. Geol.* 18, 165–193.
- 239 London, D., 2008. Pegmatites, *Can. Mineral. Spec. Publ.* 10, 368 p.
- 240 London, D., 2005. Granitic pegmatites: an assessment of current concepts and directions for
241 the future. *Lithos* 80, 281–303. doi:10.1016/j.lithos.2004.02.009
- 242 Ludwig, K.R., 2001. Isoplot/Ex Version 2.49. A Geochronological Toolkit for Microsoft
243 Excel. Berkeley Geochronology Center, Special Publication vol. 1a, pp. 1–55.
- 244 Ludwig, K.R., 1998. On the Treatment of Concordant Uranium-Lead Ages. *Geochim.*
245 *Cosmochim. Ac.* 62, 665–676. doi:10.1016/S0016-7037(98)00059-3
- 246 Lumbers, S.B., 1979. The Grenville Province of Ontario, in: 5th Ann. Meeting Int. Union
247 Geol. Sci, Subcomm. Precamb. Stratigraphy. pp. 1–35.
- 248 Lumbers, S.B., 1964. Preliminary report on the relationship of mineral deposits to intrusive
249 rocks and metamorphism in part of the Grenville Province of southeastern Ontario.
250 Ont. Dep. Mines Rep. No. PR1964-4.
- 251 Martin, R.F., De Vito, C., 2005. The Patterns of Enrichment in Felsic Pegmatites Ultimately
252 Depend on Tectonic Setting. *Can. Mineral.* 43, 2027–2048.
253 doi:10.2113/gscanmin.43.6.2027
- 254 Masson, S.L., Gordon, J.B., 1981. Radioactive mineral deposits of the Pembroke-Renfrew
255 area. *Ont. Geol. Surv. Mineral Deposits Circ.*, No. 23.

- 256 McDonough, W.F., Sun, S. -s., 1995. The composition of the Earth. *Chem. Geol.* 120, 223–
257 253. doi:10.1016/0009-2541(94)00140-4
- 258 Melcher, F., Graupner, T., Gäbler, H.-E., Sitnikova, M., Henjes-Kunst, F., Oberthür, T.,
259 Gerdes, A., Dewaele, S., 2015. Tantalum–(niobium–tin) mineralisation in African
260 pegmatites and rare metal granites: Constraints from Ta–Nb oxide mineralogy,
261 geochemistry and U–Pb geochronology. *Ore Geol. Rev.* 64, 667–719.
262 doi:10.1016/j.oregeorev.2013.09.003
- 263 Montel, J.-M., 1993. A model for monazite/melt equilibrium and application to the generation
264 of granitic magmas. *Chem. Geol.* 110, 127–146. doi:10.1016/0009-2541(93)90250-M
- 265 Moukhsil, A., Lacoste, P., Gobeil, A., David, J., 2009. Synthèse géologique de la région de
266 Baie-Comeau. Ministère des Ressources naturelles et de la Faune, Québec, RG 2009-
267 03, 30 p.
- 268 Moukhsil, A., Lacoste, P., Simard, M., Perreault, S., 2007. Géologie de la région
269 septentrionale de Baie-Comeau (22F07, 22F08, 22F09, 22F15 et 22F16). Ministère
270 des Ressources naturelles et de la Faune, Québec, RP 2007-04, 16 p.
- 271 Moukhsil, A., Solgadi, F., Belkacim, S., Elbasbas, A., Augland, L.E., 2014. Géologie de la
272 région du lac Okaopéo, Côte-Nord. Ministère de l’Energie et des Ressources
273 Naturelles, Québec, RG 2014-03, 34 p.
- 274 Moukhsil, A., Solgadi, F., Clark, T., Blouin, S., Indares, A., Davis, D.W., 2013a. Géologie du
275 nord-ouest de la région du barrage Daniel-Johnson (Manic 5), Côte-Nord. Ministère
276 des Ressources Naturelles, Québec, RG 2013-01, 46 p.

- 277 Moukhsil, A., Solgadi, F., Indares, A., Belkacim, S., 2013b. Géologie de la région
278 septentrionale du réservoir aux Outardes 4, Côte-Nord. Ministère des Ressources
279 Naturelles, Québec, RG 2013-03, 33 p.
- 280 Moukhsil, A., Solgadi, F., Lacoste, P., Gagnon, M., David, J., 2012. Géologie de la région du
281 lac du Milieu (SNRC 22O03, 22O04, 22O06, 22J13 et 22J14). Ministère des
282 Ressources Naturelles et de la Faune, Québec, RG 2012-01, 33 p.
- 283 Paquette, J.L., Tiepolo, M., 2007. High resolution (5 μm) U–Th–Pb isotope dating of
284 monazite with excimer laser ablation (ELA)-ICPMS. *Chem. Geol.* 240, 222–237.
285 doi:10.1016/j.chemgeo.2007.02.014
- 286 Perreault, S., Lafrance, B., 2015. Kwyjibo, a REE-enriched iron oxides-copper-gold (IOCG)
287 deposit, Grenville Province, Québec. Symposium on critical and strategic materials.
288 British Columbia Geological Survey Paper 3, 139–145.
- 289 Petrík, I., Broska, I., Lipka, J., Siman, P., 1995. Granitoid Allanite-(Ce) Substitution
290 Relations, Redox Conditions and REE Distributions (on an Example of I-Type
291 Granitoids, Western Carpathians, Slovakia). *Geol. Carpath.* 46, 79–94.
- 292 Rapp, R.P., Watson, E.B., 1986. Monazite solubility and dissolution kinetics: implications for
293 the thorium and light rare earth chemistry of felsic magmas. *Contr. Mineral. Petrol.* 94,
294 304–316. doi:10.1007/BF00371439
- 295 Rivers, T., 2012. Upper-crustal orogenic lid and mid-crustal core complexes: signature of a
296 collapsed orogenic plateau in the hinterland of the Grenville Province. *Can. J. Earth
297 Sci.* 49, 1–42. doi:10.1139/e11-014

- 298 Rivers, T., 2009. The Grenville Province as a large hot long-duration collisional orogen –
299 insights from the spatial and thermal evolution of its orogenic fronts. *Geol. Soc.,*
300 *Lond., Spec. Publ.* 327, 405–444. doi:10.1144/SP327.17
- 301 Rivers, T., 2008. Assembly and preservation of lower, mid, and upper orogenic crust in the
302 Grenville Province—Implications for the evolution of large hot long-duration orogens.
303 *Precambrian Res.* 167, 237–259. doi:10.1016/j.precamres.2008.08.005
- 304 Rivers, T., 1997. Lithotectonic elements of the Grenville Province: review and tectonic
305 implications. *Precambrian Res.* 86, 117–154. doi:10.1016/S0301-9268(97)00038-7
- 306 Rivers, T., 1980. Revised stratigraphic nomenclature for Aphebian and other rock units,
307 southern Labrador Trough, Grenville Province. *Can. J. Earth Sci.* 17, 668–670.
308 doi:10.1139/e80-062
- 309 Rivers, T., Culshaw, N., Hynes, A., Indares, A., Jamieson, R., Martignole, J., 2012. The
310 Grenville Orogen - A Post-LITHOPROBE Perspective, in: *Tectonic Styles in Canada:*
311 *The LITHOPROBE Perspective*, Geological Association of Canada, Special Paper 49.
312 J.A. Percival, F.A. Cook, and R.M. Clowes, pp. 97–236.
- 313 Rivers, T., Ketchum, J., Indares, A., Hynes, A., 2002. The High Pressure belt in the Grenville
314 Province: architecture, timing, and exhumation. *Can. J. Earth Sci.* 39, 867–893. doi:
315 10.1139/E02-025.
- 316 Rivers, T., Martignole, J., Gower, C.F., Davidson, A., 1989. New tectonic divisions of the
317 Grenville Province, Southeast Canadian Shield. *Tectonics* 8, 63–84.
318 doi:10.1029/TC008i001p00063

- 319 Rivers, T., Schwerdtner, W., 2015. Post-peak Evolution of the Muskoka Domain, Western
320 Grenville Province: Ductile Detachment Zone in a Crustal-scale Metamorphic Core
321 Complex. *Geosci. Can.* 42, 403–436. doi:10.12789/geocanj.2015.42.080
- 322 Sangster, A.L., Gauthier, M., Gower, C.F., 1992. Metallogeny of structural zones, Grenville
323 Province, northeastern North America. *Precambrian Res.* 58, 401–426.
324 doi:10.1016/0301-9268(92)90127-A
- 325 Saucier, G., Noreau, C., Casgrain, P., Côté, P., Larochelle, E., Bilodeau, M., Hayden, A.,
326 Poirier, E., Garon, M., Bertrand, V., Kissiova, M., Malloux, M., Rouger, M., Camus,
327 Y., Gagnon, G., 2013. NI-43-101 report-feasibility study for the Kipawa project
328 Temiscamingue area, Québec, Canada. Matamec Explorations Inc., Montréal.
- 329 Shand, S.J., 1943. *The Eruptive Rocks*, 2nd edition. ed. New York: John Wiley, 444 p.
- 330 Soucy La Roche, R., Gervais, F., Tremblay, A., Crowley, J.L., Ruffet, G., 2015. Tectono-
331 metamorphic history of the eastern Taureau shear zone, Mauricie area, Québec:
332 Implications for the exhumation of the mid-crust in the Grenville Province.
333 *Precambrian Res.* 257, 22–46. doi:10.1016/j.precamres.2014.11.012
- 334 Spear, F.S., Pyle, J.M., 2002. Apatite, Monazite, and Xenotime in Metamorphic Rocks. *Rev.*
335 *Mineral. Geochem.* 48, 293–335. doi:10.2138/rmg.2002.48.7
- 336 Stepanov, A., Mavrogenes, J.A., Meffre, S., Davidson, P., 2014. The key role of mica during
337 igneous concentration of tantalum. *Contrib. Mineral. Petrol.* 167, 1009–1016.
338 doi:10.1007/s00410-014-1009-3
- 339 Tucker, R.D., Gower, C.F., 1994. A U-Pb geochronological framework for the Pinware
340 Terrane, Grenville Province, Southeast Labrador. *J. Geol.* 102, 67–78.

- 341 Van Achterbergh, E., Ryan, C.G., Jackson, S.E., Griffin, W.L., 2001. Data reduction software
342 for LA-ICP-MS: appendix. Laser-Ablation-ICPMS in the earth sciences—principles
343 and applications. Mineralogical Association of Canada (short course series) 29, 239–
344 243.
- 345 van Breemen, O., Currie, K. I., 2004. Geology and U–Pb geochronology of the Kipawa
346 Syenite Complex — a thrust related alkaline pluton — and adjacent rocks in the
347 Grenville Province of western Quebec. *Can. J. Earth Sci.* 41, 431–455.
- 348 van Gool, J.A.M., Rivers, T., Calon, T., 2008. Grenville Front zone, Gagnon terrane,
349 southwestern Labrador: Configuration of a midcrustal foreland fold-thrust belt.
350 *Tectonics* 27, TC1004. doi:10.1029/2006TC002095
- 351 Van Lichtervelde, M., Grand’Homme, A., Saint-Blanquat, M. de, Olivier, P., Gerdes, A.,
352 Paquette, J.-L., Melgarejo, J.C., Druguet, E., Alfonso, P., 2016. U-Pb geochronology
353 on zircon and columbite-group minerals of the Cap de Creus pegmatites, NE Spain.
354 *Miner. Petrol.*, 1–21. doi:10.1007/s00710-016-0455-1
- 355 White, A.J.R., Chappell, B.W., 1977. Ultrametamorphism and granitoid genesis.
356 *Tectonophysics* 43, 7–22. doi:10.1016/0040-1951(77)90003-8
- 357 Zارايسкий, G.P., Aksyuk, A.M., Devyatova, V.N., Udoratina, O.V., Chevychelov, V.Y., 2009.
358 The Zr/Hf ratio as a fractionation indicator of rare-metal granites. *Petrol.* 17, 25.
359 doi:10.1134/S0869591109010020

360

361 **Figures captions**

362 **Figure 1:** a: Position of the Grenville orogen in Laurentia. Paleozoic and younger cover
363 omitted (modified from Hoffman, 1989; Rivers, 2008; Rivers et al., 2012). The northern
364 dashed line represents the boundary between Internal and External Paleoproterozoic Laurentia
365 and the southern dashed line represents the Grenville Front (GF). Abbreviations: 1 = exposed
366 Grenville Province, light grey represents the inferred extension of subsurface allochthonous
367 Grenville Province; 2 = Granite-Rhyolite Igneous Province, ca. 1.50-1.34 Ga and reworked
368 equivalents in the Grenville Province; 3 = Mid-Continental Rift system; 4 = Paleoproterozoic
369 orogens, ca. 1.9-1.8 Ga, ca. 1.65 Ga and reworked equivalents in the Grenville Province; 5 =
370 Archean cratons; GF = Grenville Front. b: Simplified tectonic map of the Grenville Province
371 (modified after Rivers, 2008; Rivers et al., 2012). Letters in circle represent the localization of
372 the main Grenvillian granitic pegmatites field as reviewed in Ayres and Černý (1982) and
373 Černý (1990): A = Central Gneiss Belt; B = Central Metasedimentary Belt; C = Central
374 Granulite Terrain; D = eastern part of the Grenville Province. Abbreviations: ABT =
375 Allochthon Boundary Thrust; Cn = Canyon domain; G = Gagnon Terrane; GF = Grenville
376 Front; HJ = Hart-Jaune terrane; L = Lelukuau terrane; Ts = Tshenukutish terrane.

377 **Figure 2:** Geological map of the central Grenville (Quebec) showing the position of the
378 studied Lac Okaopéo region (NTS sheets 22K/01, 22K/02, 22K/07, 22K/08, 22K/09, 22K/10,
379 modified after Moukhsil et al., 2014). Abbreviations: ABT = Allochthon Boundary Thrust;
380 MIZ = Manicouagan Imbricate Zone.

381 **Figure 3:** Simplified geological map of the studied Lac Okaopéo region (modified after
382 Moukhsil et al., 2014) showing the geology of the environment of the REE occurrences
383 identified in 2013 by Moukhsil et al. (2014). Stars and diamonds represent monazite-bearing
384 and allanite-bearing pegmatitic granite outcrops respectively. Coordinates of the REE

385 occurrences are proposed in Table 1. ¹: Augland et al. (2015); ²: Gobeil et al. (2002); ³: David
386 (2006); ⁴: Dunning and Indares (2010); ⁵: David et al. (2009); ⁶: Moukhsil et al. (2013a); ⁷:
387 Moukhsil et al. (2012); ⁸: Lasalle et al. (2013). Abbreviation: PGD = pegmatitic granite dyke.

388 **Figure 4:** Example of detailed map for the 13-AM-13 monazite-bearing pegmatitic granite
389 outcrop from the Lac Okaopéo region showing the relationships between the different
390 identified facies of the pegmatitic granite and the sampling areas. The detailed map for the six
391 other outcrops are proposed in appendices A and B. Abbreviations: PGD = pegmatitic granite
392 dyke.

393 **Figure 5:** Structural measurements of the investigated pegmatitic granite dykes from the Lac
394 Okaopéo region and of the foliation of their host rocks. a: structural measurements from the
395 outcrops of paragneisses-hosted monazite-bearing pegmatitic granite dykes; b: structural
396 measurements from the outcrops of metaplutonic complexes-hosted allanite-bearing
397 pegmatitic granite dykes. Stars and diamonds represent monazite-bearing and allanite-bearing
398 pegmatitic granite outcrops respectively. Note that a larger number of measurements are
399 reported for outcrops of metaplutonic complexes-hosted pegmatitic granite dykes on which
400 allanite-bearing dykes are expressed as dyke swarms. In addition, the concordant/discordant
401 veins connected to the main dyke of the 13-AE-2149 outcrop form a network of undulating
402 veins that do not allow clear 3D observations. Therefore, these veins have not been measured.
403 Abbreviations: Aln-bearing PGD = allanite-bearing pegmatitic granite; Mnz-bearing PGD =
404 monazite-bearing pegmatitic granite.

405 **Figure 6:** Representative photographs of the monazite-bearing pegmatitic granite outcrops
406 from the Lac Okaopéo region (from the outcrops 13-AM-07, -13 and 13-TC-5008). a: general
407 view of the 13-AM-13 outcrop composed of a pegmatitic granite intruding paragneisses from
408 the Plus-Value Complex; b: detailed view of Stockscheider-like contact between the 13-AM-

409 07 pegmatitic granite dyke and the intruded paragneisses marked by the crystallization of
410 feldspar from the dyke perpendicular to the contact; c: locally diffuse contact between the 13-
411 TC-5008 pegmatitic granite dyke and the intruded paragneisses delineated by garnet-biotite
412 aggregates; d: typical transition between the fine and coarse grained facies of the 13-AM-13
413 pegmatitic granite dyke underlined by biotite aggregates. Note that the abundance of biotite in
414 the fine grained facies on this photograph is related to the vicinity of the coarse grained facies;
415 e: detailed view of a garnet phenocryst in the fine grained facies; f: monazite crystals from the
416 fine grained facies; g: typical pegmatitic facies essentially composed of a
417 quartz+feldspar+biotite assemblage in which feldspar and biotite crystals can reach over 5
418 cm; h: arborescent textures made by skeletal crystals reaching up to 15 cm long in the 13-TC-
419 5008 pegmatitic granite dyke. Abbreviations: Bt = biotite; Grt = garnet; Fsp = feldspar; Mnz
420 = monazite; Mnz-bearing = monazite-bearing pegmatitic granite; PGD = pegmatitic granite
421 dyke; Qz = quartz.

422 **Figure 7:** Representative photographs of the allanite-bearing pegmatitic granite outcrops from
423 the Lac Okaopéo region (from the outcrops 13-TC-5072, 13-FS-1202 and 13-AE-2149). a:
424 general view of the dome-shaped 13-TC-5072 outcrop composed of a pegmatitic granite
425 intruding as a dyke swarm a metamonzogranite from the Bardoux Plutonic Suite; b: detailed
426 view of the typical zoning observed in the 13-FS-1202 pegmatitic granite. Note that the
427 allanite phenocrysts are associated with a coarse grained facies; c: typical dyke zonation of
428 the 13-TC-5072 pegmatitic dykes, with a southeastern boundary (1) marked by a thin zone of
429 reaction with the host rock developed over a few millimeters with almost no biotite, followed
430 by a fine grained facies with increasing grain size and proportions of biotite (2, 3) up to a
431 pegmatitic core (4). This core is followed by a progressive fine grained facies with decreasing
432 grain size zone (5). The northern contact (6) is marked by the development of K-feldspar
433 phenocrysts perpendicular to the contact. Note that these phenocrysts are locally disconnected

434 to the contact that contrast with a Stockscheider-like texture as represented in Fig. 6b, and that
435 dyke is discordant to the foliation of the intruded metamonzogranite; d: typical allanite
436 phenocrysts in pegmatitic granite dykes intruding the metamonzogranite; e: general view of
437 the 13-AE-2149 outcrop composed of a pegmatitic granite dyke intruding a layered
438 metamangerite from the Castoréum Plutonic Suite; f: detailed view of one of the pegmatitic
439 granite vein from the 13-AE-2149 outcrop discordant to the foliation of its host rock and its
440 connection with the main pegmatitic granite dyke expressed on this outcrop, here with a sub-
441 concordant contact with the layered metamangerite; g: detailed view of the whole 13-AE-
442 2149 shallow-dipping dyke zonation from its hanging wall to its lower contact, both marked
443 by a pegmatitic facies with large allanite crystals, through a layered fine grained facies
444 making the core of the core of the dyke and that also carries disseminated and smaller allanite
445 grains. Abbreviations: Aln = allanite; Aln-bearing = allanite-bearing pegmatitic granite; Bt =
446 biotite; K-Fsp = K-feldspar; PGD = pegmatitic granite dyke.

447 **Figure 8:** Typical petrography of monazite-bearing pegmatitic granite dykes from the Lac
448 Okaopéo region. a: major phases composing the monazite-bearing granite (polarized and
449 analysed light); b: syn- to late-zircon growth monazite crystal (SEM); c: late-magmatic
450 crystallization of Th-U±REE silicates filling fractures of monazite crystals (SEM); d: late-
451 sericite affecting plagioclase (polarized and analysed light). Abbreviations: Bt = biotite; Mc =
452 microcline; Mnz = monazite; Mnz-PGD = monazite-bearing pegmatitic granite dyke; Pl =
453 plagioclase; Qz = quartz; Ser = sericite; Silic. = silicates; Zrc = zircon.

454 **Figure 9:** Chemical mapping of monazite grains from the 13-AM-13 and 13-TC-5008
455 monazite-bearing pegmatitic granite dykes from the Lac Okaopéo region. Numbers in figures
456 a and d refer to the U-Pb dating analyses conducted using LA-ICP-MS, and reported in Table
457 5. a to c: BSE image with spot positions of LA-ICP-MS U-Pb dating and Ce and Th X-ray

458 maps of a representative oscillatory zoned monazite grain from the 13-AM-13 monazite-
459 bearing pegmatitic granite; d to f: BSE image with spot positions of LA-ICP-MS U-Pb dating
460 and Ce and Th X-ray maps of a representative rather homogeneous and weakly zoned
461 monazite grain from the 13-TC-5008 monazite-bearing pegmatitic granite. Abbreviations:
462 Mnz = monazite Mnz-PGD = monazite-bearing pegmatitic granite dyke.

463 **Figure 10:** Chemical compositions of the different zones identified in monazite grains from
464 the 13-AM-13 and 13-TC-5008 pegmatitic granite samples from the Lac Okaopéo region. a:
465 ternary plot of the monazite compositions from the 13-AM-13 monazite-bearing pegmatitic
466 granite. For the three identified zones, the monazite grains are dominated by monazite-(Ce)
467 compositions, but evolve towards monazite-(La) compositions with increasing Th and Si
468 proportion over LREE and P; b: Th+U+Si vs REE+Y+P diagram with compositional trends of
469 huttonite and brabantite end-members for monazite grains from the 13-AM-13 pegmatitic
470 granite. The huttonite substitution tends to be dominant with increasing Th and Si proportion
471 over LREE and P; c: ternary plot of the monazite compositions from the 13-TC-5008
472 monazite-bearing pegmatitic granite. For the three identified zones, the monazite grains are
473 clustered into the monazite-(Ce) composition field with no significant changes with increasing
474 Ti and Si proportion over LREE and P; d: Th+U+Si vs REE+Y+P diagram with
475 compositional trends of huttonite and brabantite end-members for monazite grains from the
476 13-TC-5008 pegmatitic granite. Note these grains are mainly characterized by the huttonite
477 end-member with no significant changes with increasing Ti and Si proportion over LREE and
478 P. Abbreviations: Mnz = monazite; PGD = pegmatitic granite dyke.

479 **Figure 11:** Typical petrography of allanite-bearing pegmatitic granite dykes from the Lac
480 Okaopéo region. a: major phases composing the allanite-bearing granite dykes (polarized and
481 analysed light); b: allanite crystal displaying an Aln_1 oscillatory zoned core corroded by an

482 Aln₂ overgrowth of similar composition (Table 4) and altered by a rim associated with fluids
483 circulation probably related to the magmatic-hydrothermal transition (polarized and analysed
484 light); c: allanite grains display rims probably associated with the late-sericitization of
485 feldspar. Note the syn- to late-zircon growth crystallization of the allanite phenocrysts
486 (polarized and analysed light); d: typical millimetric allanite phenocryst from the 13-FS-1202
487 pegmatitic granite showing LREE-rich and Fe-Ca-LREE(Ce)-rich zones (Table 4) surrounded
488 by an alteration rim probably associated with fluids circulation probably related to the
489 magmatic-hydrothermal transition; e: veinlets of Ca+REE carbonates on the boundary or
490 filling fractures of allanite crystals most probably associated with fluids circulation at the
491 magmatic-hydrothermal transition (SEM); f: veinlets of Ca+REE silicates on the boundary or
492 filling fractures of allanite crystals most probably associated with fluids circulation at the
493 magmatic-hydrothermal transition (SEM). Abbreviations: Aln = allanite; Aln-PGD = allanite-
494 bearing pegmatitic granite dyke; Bt = biotite; Carb. = carbonates; Mc = microcline; Pl =
495 plagioclase; Qz = quartz; Ser = sericite; Silic. = silicates; Zrc = zircon.

496 **Figure 12:** Chemical compositions of the different zones identified in allanite grains from the
497 13-TC-5072 and 13-FS-1202 pegmatitic granite samples from the Lac Okaopéo region. a:
498 REE vs Al composition of allanite grains from the 13-TC-5072 allanite-bearing pegmatitic
499 granite obtained on EMP (Petřík et al., 1995). Note the clustering of compositions of the
500 different zones close to the allanite pole; b: REE vs Al composition of allanite grains from the
501 13-FS-1202 allanite-bearing pegmatitic granite obtained on EMP (Petřík et al., 1995). Note
502 the alteration trend that lead to more 'epidote like' compositions. Abbreviation: Aln =
503 allanite; PGD = pegmatitic granite dyke.

504 **Figure 13:** Whole rock geochemistry of the REE-richest facies of the investigated pegmatitic
505 granite dykes from the Lac Okaopéo region, compared to data of REE-rich granitic

506 pegmatites samples from Lentz (1996). a: peraluminous, metaluminous and peralkaline fields
507 showing the peraluminous character of the pegmatitic granite samples; b: chondrite
508 normalized REE patterns of the pegmatitic granite samples. Note that six of them display a
509 similar tendency of strong fractionation of LREE over HREE that contrast with lower
510 fractionation of the 13-AE-2149 dyke. The Σ REE increases with decreasing Eu/Eu^*
511 (normalization after McDonough and Sun, 1995); c: U+Th (ppm) vs Σ REE (ppm) diagram
512 showing the close relationship between an increase in REE and an increase in U and Th for all
513 the investigated pegmatitic granite samples; d: Na_2O (wt.%) vs CaO (wt.%) diagram that
514 evidence a coeval increase of Na_2O , CaO and the REE associated with a decrease in K_2O for
515 all the investigated pegmatitic granite samples; e: Nb/Ta vs Zr/Hf diagram showing a
516 contradictory behavior of Nb and Ta between the monazite-bearing and the allanite-bearing
517 samples, as Nb/Ta increases with the Σ REE in the former and decreases with the Σ REE in the
518 latter. Note that the Zr/Hf ratio remain quite stable for both series; f: CaO (wt.%) vs P_2O_5
519 (wt.%) diagram showing that the formation of monazite (Mnz-bearing pegmatitic granite
520 samples) is associated with increasing CaO and P_2O_5 contents. Note that the Aln-bearing
521 pegmatitic granite samples do not display a similar pattern; g: Fe_2O_3 (total) (wt.%) vs MgO
522 (wt.%) diagram showing that the formation of allanite (Aln-bearing pegmatitic granite
523 samples) is associated with increasing Fe_2O_3 and MgO contents. Note that the Mnz-bearing
524 pegmatitic granite samples do not display a similar pattern. Abbreviation: PGD = pegmatitic
525 granite dyke.

526 **Figure 14:** U-Pb ages of monazite grains from the 13-AM-13 and 13-TC-5008 pegmatitic
527 granite dykes from the Lac Okaopéo region. a: Concordia plots for the monazite grains from
528 the 13-AM-13 pegmatitic granite ($n = 25$, data-point error ellipses are 2σ); b: Concordia plots
529 for the over 98% of concordance analyses from the 13-AM-13 pegmatitic granite ($n = 11$,

530 data-point error ellipses are 2σ); c: Concordia plots for the monazite grains from the 13-TC-

531 5008 granite (n = 22, data-point error ellipses are 2σ).

532

ACCEPTED MANUSCRIPT

533

534 **Table 1:** Location, present coordinates and results presented in this study of the REE

535 occurrences from the Lac Okaopéo region, first ordered by type of occurrence then from north

536 to south. Abbreviation: Aln-bearing = allanite-bearing pegmatitic granite dyke; Mnz-bearing

537 = monazite-bearing pegmatitic granite dyke; NTS = National Topographic System.

538

Type of REE occurrence	Outcrop n°	NTS sheet	UT M zone ¹	Easting g ¹	Northing g ¹	Localization (see Fig. 3)			Results presented in this study		
							Detail ed map	Structural measurements ²	Whole-rock geochemistry ³	Accessory mineral composition	Dating (U-Pb monazite)
<i>Mnz-bearing</i>	13-AM-07	22K10	U19	510199	5620952	North of the 22K/10 NTS sheet	Fig. A-1	Fig. 5a	Table 2	-	-
	13-AM-10	22K10	U19	511236	5618292	North of the 22K/10 NTS sheet	Fig. A-3	Fig. 5a	Table 2	-	-
	13-AM-13	22K10	U19	512052	5614036	North of the 22K/10 NTS sheet	Figs. 4, A-5	Fig. 5a	Table 2	Table 3 - Figs. 10a, b	Table 5 - Figs. 14a-b
	13-TC-5008	22K07	U19	504614	5585041	North of the 22K/07 NTS sheet	Fig. A-7	Fig. 5a	Table 2	Table 3 - Figs. 10c, d	Table 5 - Fig. 14c
<i>Aln-bearing</i>	13-TC-5072	22K10	U19	510668	5603384	South of the 22K/10 NTS sheet	Fig. B-1	Fig. 5b	Table 2	Table 4 - Figs. 12a	-
	13-FS-1202	22K10	U19	510162	5601234	South of the 22K/10 NTS sheet	Fig. B-3	Fig. 5b	Table 2	Table 4 - Figs. 12b	-
	13-AE-2149	22K07	U19	503389	5589641	North of the 22K/07 NTS sheet	Fig. B-5	Fig. 5b	Moukhsil et al. (2014)	-	-

539 ¹ Coordinates are reported as Universal Transverse Mercator (UTM).540 ² All the structural measurements (foliation of the host rocks and dykes) are available in
541 Appendix C.542 ³ Geochemical data are represented in Fig. 13.

543

544

545 **Table 2:** Whole rock geochemistry of the REE-richest facies of the pegmatitic granite dykes
 546 from the Lac Okaopéo region, first ordered by type of occurrence then from north to south.
 547 Data for the 13-AE-2149 pegmatitic granite is from (Moukhsil et al., 2014). Abbreviations:
 548 A/CNK = Al/(Na + K + Ca/2) (Shand, 1943); Allanite-bearing = allanite-bearing pegmatitic
 549 granite dyke; A/NK = Al/(Na + K) (Shand, 1943); ASI = Aluminum Saturation Index given
 550 by the expression $ASI = Al/(Ca - 1.67 \times P + Na + K)$ (Frost et al., 2001; Shand, 1943);
 551 Monazite-bearing = monazite-bearing pegmatitic granite dyke.

Type of REE occurrence	Monazite-bearing	Allanite-bearing					
Sample	13-AM-07	13-AM-10	13-AM-13	13-TC-5008	13-TC-5072	13-FS-1202	13-AE-2149
SiO ₂ (wt.%)	71.03	70.80	60.24	70.79	70.27	70.85	55.84
TiO ₂	0.24	0.50	0.89	0.69	0.34	0.43	0.63
Al ₂ O ₃	15.93	13.85	18.58	12.90	14.18	14.83	15.05
Fe ₂ O ₃ (total)	1.23	1.80	4.60	3.67	2.38	3.48	12.42
MnO	0.01	0.01	0.03	0.02	0.02	0.05	0.22
MgO	0.36	0.48	1.16	0.71	0.30	0.52	0.85
CaO	2.29	0.87	3.10	0.88	1.38	2.99	5.54
Na ₂ O	3.53	2.26	4.02	1.99	2.74	4.14	4.28
K ₂ O	4.32	6.68	4.36	6.25	5.90	1.33	1.93
P ₂ O ₅	0.29	0.09	0.40	0.10	0.15	0.02	0.22
Cr ₂ O ₃	< 0.01	< 0.01	< 0.01	< 0.01	< 0.01	< 0.01	< 0.01
LOI	0.63	0.92	0.82	0.60	0.73	1.01	0.83
Total	99.87	98.26	98.19	98.58	98.39	99.64	97.80
ASI	1.30	1.19	1.36	1.20	1.18	1.35	1.08
A/CNK	1.28	1.30	1.27	1.29	1.24	1.30	0.87
A/NK	2.03	1.55	2.22	1.57	1.64	2.71	2.42
Sr (ppm)	448.00	342.00	550.00	213.00	164.00	275.00	147.00
Ba	1191.00	2424.00	899.00	1662.00	661.00	147.00	181.00
Nb	5.60	8.40	21.00	15.70	7.50	17.30	132.00
V	16.00	23.00	27.00	27.00	7.00	15.00	38.00
Co	2.00	2.00	6.00	5.00	2.00	3.00	6.00
Ga	39.00	22.00	60.00	26.00	29.00	53.00	79.00
Ge	4.70	2.10	6.90	2.40	2.90	7.40	9.70
In	< 0.1	< 0.1	< 0.1	< 0.1	< 0.1	< 0.1	0.20
Sn	< 1	< 1	< 1	< 1	< 1	2.00	4.00
Cs	0.50	0.70	1.50	0.70	0.30	1.00	0.70
Pb	35.00	29.00	34.00	22.00	31.00	17.00	41.00
Be	2.00	< 1	3.00	< 1	< 1	4.00	9.00
Hf	23.40	4.40	41.50	9.00	7.40	50.80	171.00
Ta	0.10	0.25	0.40	0.35	0.11	0.30	3.20
W	0.90	0.80	1.10	0.80	1.40	0.80	3.00

Tl	0.97	1.08	1.40	1.10	0.97	0.75	0.34
Bi	< 0.1	< 0.1	< 0.1	< 0.1	< 0.1	< 0.1	< 0.1
Th	561.00	102.00	1300.00	123.00	70.50	392.00	766.00
U	11.00	2.02	19.10	1.66	1.11	6.88	30.30
Rb	98.00	141.00	214.00	172.00	122.00	58.00	42.00
Y	29.50	5.90	52.90	10.00	15.80	83.50	544.00
Zr	860.00	195.00	1480.00	388.00	290.00	1760.00	6340.00
Nb/Ta	56	34	53	45	68	58	41
Zr/Hf	37	44	36	43	39	35	37
Th/U	51	50	68	74	64	57	25
La	1560.00	433.00	1800.00	538.00	674.00	1870.00	2150.00
Ce	2720.00	690.00	3370.00	884.00	1160.00	3580.00	4130.00
Pr	271.00	64.10	370.00	92.20	120.00	406.00	470.00
Nd	843.00	202.00	1250.00	300.00	377.00	1400.00	1710.00
Sm	84.60	17.50	159.00	30.40	37.70	179.00	297.00
Eu	3.47	2.37	4.74	2.40	2.62	4.71	9.39
Gd	28.60	5.70	65.20	11.80	13.00	73.30	180.00
Tb	2.07	0.41	5.03	0.78	1.09	6.81	24.90
Dy	8.41	1.55	16.30	2.99	4.33	25.70	123.00
Ho	1.12	0.22	1.93	0.43	0.67	3.58	21.80
Er	2.42	0.52	3.81	0.91	1.51	7.73	59.00
Tm	0.23	0.06	0.35	0.09	0.17	0.90	8.34
Yb	1.13	0.35	1.56	0.43	0.74	4.87	51.80
Lu	0.17	0.05	0.22	0.06	0.10	0.72	7.22
ΣLREE	5479	1407	6949	1845	2369	7435	8757
ΣHREE	47	11	99	19	24	128	485
ΣREE	5526	1418	7048	1864	2393	7563	9242
La_N/Yb_N¹	938	840	784	850	619	261	28
Eu/Eu*¹	0.22	0.72	0.14	0.39	0.36	0.13	0.12
Cd	< 0.5	< 0.5	< 0.5	< 0.5	< 0.5	< 0.5	< 0.5
Cu	5.00	3.00	20.00	2.00	2.00	6.00	16.00
Ag	< 0.3	< 0.3	< 0.3	< 0.3	< 0.3	3.60	-
Ni	< 1	< 1	3.00	2.00	< 1	< 1	3.00
Mo	2.00	< 1	4.00	1.00	5.00	< 1	6.00
Zn	27.00	32.00	110.00	103.00	46.00	56.00	288.00
S	300.00	300.00	1100.00	100.00	< 100	300.00	600.00
Au	< 2	< 2	< 2	< 2	< 2	< 2	< 2

*Turlin et al. - Unusual LREE-rich, post-tectonic, monazite- or allanite-bearing pegmatitic
granites
in the central Grenville Province, Québec*

As	< 0.5	< 0.5	< 0.5	< 0.5	3.30	< 0.5	< 0.5
Br	< 0.5	< 0.5	< 0.5	< 0.5	< 0.5	< 0.5	< 0.5
Cr	58.00	47.00	70.00	49.00	59.00	75.00	48.00
Ir	< 5	< 5	< 5	< 5	< 5	< 5	< 5
Sc	1.10	1.70	3.50	1.70	2.60	6.70	31.90
Sb	< 0.1	< 0.1	< 0.1	< 0.1	< 0.1	< 0.1	< 0.1
Se	< 3	< 3	< 3	< 3	< 3	< 3	< 3

552 ¹ Normalization after McDonough and Sun (1995).

553

ACCEPTED MANUSCRIPT

554 **Table 3:** Analyses of monazite grains from the 13-AM-13 and the 13-TC-5008 pegmatitic
555 granite dykes from the Lac Okaopéo region. Data were obtained using EMP and were
556 performed on LREE-rich, intermediate and Th-Si-rich zones of monazite grains. They are
557 reported with confidence interval of 95% in brackets (n = number of analyses). Abbreviations:
558 Brab. = brabantite; Hutt. = huttonite; Mnz. = monazite; Xen. = xenotime.

<i>Sample</i>		<i>13-AM-13</i>			<i>13-TC-5008</i>		
<i>Zonation type</i>		<i>LREE(Ce)-rich</i>	<i>Intermediate</i>	<i>Th-Si-rich</i>	<i>LREE(Ce)-rich</i>	<i>Intermediate</i>	<i>Th-Si-rich</i>
Oxides/wt.%	P ₂ O ₅	29.07 (0.22)	27.59 (0.33)	25.63 (0.40)	28.99 (0.17)	28.87 (0.10)	28.43 (0.20)
	SiO ₂	0.99 (0.12)	1.92 (0.19)	3.14 (0.24)	1.03 (0.11)	1.09 (0.05)	1.38 (0.14)
	CaO	0.89 (0.15)	0.93 (0.11)	0.89 (0.12)	0.31 (0.03)	0.31 (0.02)	0.37 (0.03)
	Y ₂ O ₃	0.26 (0.06)	0.17 (0.03)	0.10 (0.02)	0.09 (0.04)	0.07 (0.02)	0.08 (0.05)
	La ₂ O ₃	15.59 (0.38)	14.48 (0.16)	14.04 (0.17)	17.98 (0.18)	18.07 (0.12)	17.91 (0.25)
	Ce ₂ O ₃	30.44 (0.50)	28.57 (0.32)	26.69 (0.34)	31.88 (0.25)	31.77 (0.15)	31.07 (0.29)
	Pr ₂ O ₃	3.47 (0.04)	3.30 (0.04)	3.04 (0.05)	3.39 (0.05)	3.37 (0.04)	3.30 (0.05)
	Nd ₂ O ₃	10.83 (0.09)	10.52 (0.16)	9.43 (0.17)	10.62 (0.16)	10.53 (0.11)	10.28 (0.22)
	Sm ₂ O ₃	1.40 (0.08)	1.34 (0.06)	1.07 (0.05)	1.10 (0.05)	1.09 (0.03)	1.05 (0.06)
	Gd ₂ O ₃	0.67 (0.06)	0.63 (0.03)	0.47 (0.03)	0.44 (0.04)	0.45 (0.02)	0.43 (0.05)
	PbO	0.57 (0.22)	0.44 (0.18)	0.95 (0.20)	0.02 (0.03)	0.01 (0.02)	0.07 (0.13)
	ThO ₂	7.06 (0.46)	11.07 (0.68)	15.93 (0.80)	4.57 (0.48)	4.85 (0.24)	6.19 (0.52)
	UO ₂	0.10 (0.01)	0.11 (0.01)	0.10 (0.01)	0.05 (0.01)	0.05 (0.01)	0.07 (0.02)
	Total	101.34	101.07	101.49	100.48	100.52	100.63

*Turlin et al. - Unusual LREE-rich, post-tectonic, monazite- or allanite-bearing pegmatitic
granites
in the central Grenville Province, Québec*

	(0.24)	(0.24)	(0.20)	(0.17)	(0.12)	(0.15)
Oxygens	4	4	4	4	4	4
Cations						
P	0.963 (0.005)	0.927 (0.008)	0.876 (0.010)	0.965 (0.004)	0.962 (0.002)	0.950 (0.005)
Si	0.039 (0.005)	0.076 (0.008)	0.127 (0.010)	0.041 (0.004)	0.043 (0.002)	0.055 (0.005)
ΣT-site	1.002 (0.001)	1.004 (0.001)	1.003 (0.001)	1.006 (0.001)	1.005 (0.001)	1.005 (0.001)
Ca	0.037 (0.006)	0.039 (0.005)	0.039 (0.005)	0.013 (0.001)	0.013 (0.001)	0.016 (0.001)
Y	0.005 (0.001)	0.004 (0.001)	0.002 (0.000)	0.002 (0.001)	0.001 (0.000)	0.002 (0.001)
La	0.225 (0.006)	0.212 (0.002)	0.209 (0.002)	0.261 (0.003)	0.262 (0.002)	0.261 (0.004)
Ce	0.436 (0.008)	0.415 (0.004)	0.395 (0.004)	0.459 (0.003)	0.458 (0.002)	0.449 (0.004)
Pr	0.049 (0.001)	0.048 (0.001)	0.045 (0.001)	0.049 (0.001)	0.048 (0.001)	0.047 (0.001)
Nd	0.151 (0.001)	0.149 (0.002)	0.136 (0.002)	0.149 (0.002)	0.148 (0.002)	0.145 (0.003)
Sm	0.019 (0.001)	0.018 (0.001)	0.015 (0.001)	0.015 (0.001)	0.015 (0.000)	0.014 (0.001)
Gd	0.009 (0.001)	0.008 (0.000)	0.006 (0.000)	0.006 (0.001)	0.006 (0.000)	0.006 (0.001)
Pb	0.006 (0.002)	0.005 (0.002)	0.010 (0.002)	0.000 (0.000)	0.000 (0.000)	0.001 (0.001)
Th	0.063 (0.004)	0.100 (0.006)	0.147 (0.008)	0.041 (0.004)	0.043 (0.002)	0.056 (0.005)
U	0.001 (0.000)	0.001 (0.000)	0.001 (0.000)	0.000 (0.000)	0.000 (0.000)	0.001 (0.000)
Σa-site	1.003 (0.002)	1.000 (0.002)	1.004 (0.003)	0.995 (0.002)	0.996 (0.002)	0.997 (0.002)
% Hutt.	3.78 (0.46)	7.47 (0.76)	12.27 (0.98)	4.02 (0.45)	4.27 (0.22)	5.39 (0.54)
% Brab.	8.66 (1.20)	8.85 (0.81)	9.62 (0.95)	2.77 (0.27)	2.68 (0.20)	3.37 (0.27)

*Turlin et al. - Unusual LREE-rich, post-tectonic, monazite- or allanite-bearing pegmatitic
granites
in the central Grenville Province, Québec*

% Mnz.	87.56	83.68	78.11	93.21	93.05	91.24
+ Xen.	(0.92)	(0.85)	(0.96)	(0.48)	(0.27)	(0.53)
n	20	23	29	17	27	22

559

560

ACCEPTED MANUSCRIPT

561 **Table 4:** Analyses of allanite grains from the 13-TC-5072 and 13-FS-1202 pegmatitic granite
 562 dykes from the Lac Okaopéo region. Data were obtained using EMP and were performed on
 563 LREE(Ce)-rich zones, intermediate zones and alteration rims of allanite grains from the 13-
 564 TC-5072 pegmatitic granite, and on LREE(Ce)-rich zones, Fe-Ca-LREE(Ce)-rich zones and
 565 alteration rims of allanite grains from the 13-FS-1202 pegmatitic granite. They are reported
 566 with confidence interval of 95% in brackets (n = number of analyses). Abbreviations: Aln =
 567 allanite.

<i>Sample</i>		<i>13-TC-5072</i>			<i>13-FS-1202</i>		
Zonation		Intermediate	LREE(Ce)-rich	Alteration	Fe-Ca-	Alteration	
type		(Aln₁)	(Aln₂)	rims	LREE(Ce)-rich	rims	
Oxides/wt.%	SiO ₂	31.97 (0.25)	31.82 (0.54)	32.30 (0.44)	33.52 (0.28)	32.81 (0.37)	35.77 (0.81)
	P ₂ O ₅	0.22 (0.01)	0.21 (0.01)	0.25 (0.02)	0.23 (0.02)	0.24 (0.00)	0.22 (0.02)
	CaO	9.88 (0.12)	10.02 (0.23)	9.75 (0.20)	10.73 (0.25)	11.27 (0.19)	9.55 (0.47)
	Y ₂ O ₃	0.00 (0.00)	0.00 (0.00)	0.00 (0.00)	0.00 (0.00)	0.00 (0.00)	0.00 (0.00)
	La ₂ O ₃	6.20 (0.25)	6.41 (0.31)	6.17 (0.15)	5.35 (0.05)	5.34 (0.09)	4.79 (0.13)
	Ce ₂ O ₃	11.69 (0.32)	11.83 (0.48)	11.55 (0.25)	10.49 (0.19)	10.53 (0.17)	9.97 (0.31)
	Pr ₂ O ₃	1.35 (0.05)	1.32 (0.05)	1.30 (0.03)	1.29 (0.01)	1.29 (0.02)	1.25 (0.03)
	Nd ₂ O ₃	3.73 (0.13)	3.79 (0.17)	3.71 (0.10)	3.95 (0.03)	3.90 (0.06)	3.85 (0.11)
	Sm ₂ O ₃	0.33 (0.02)	0.35 (0.02)	0.34 (0.01)	0.48 (0.01)	0.48 (0.01)	0.50 (0.02)
	Gd ₂ O ₃	0.00 (0.00)	0.00 (0.00)	0.00 (0.00)	0.00 (0.00)	0.00 (0.00)	0.00 (0.00)
	ΣREE ₂ O ₃	23.30 (0.73)	23.70 (1.01)	23.07 (0.52)	21.57 (0.24)	21.54 (0.34)	20.36 (0.55)
	FeO	11.11	10.54	9.76	8.41	9.73	7.97

*Turlin et al. - Unusual LREE-rich, post-tectonic, monazite- or allanite-bearing pegmatitic
granites
in the central Grenville Province, Québec*

	(0.94)	(0.36)	(0.31)	(0.21)	(0.28)	(0.47)
K ₂ O	0.01	0.02	0.03	0.01	0.02	0.03
	(0.01)	(0.00)	(0.01)	(0.00)	(0.01)	(0.01)
MgO	0.43	0.34	0.33	0.31	0.41	0.35
	(0.12)	(0.03)	(0.03)	(0.04)	(0.05)	(0.07)
Al ₂ O ₃	18.94	18.63	18.92	18.88	18.44	18.93
	(0.53)	(0.22)	(0.25)	(0.17)	(0.19)	(0.36)
TiO ₂	0.95	0.92	1.05	0.85	0.81	0.95
	(0.06)	(0.04)	(0.07)	(0.03)	(0.04)	(0.07)
MnO	0.27	0.29	0.30	0.34	0.30	0.33
	(0.07)	(0.03)	(0.02)	(0.02)	(0.01)	(0.02)
SrO	0.09	0.13	0.14	0.26	0.23	0.25
	(0.04)	(0.02)	(0.02)	(0.01)	(0.01)	(0.03)
PbO	0.04	0.04	0.04	0.03	0.04	0.04
	(0.00)	(0.00)	(0.01)	(0.00)	(0.00)	(0.00)
ThO ₂	0.69	0.62	0.73	1.12	1.00	1.19
	(0.06)	(0.04)	(0.04)	(0.04)	(0.07)	(0.08)
UO ₂	0.01	0.01	0.01	0.01	0.01	0.01
	(0.01)	(0.00)	(0.00)	(0.00)	(0.00)	(0.00)
F	0.46	0.70	0.63	0.52	0.55	0.44
	(0.11)	(0.21)	(0.09)	(0.02)	(0.02)	(0.03)
Total	98.37	97.98	97.31	96.79	97.38	96.39
	(0.88)	(0.35)	(0.45)	(0.28)	(0.27)	(0.85)
Oxygens	12.5	12.5	12.5	12.5	12.5	12.5
Cations						
Si	2.968	2.961	2.999	3.090	3.033	3.240
	(0.021)	(0.038)	(0.024)	(0.020)	(0.022)	(0.051)
P	0.017	0.017	0.019	0.018	0.019	0.017
	(0.001)	(0.000)	(0.002)	(0.001)	(0.000)	(0.001)
Ca	0.983	0.999	0.971	1.061	1.119	0.929
	(0.016)	(0.020)	(0.022)	(0.025)	(0.022)	(0.047)
Y	0.000	0.000	0.000	0.000	0.000	0.000
	(0.000)	(0.000)	(0.000)	(0.000)	(0.000)	(0.000)
La	0.212	0.220	0.212	0.182	0.182	0.161
	(0.009)	(0.012)	(0.006)	(0.002)	(0.003)	(0.005)
Ce	0.397	0.404	0.393	0.354	0.357	0.332
	(0.011)	(0.019)	(0.010)	(0.007)	(0.006)	(0.012)

*Turlin et al. - Unusual LREE-rich, post-tectonic, monazite- or allanite-bearing pegmatitic
granites
in the central Grenville Province, Québec*

Pr	0.046 (0.002)	0.045 (0.002)	0.044 (0.001)	0.043 (0.001)	0.044 (0.001)	0.041 (0.001)
Nd	0.124 (0.004)	0.126 (0.006)	0.123 (0.004)	0.130 (0.001)	0.129 (0.002)	0.125 (0.004)
Sm	0.010 (0.001)	0.011 (0.001)	0.011 (0.000)	0.015 (0.000)	0.015 (0.000)	0.015 (0.001)
Gd	0.000 (0.000)	0.000 (0.000)	0.000 (0.000)	0.000 (0.000)	0.000 (0.000)	0.000 (0.000)
ΣREE	0.789 (0.025)	0.806 (0.039)	0.783 (0.020)	0.725 (0.009)	0.727 (0.012)	0.675 (0.021)
Fe	0.862 (0.073)	0.820 (0.026)	0.759 (0.025)	0.649 (0.017)	0.754 (0.023)	0.605 (0.036)
K	0.002 (0.001)	0.002 (0.001)	0.004 (0.001)	0.002 (0.000)	0.002 (0.001)	0.004 (0.001)
Mg	0.059 (0.017)	0.048 (0.005)	0.046 (0.004)	0.042 (0.006)	0.056 (0.007)	0.047 (0.009)
Al	2.072 (0.053)	2.044 (0.018)	2.071 (0.018)	2.050 (0.015)	2.010 (0.018)	2.024 (0.035)
Ti	0.066 (0.004)	0.065 (0.003)	0.073 (0.005)	0.059 (0.002)	0.056 (0.003)	0.065 (0.005)
Mn	0.021 (0.005)	0.023 (0.003)	0.024 (0.002)	0.027 (0.002)	0.023 (0.001)	0.025 (0.002)
Sr	0.005 (0.002)	0.007 (0.001)	0.008 (0.001)	0.014 (0.001)	0.012 (0.001)	0.013 (0.002)
Pb	0.001 (0.000)	0.001 (0.000)	0.001 (0.000)	0.001 (0.000)	0.001 (0.000)	0.001 (0.000)
Th	0.015 (0.001)	0.013 (0.001)	0.015 (0.001)	0.024 (0.001)	0.021 (0.002)	0.025 (0.002)
U	0.000 (0.000)	0.000 (0.000)	0.000 (0.000)	0.000 (0.000)	0.000 (0.000)	0.000 (0.000)
F	0.135 (0.032)	0.207 (0.063)	0.185 (0.028)	0.153 (0.006)	0.160 (0.006)	0.127 (0.009)
Total	7.996 (0.027)	8.012 (0.022)	7.958 (0.023)	7.913 (0.019)	7.994 (0.018)	7.994 (0.018)
n	14	26	47	91	122	52

ACCEPTED MANUSCRIPT

570 **Table 5:** U-Pb monazite dating using LA-ICP-MS from the 13-AM-13 and 13-TC-5008

571 monazite-bearing pegmatitic granite dykes from the Lac Okaopéo region. Abbreviations:

572 Conc. (%) = degree of concordance.

573

Sampl e	Analysi s no.	Isotopic ratios	Ages / Ma									
		$^{206}\text{Pb}/^{238}\text{U}$	1σ	$^{207}\text{Pb}/^{235}\text{U}$	1σ	$^{207}\text{Pb}/^{206}\text{Pb}$	1σ	$^{206}\text{Pb}/^{238}\text{U}$	1σ	$^{207}\text{Pb}/^{235}\text{U}$	1σ	Conc . (%)
13- AM-13	1-1	0.1641	0.002 0	1.645	0.02 2	1006.2	24.6 2	979.3	10. 9	987.6	8.6	98.2
	1-2	0.1589	0.001 9	1.593	0.02 1	1005.2	23.8 4	950.9	10. 6	967.4	8.3	96.2
	1-3	0.1646	0.002 0	1.650	0.02 2	1005.5	24.1 2	982.3	11. 0	989.5	8.5	98.4
	1-4	0.1620	0.002 0	1.628	0.02 4	1010.8	27.5 8	967.8	10. 9	981.1	9.4	97.1
	1-5	0.1560	0.001 9	1.564	0.02 0	1006.6	22.9 7	934.4	10. 4	956.1	8.0	95.0
2	2-1	0.1640	0.002 0	1.641	0.02 1	1001.1	22.5 4	979.1	10. 9	985.9	8.1	98.5
	2-2	0.1573	0.001 9	1.571	0.02 0	997.4	22.4 8	941.9	10. 5	958.7	7.9	96.1
	2-3	0.1626	0.002 0	1.630	0.02 2	1004.8	23.5 9	971.5	10. 8	981.7	8.3	97.7
	2-4	0.1666	0.002 0	1.671	0.02 4	1007.5	26.0 5	993.1	11. 2	997.6	9.1	99.0
	2-5	0.1595	0.001 9	1.597	0.02 2	1003.7	24.5 7	953.7	10. 7	968.9	8.5	96.5
3	3-1	0.1687	0.002 0	1.703	0.02 4	1019.6	25.5 9	1005.2	11. 3	1009.7	9.0	99.0
	3-2	0.1601	0.001 9	1.605	0.02 1	1005.2	22.8 9	957.5	10. 7	972.1	8.1	96.7
4	4-1	0.1587	0.001 9	1.590	0.02 1	1005.0	23.1 9	949.4	10. 6	966.3	8.1	96.1

*Turlin et al. - Unusual LREE-rich, post-tectonic, monazite- or allanite-bearing pegmatitic
granites
in the central Grenville Province, Québec*

	4-2	0.1606	0.001 9	1.608	0.02 1	1004.1	23.3 1	959.9	10. 7	973.4	8.2	96.9
	5-1	0.1629	0.002 0	1.636	0.02 2	1009.7	23.4 6	972.8	10. 9	984.2	8.3	97.5
	5-2	0.1628	0.002 0	1.631	0.02 2	1005.0	23.5 0	972.3	10. 9	982.4	8.3	97.8
	5-4	0.1613	0.001 9	1.622	0.02 2	1012.2	23.6 9	964.0	10. 8	978.8	8.3	96.7
	6-1	0.1680	0.002 1	1.681	0.02 5	1001.9	27.4 5	1001.0	11. 3	1001.3	9.5	99.9
	6-2	0.1641	0.002 0	1.650	0.02 3	1013.1	24.5 1	979.2	11. 0	989.7	8.6	97.7
	6-3	0.1688	0.002 0	1.684	0.02 3	996.8	24.4 0	1005.3	11. 2	1002.6	8.6	100.6
	6-4	0.1687	0.002 0	1.669	0.02 3	978.4	25.5 8	1005.2	11. 3	996.8	8.9	101.9
	6-5	0.1687	0.002 0	1.669	0.02 3	979.7	25.2 0	1004.9	11. 3	997.0	8.8	101.8
	7-1	0.1613	0.002 0	1.620	0.02 2	1009.7	24.9 2	964.1	10. 8	978.1	8.7	96.9
	7-2	0.1663	0.002 0	1.666	0.02 6	1004.2	29.0 3	991.7	11. 3	995.6	9.9	99.1
	7-3	0.1675	0.002 0	1.677	0.02 4	1004.3	25.6 6	998.1	11. 2	1000.0	9.0	99.6
13-TC-5008	1-1	0.1700	0.002 1	1.678	0.02 3	974.6	24.7	1012.3	11. 6	1000.4	8.8	102.6
	1-2	0.1689	0.002 1	1.703	0.02 7	1018.8	29.2	1005.8	11. 7	1009.8	10. 1	99.1
	2-1	0.1689	0.002 1	1.745	0.02 7	1067.5	28.3	1005.9	11. 7	1025.4	10. 0	96.1
	2-2	0.1692	0.002 1	1.692	0.02 7	1001.0	29.7	1007.6	11. 8	1005.5	10. 2	100.4
	3-1	0.1689	0.002 2	1.724	0.03 2	1041.7	35.6	1006.1	12. 0	1017.3	12. 0	97.7
	3-2	0.1692	0.002 1	1.700	0.02 4	1010.8	25.3	1007.7	11. 6	1008.6	9.0	99.8

*Turlin et al. - Unusual LREE-rich, post-tectonic, monazite- or allanite-bearing pegmatitic
granites
in the central Grenville Province, Québec*

	4-2	0.1683	0.002 1	1.700	0.02 6	1020.8	27.9	1003.0	11. 6	1008.5	9.7	98.8
	5-1	0.1694	0.002 1	1.688	0.02 5	993.4	27.0	1008.8	11. 7	1003.9	9.4	101.1
	5-2	0.1688	0.002 1	1.690	0.02 7	1003.3	29.2	1005.3	11. 7	1004.6	10. 0	100.1
	5-3	0.1686	0.002 1	1.659	0.02 7	967.2	31.2	1004.6	11. 8	992.8	10. 5	102.6
	5-4	0.1686	0.002 1	1.699	0.02 5	1015.5	27.5	1004.6	11. 6	1008.0	9.6	99.3
	6-1	0.1686	0.002 1	1.684	0.02 6	998.4	28.5	1004.4	11. 7	1002.4	9.8	100.4
	7-1	0.1686	0.002 1	1.706	0.02 8	1024.6	30.8	1004.4	11. 8	1010.7	10. 6	98.6
	7-2	0.1695	0.002 2	1.694	0.02 9	1000.0	32.2	1009.4	11. 9	1006.4	10. 9	100.6
	8-1	0.1684	0.002 1	1.630	0.02 7	933.9	31.8	1003.3	11. 8	981.7	10. 5	105.1
	8-2	0.1688	0.002 2	1.669	0.03 0	978.2	34.7	1005.5	12. 0	996.9	11. 5	101.9
	8-3	0.1696	0.002 2	1.691	0.03 0	994.7	33.5	1009.9	12. 0	1005.0	11. 3	101.0
	9-1	0.1678	0.002 2	1.714	0.03 1	1043.3	34.0	1000.2	11. 9	1013.7	11. 5	97.2
	9-2	0.1690	0.002 1	1.715	0.02 9	1031.4	31.1	1006.4	11. 8	1014.2	10. 7	98.3
	9-3	0.1689	0.002 2	1.685	0.02 9	995.9	32.9	1006.1	11. 9	1002.8	11. 1	100.7
	9-4	0.1698	0.002 3	1.694	0.03 6	996.9	41.4	1010.8	12. 4	1006.3	13. 6	100.9
	9-5	0.1684	0.002 2	1.701	0.03 3	1021.3	37.0	1003.4	12. 1	1008.9	12. 4	98.8

574

575

Turlin et al. - Unusual LREE-rich, post-tectonic, monazite- or allanite-bearing pegmatitic granites in the central Grenville Province, Québec

576 **Table 6:** Summary of the main characteristics of the REE-rich pegmatitic granite dykes from
 577 the Lac Okaopéo region, first ordered by type of occurrence then from north to south.
 578 Abbreviations: Aln-bearing = allanite-bearing pegmatitic granite dyke; ASI = Aluminum
 579 Saturation Index given by the expression $ASI = Al / (Ca - 1.67 \times P + Na + K)$ (Frost et al.,
 580 2001; Shand, 1943); Mnz-bearing = monazite-bearing pegmatitic granite dyke.

Type of REE occurrence	Outcrop n°	Field expression	Dip	Contact	Texture (from contact towards core)	Accessory minerals ¹	Geochemical features	Geochronology (U-Pb on monazite)	
						Type	REE-bearing phase composition		
<i>Mnz-bearing</i>	13-AM-07	Single dyke	Steep-dipping	Slightly diffuse – Discordant	Stockschi-der contact – fine-grained – pegmatitic	Zircon-monazite	-	<i>High:</i> ASI, Σ LREE, La _N /Yb _N , Th, Zr/Hf, Zr and Hf, Nb/Ta <i>Low:</i> Σ HREE, Eu/Eu*, Nb and Ta <i>Positive correlation:</i> P ₂ O ₅ and CaO with Σ REE	-
	13-AM-10	Single dyke	Steep-dipping		Fine-grained	Zircon-monazite	-		-
	13-AM-13	Single dyke	Steep-dipping		Patchy zoning (fine-grained to pegmatitic)	Zircon-monazite-(Ce)-minor garnet and Ti-oxides)	LREE-rich cores/Th-Si-rich overgrowths		996.7±5.3 Ma
	13-TC-5008	Single dyke	Steep-dipping	Locally diffuse – Discordant	Patchy zoning (coarse-grained to skeletal Bt-rich)	Zircon-monazite-(Ce)-minor garnet)	Rather homogeneous		1005.4±4.4 Ma
<i>Aln-bearing</i>	13-TC-5072	Dyke swarm	Steep-dipping	Slightly diffuse – Discordant to sub-concordant	Fine-grained – pegmatitic	Zircon-allanite-(Ce)	Homogeneous cores – Fe-rich rims	<i>High:</i> ASI, Σ LREE, La _N /Yb _N , Th, Zr/Hf, Zr and Hf, Nb/Ta <i>Low:</i> Σ HREE, Eu/Eu*, Nb and Ta <i>Positive correlation:</i> Fe ₂ O ₃ (total) and MgO with Σ REE	-
	13-FS-1202	Dyke swarm	Steep-dipping	Slightly diffuse – Discordant	Patchy to layered zoning (fine-grained to	Zircon-allanite-(Ce)	LREE-rich – Fe-Ca-LREE-rich cores – Si-rich/LREE-		-

Turlin et al. - Unusual LREE-rich, post-tectonic, monazite- or allanite-bearing pegmatitic granites in the central Grenville Province, Québec

	13-AE-2149	Single dyke connected to concordant/discordant veins	Shallow-dipping	Very diffuse – Discordant to sub-concordant	pegmatitic) Pegmatitic contacts – fine-grained core	Zircon-allanite(-rare apatite)	poor rims	$\frac{La_N}{Yb_N}$, $\frac{Nb}{Ta}$, $\frac{Eu}{Eu^*}$ <i>Lower</i> ² : ASI, <i>Higher</i> ² : $\Sigma LREE$, $\Sigma HREE$, Zr and Hf, Nb and Ta <i>Intermediate</i> ² : Th, Zr/Hf	-
--	-------------------	--	-----------------	---	---	--------------------------------	-----------	---	---

581 ¹ All samples are dominated by a quartz+K-feldspar+plagioclase±biotite assemblage.

582 ² In comparison with the other dykes investigated in this study.

583

584 **Appendix C:** Planar fabrics measured on the pegmatitic granite dykes from the Lac Okaopéo
585 region, first ordered by type of occurrence then from north to south. Planar structures are
586 plotted in stereograms in Fig. 5 and are represented on detailed mapping of each outcrop from
587 Appendices A and B.

ACCEPTED MANUSCRIPT

Type of REE occurrence	Mona zite-bearing		Mona zite-bearing		Mona zite-bearing		Mona zite-bearing		Allan ite-bearing		Allani te-bearing		Allani te-bearing	
	13-AM-07		13-AM-10		13-AM-13		13-TC-5008		13-TC-5072		13-FS-1202		13-AE-2149	
Intruded unit	Plus-Valu e Complex		Plus-Valu e Complex		Plus-Valu e Complex		Plus-Valu e Complex		Bardoux Pluton ic Suite		Casto réum Pluton ic Suite		Casto réum Pluton ic Suite	
Planar structures	Folia tion ¹ ²	Dyke	Folia tion ¹ ²	Dyke	Folia tion ¹ ²	Dyke	Folia tion ¹ ²	Dyke	Folia tion ¹ ²	Dyke	Foliat ion ¹ ²	Dyke	Foliat ion ¹ ²	Dyke
	Strik e/Dip	Strik e/Dip	Strik e/Dip	Strik e/Dip	Strik e/Dip	Strik e/Dip	Strik e/Dip	Strik e/Dip	Strik e/Dip	Strik e/Dip	Strike /Dip	Strik e/Dip	Strike /Dip	Strik e/Dip
	066/83	089/78	159/55	264/58	200/56	140/62	091/61	078/83	072/76	-	037/57	251/64	278/34	292/09
	-	-	-	-	166/62	145/65	090/56	078/74	073/65	228/64	039/48	318/70	270/28	277/26
	-	-	-	-	-	-	096/57	328/64	098/62	225/56	053/67	102/79	-	-
	-	-	-	-	-	-	-	-	097/61	-	318/76	090/72	-	-
	-	-	-	-	-	-	-	-	090/71	-	337/77	-	-	-
	-	-	-	-	-	-	-	-	067/67	-	331/78	-	-	-
	-	-	-	-	-	-	-	-	087/73	030/77	025/64	275/79	-	-
	-	-	-	-	-	-	-	-	078/69	044/84	030/76	-	-	-
	-	-	-	-	-	-	-	-	079/76	053/82	042/74	-	-	-

*Turlin et al. - Unusual LREE-rich, post-tectonic, monazite- or allanite-bearing pegmatitic
granites
in the central Grenville Province, Québec*

	-	-	-	-	-	-	-	-	077/7	035/8	032/6	221/7	-	-
									9	2	8	2		
	-	-	-	-	-	-	-	-	075/4	-		068/7	-	-
									5			4		
	-	-	-	-	-	-	-	-	068/7	-	275/6	-	-	-
									9		0			
	-	-	-	-	-	-	-	-	247/7	-	046/6	233/8	-	-
									1		3	0		
	-	-	-	-	-	-	-	-	-	-	028/5	-	-	-
											3			
	-	-	-	-	-	-	-	-	-	-	034/6	200/7	-	-
											8	1		

588 ¹ Measures of the foliations of in the intruded lithologies

589 ² Measures of the contacts between the REE-rich pegmatitic granite dykes and their host rocks

590

591 **Appendix D: Operating conditions for the LA-ICP-MS equipment**

U-Pb monazite analyses	
Laboratory & Sample Preparation	
Laboratory name	Géosciences Rennes, UMR CNRS 6118, Université Rennes 1, Rennes, France
Sample type/mineral	Magmatic monazite
Sample preparation	Thin-sections
Imaging	Hitachi S-4800 SEM, GeoRessources, UMR 7359, Université de Lorraine, Vandœuvre-lès-Nancy, France
Laser ablation system	
Make, Model & type	ESI NWR193UC, Excimer
Ablation cell	ESI NWR TwoVol2
Laser wavelength	193 nm
Pulse width	< 5 ns
Fluence	6.5 J/cm ²
Repetition rate	2 Hz
Spot size	10 μm (round spot)
Sampling mode / pattern	Single spot
Carrier gas	100% He, Ar make-up gas and N ₂ (3 ml/min) combined using in-house smoothing device
Background collection	20 seconds
Ablation duration	60 seconds
Wash-out delay	10 seconds
Cell carrier gas flow (He)	0.75 l/min
ICP-MS Instrument	
Make, Model & type	Agilent 7700x, Q-ICP-MS
Sample introduction	Via conventional tubing
RF power	1350W
Sampler, skimmer cones	Ni
Extraction lenses	X type
Make-up gas flow (Ar)	0.87 l/min
Detection system	Single collector secondary electron multiplier
Data acquisition protocol	Time-resolved analysis
Scanning mode	Peak hopping, one point per peak
Detector mode	Pulse counting, dead time correction applied, and analog mode when signal intensity > ~ 10 ⁶ cps
Masses measured	²⁰⁴ (Hg + Pb), ²⁰⁶ Pb, ²⁰⁷ Pb, ²⁰⁸ Pb, ²³⁸ U
Sensitivity / Efficiency	25000 cps/ppm Pb (50μm, 10Hz)
Dwell time per isotope	10-30 ms depending on the masses
Data Processing	
Gas blank	20 seconds on-peak
Calibration strategy	Moacir Monazite used as primary reference material, Manangoutry Monazite used as secondary reference material (quality control)
Reference Material info	Moacir (Gasquet et al., 2010)
Manangoutry (Paquette and Tiepolo, 2007)	
Data processing package	Glitter (Van Achterbergh et al., 2001)
Quality control / Validation	Manangoutry: 554.8 ± 4.2 Ma (MSWD=0.94; n=8) (sample 13-AM-13)
554.4 ± 3.4 Ma (MSWD=0.94; n=8) (sample 13-TC-5008)	

592

593

Figure 1 (black and white; 2 columns fitting)

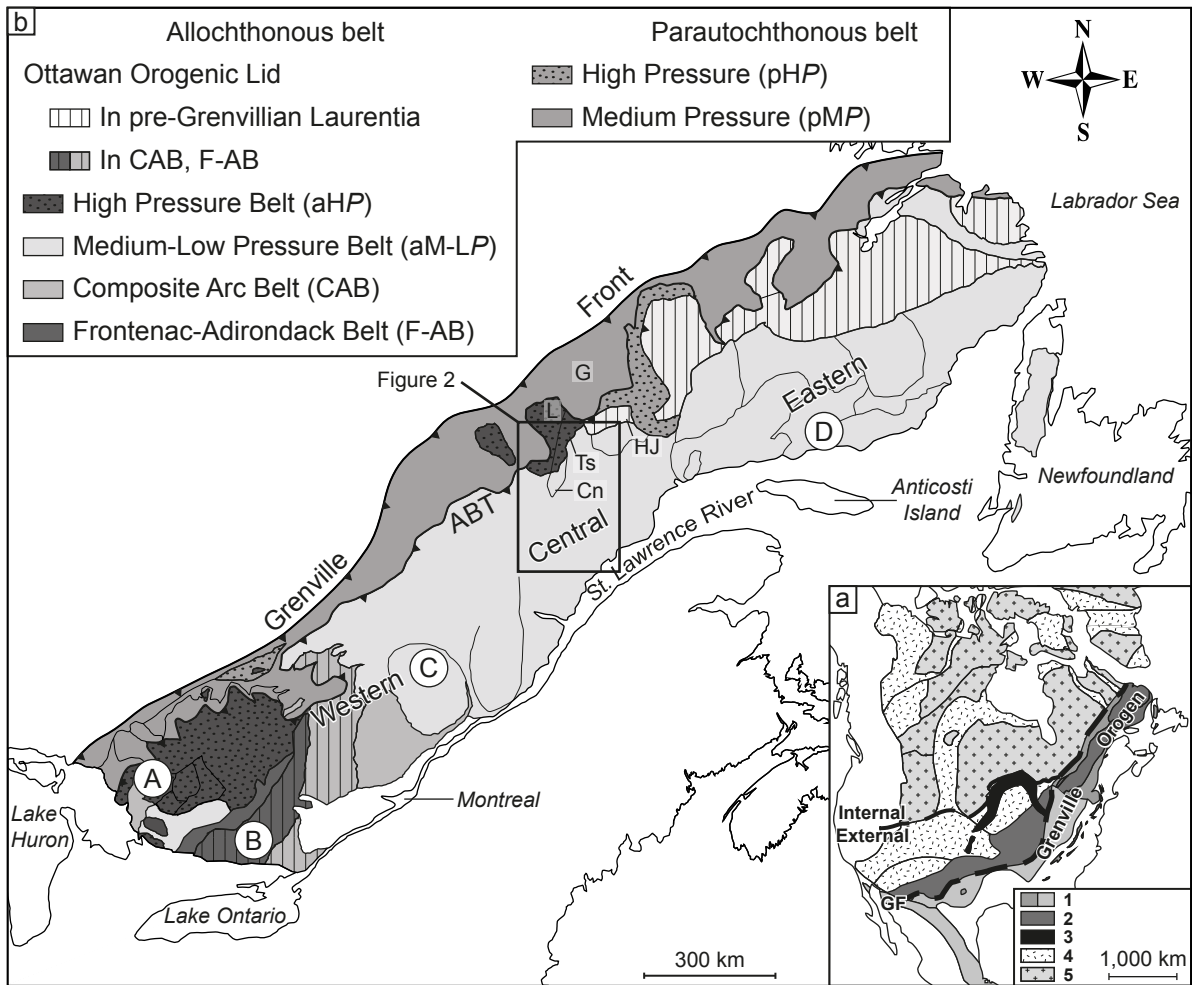
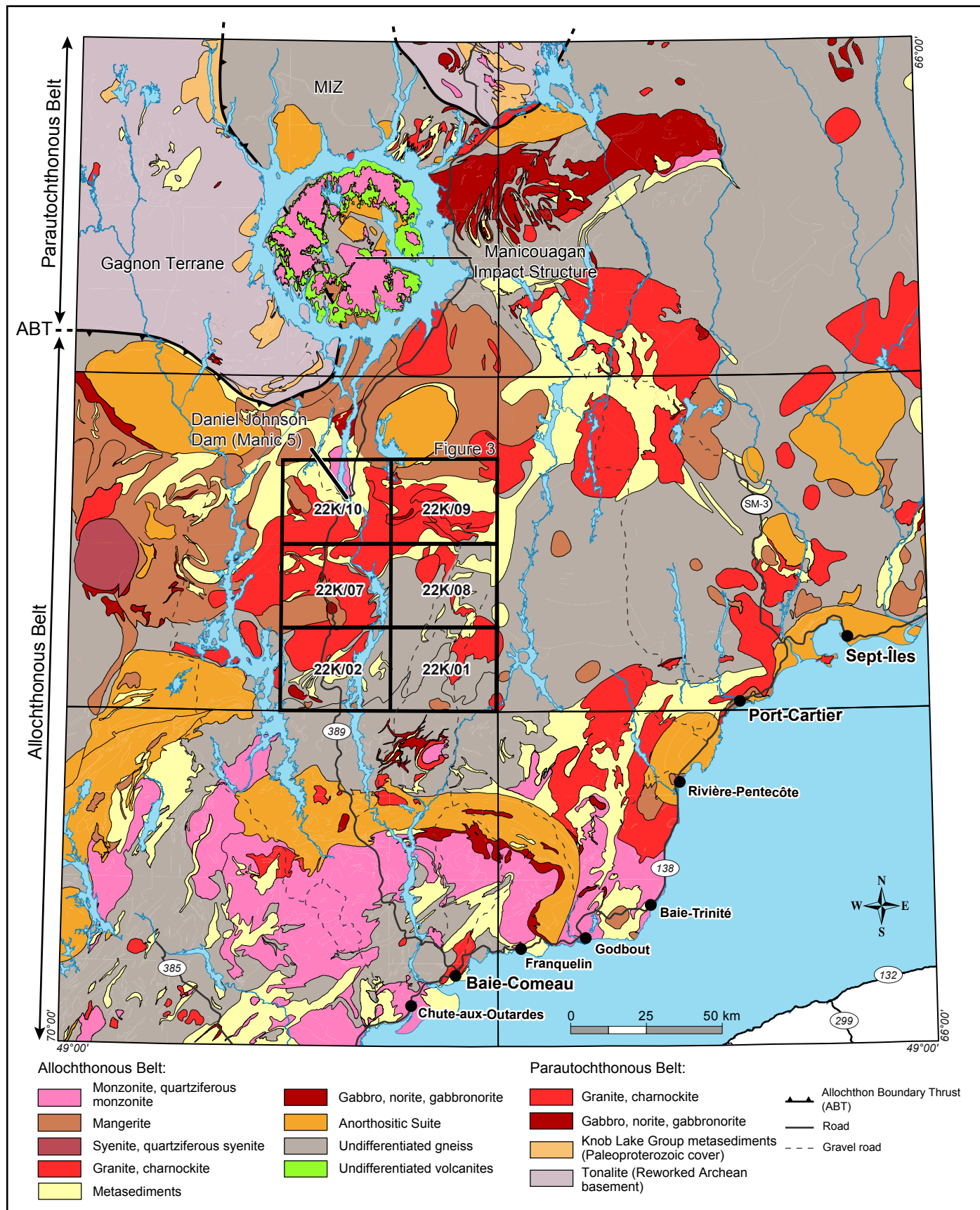
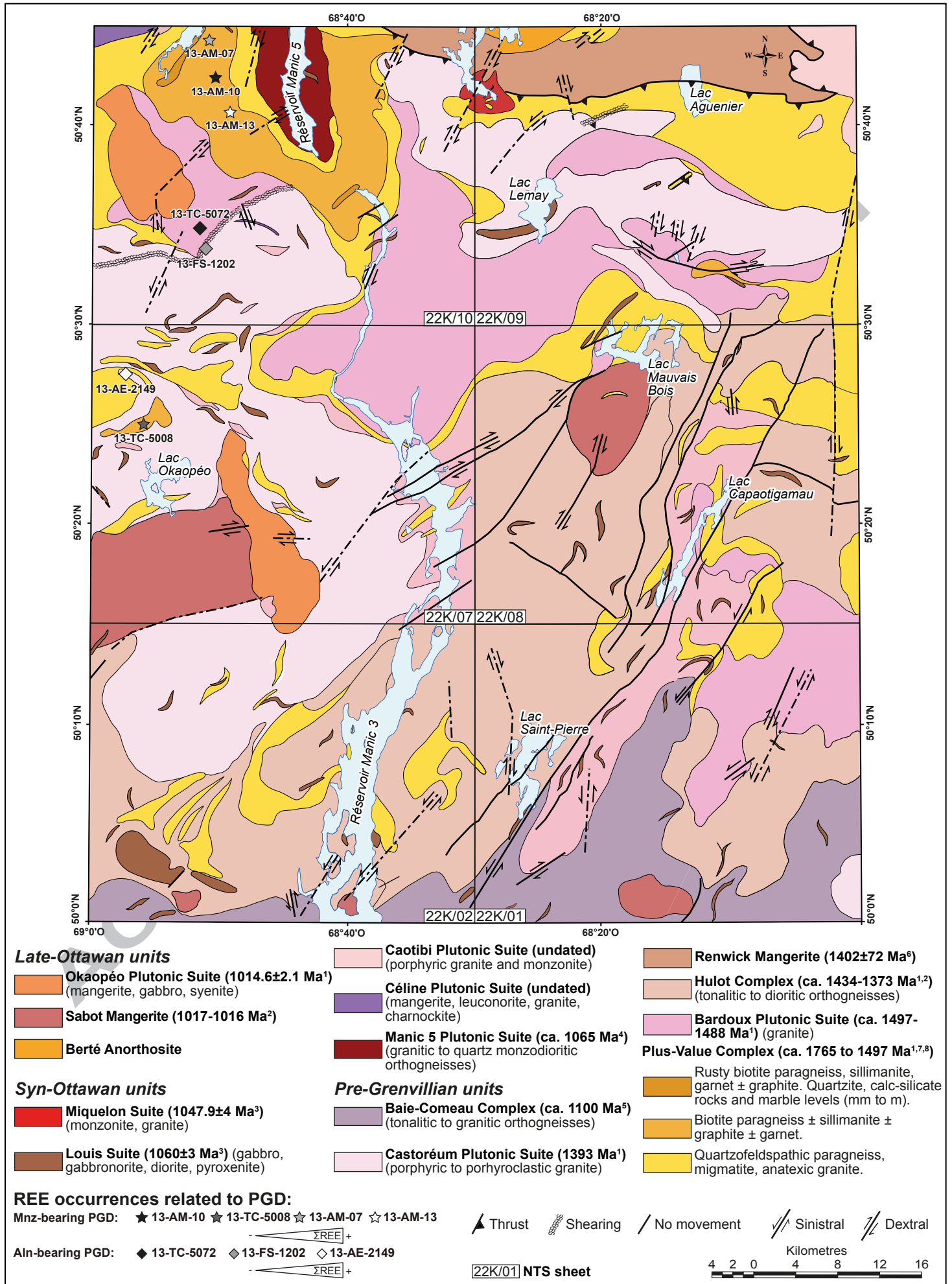


Figure 2 (color; 2 columns fitting)





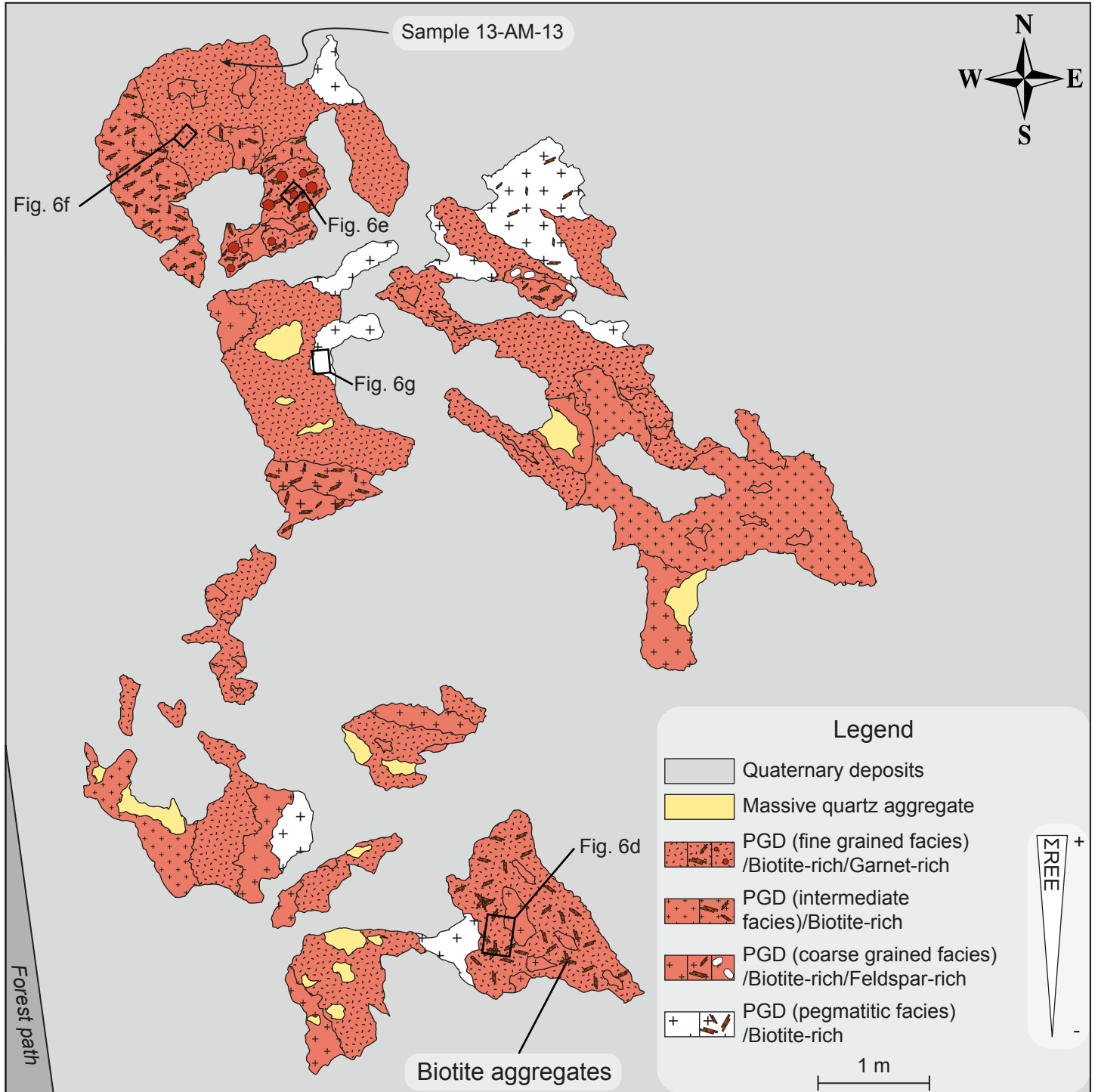


Figure 5 (black and white; 2 columns fitting)

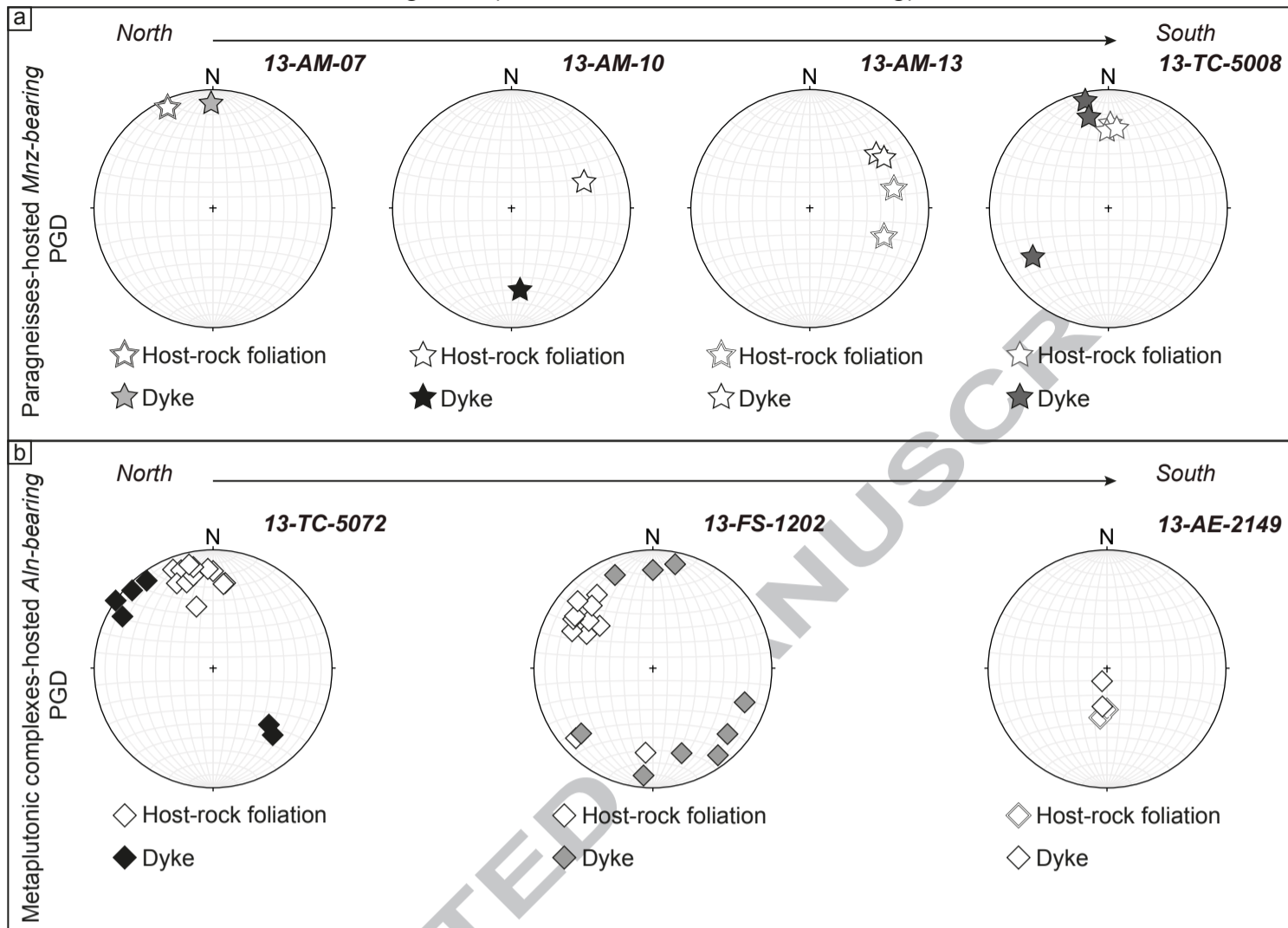


Figure 6 (color; 2 columns fitting)

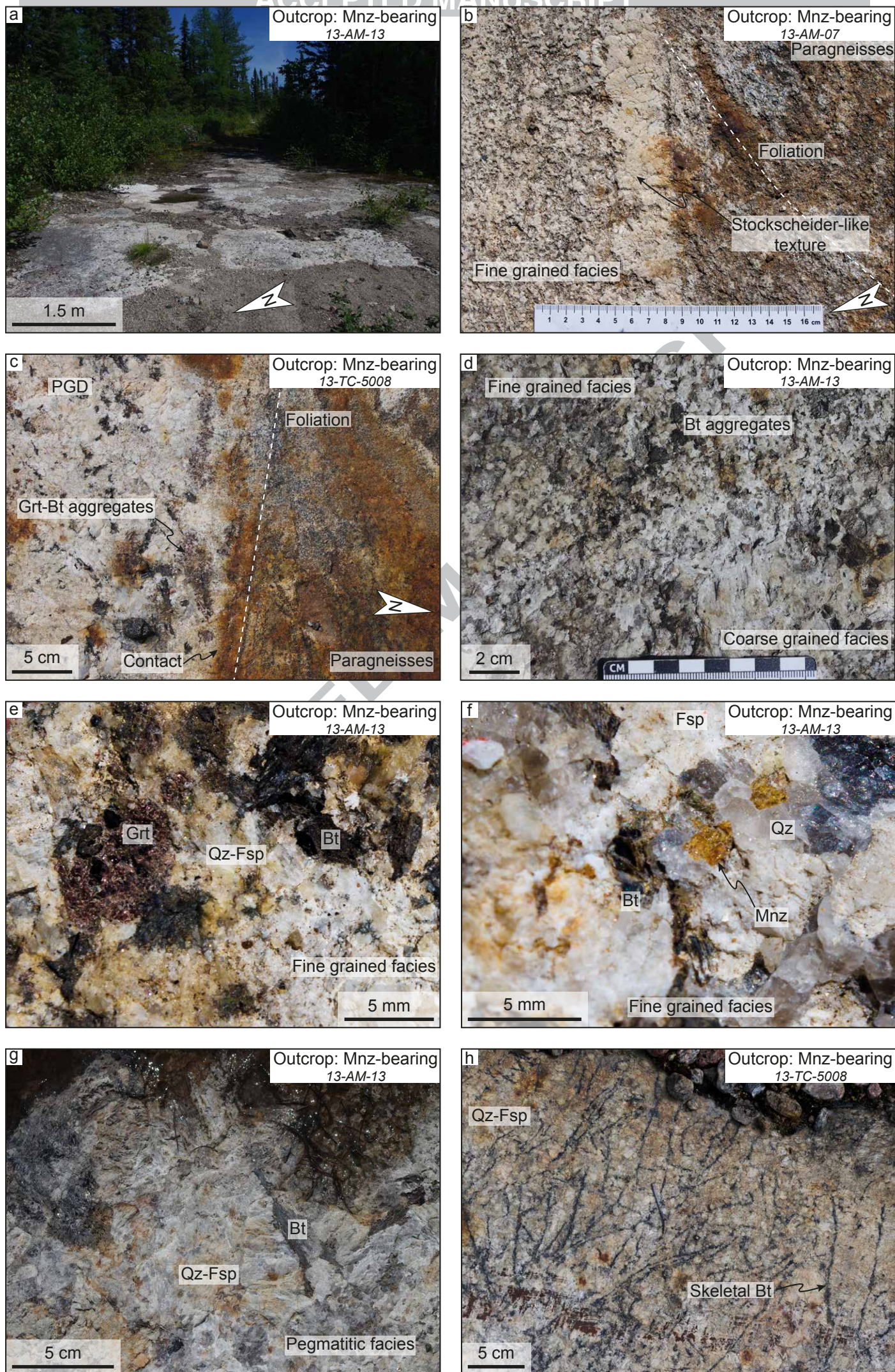


Figure 7 (color; 2 columns fitting)

ACCEPTED MANUSCRIPT

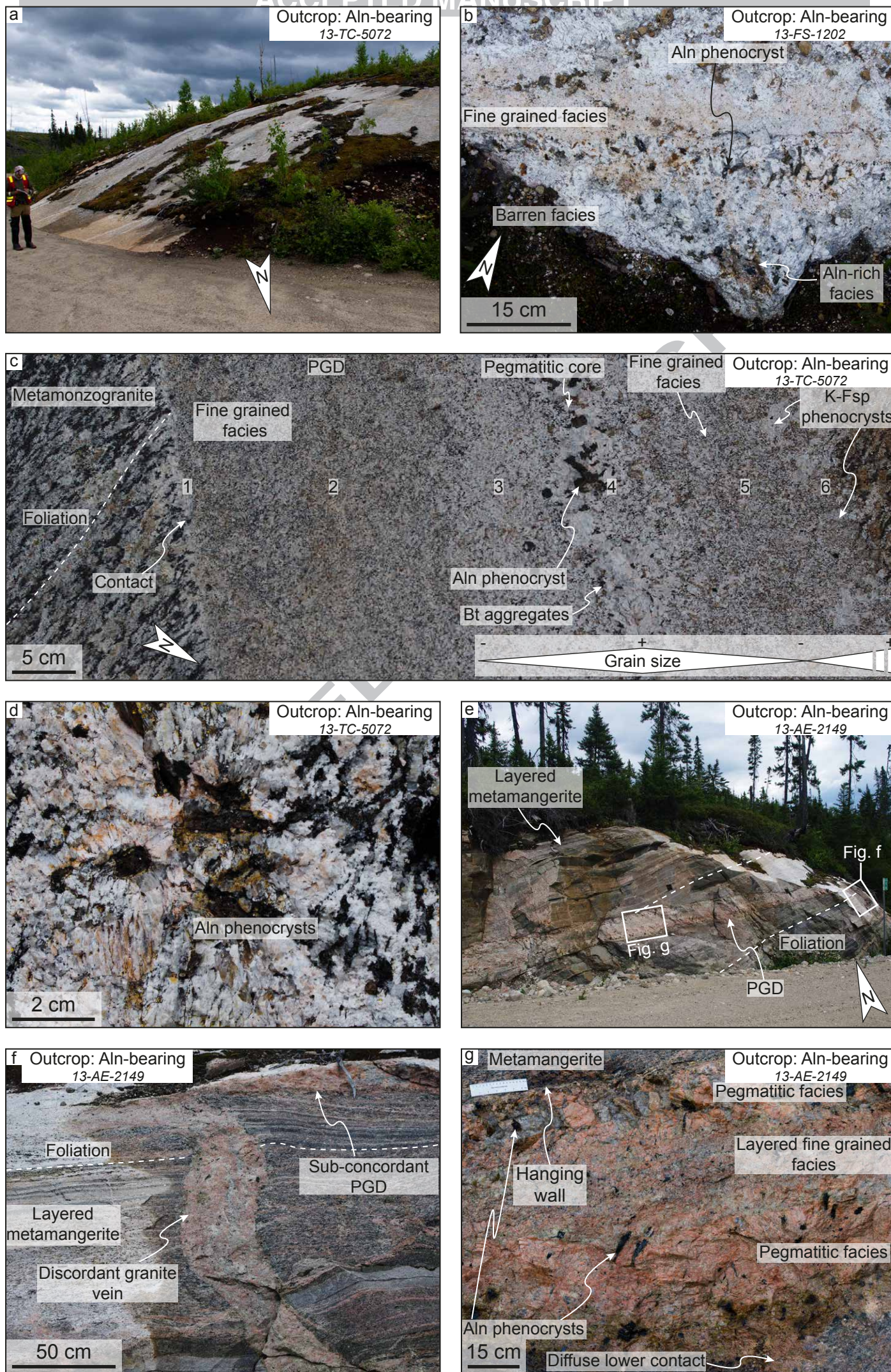


Figure 8 (color; 2 columns fitting)

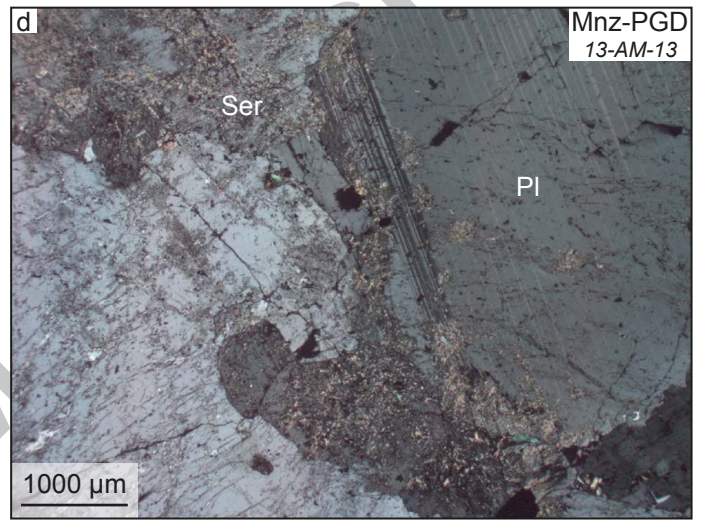
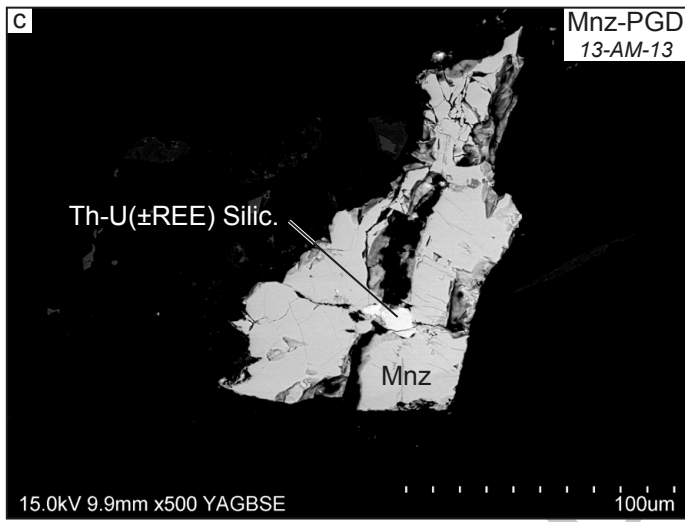
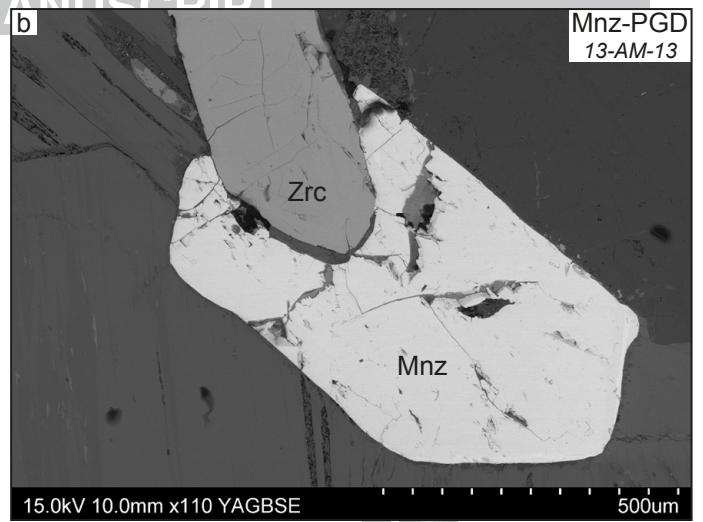
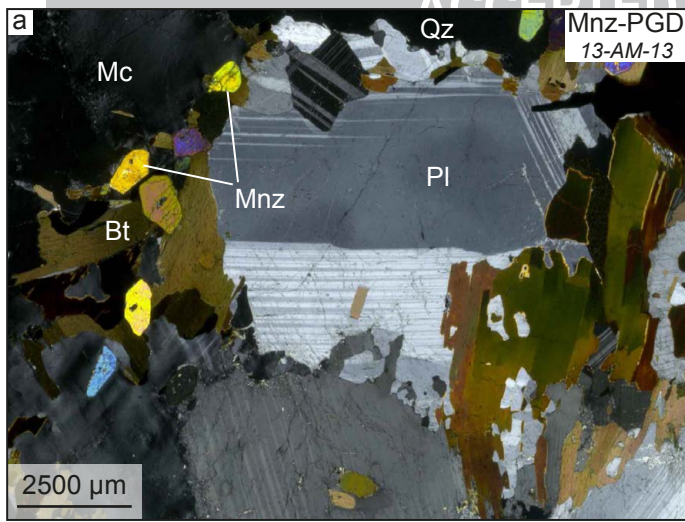
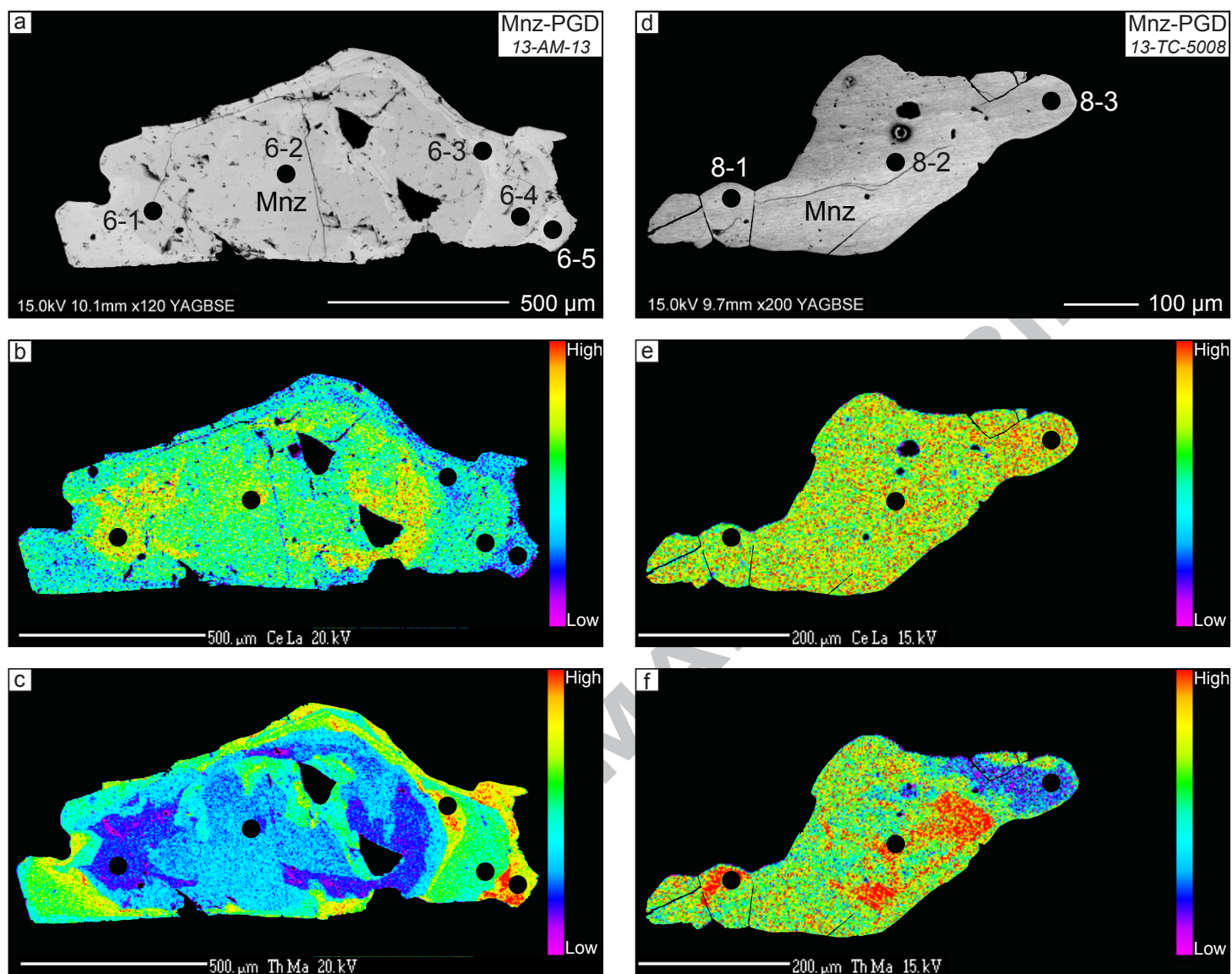


Figure 9 (color; 2 columns fitting)



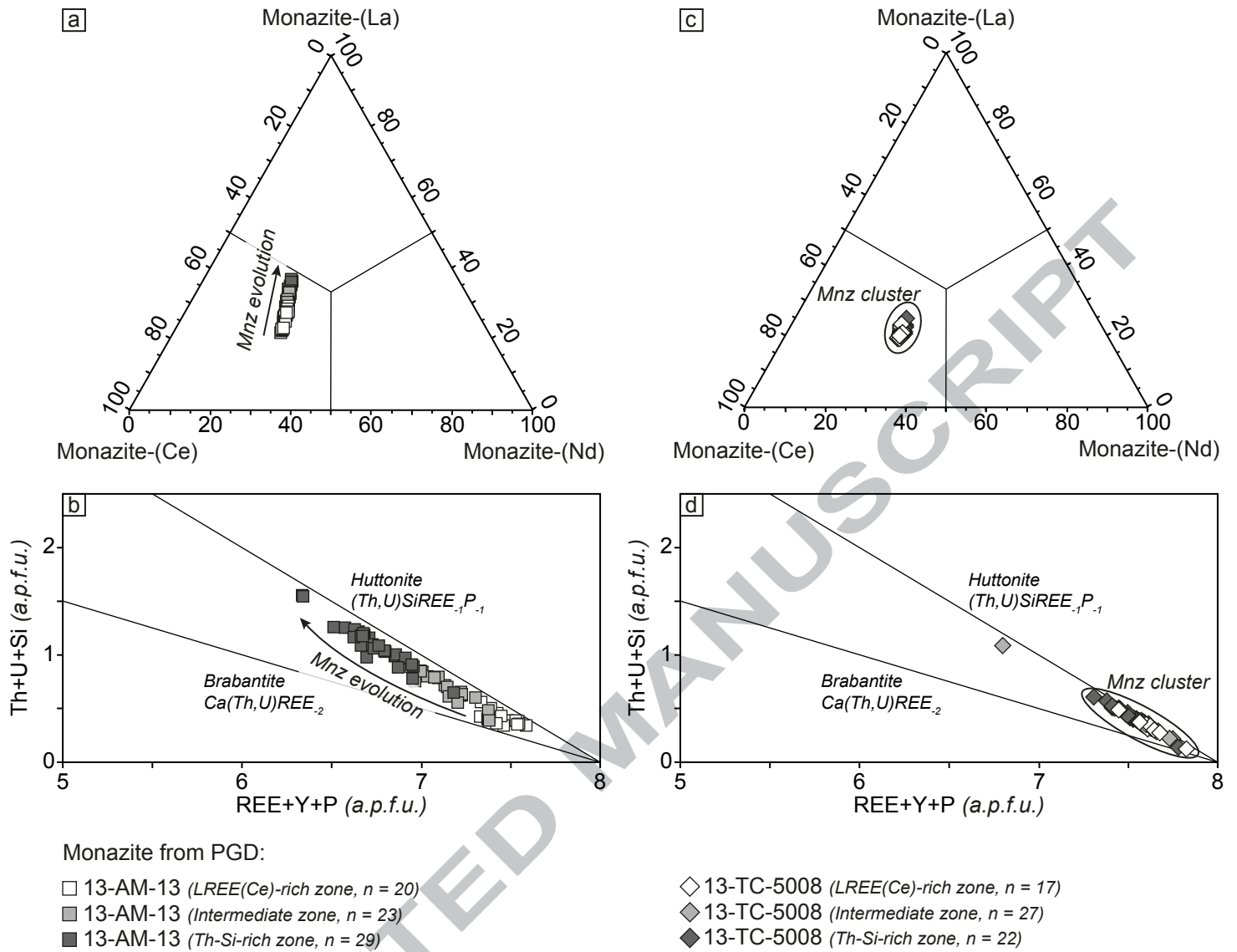


Figure 11 (color; 2 columns fitting)

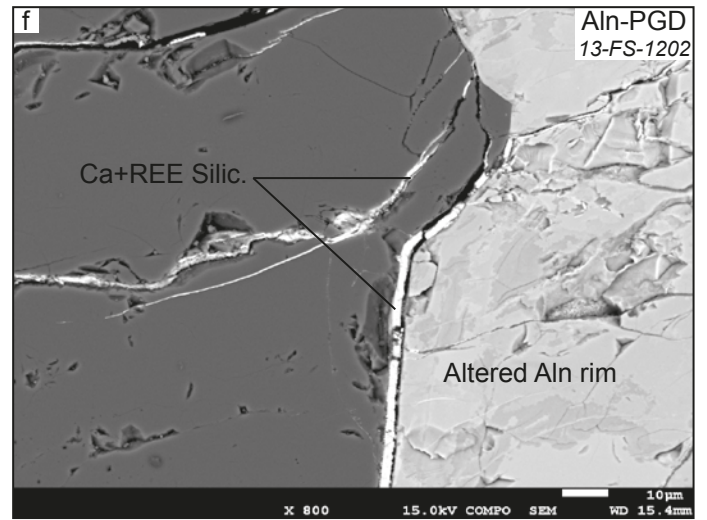
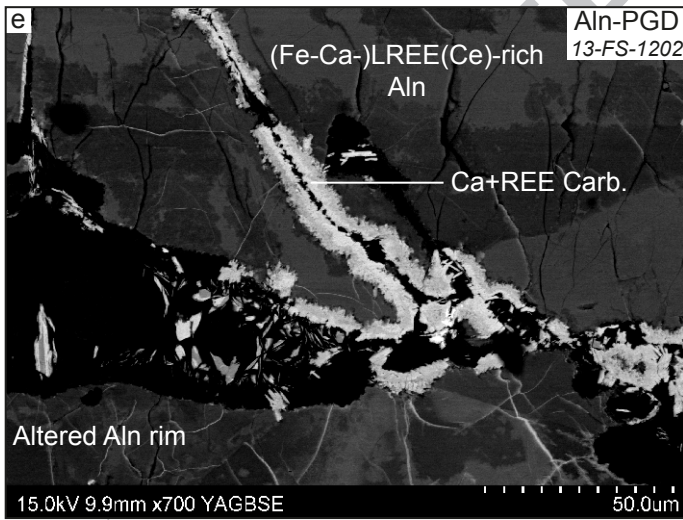
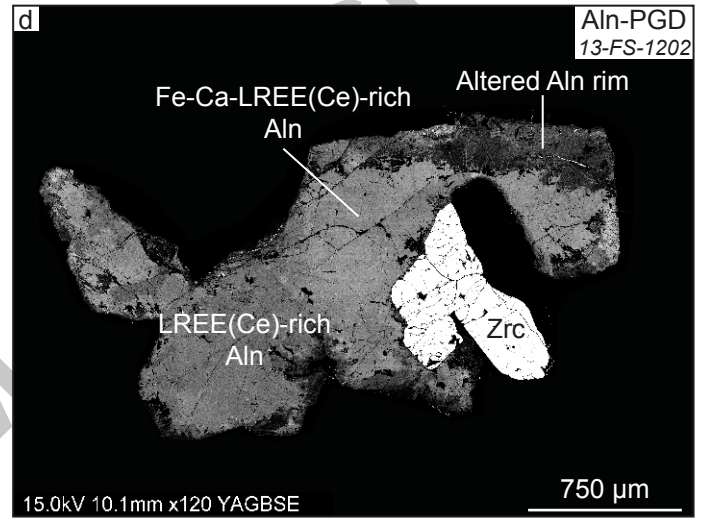
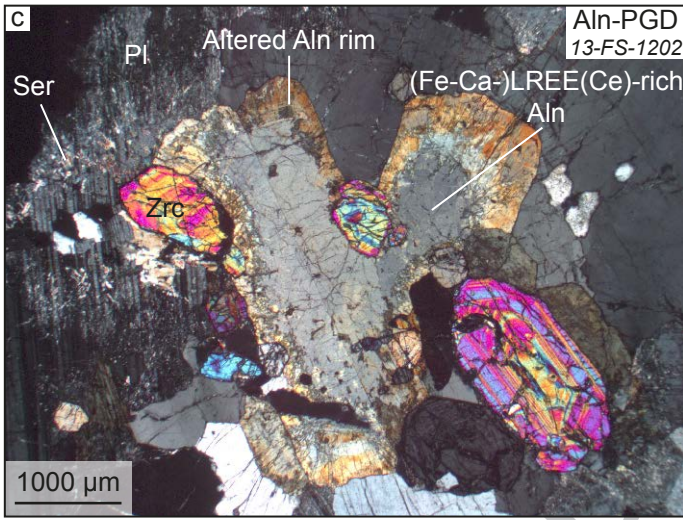
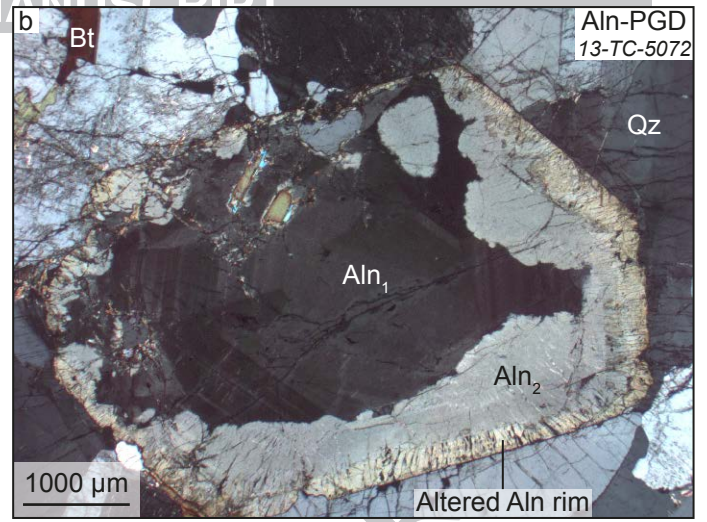
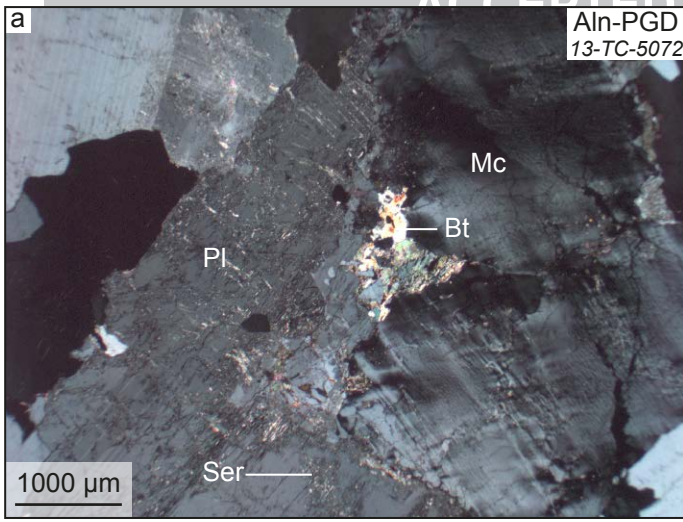
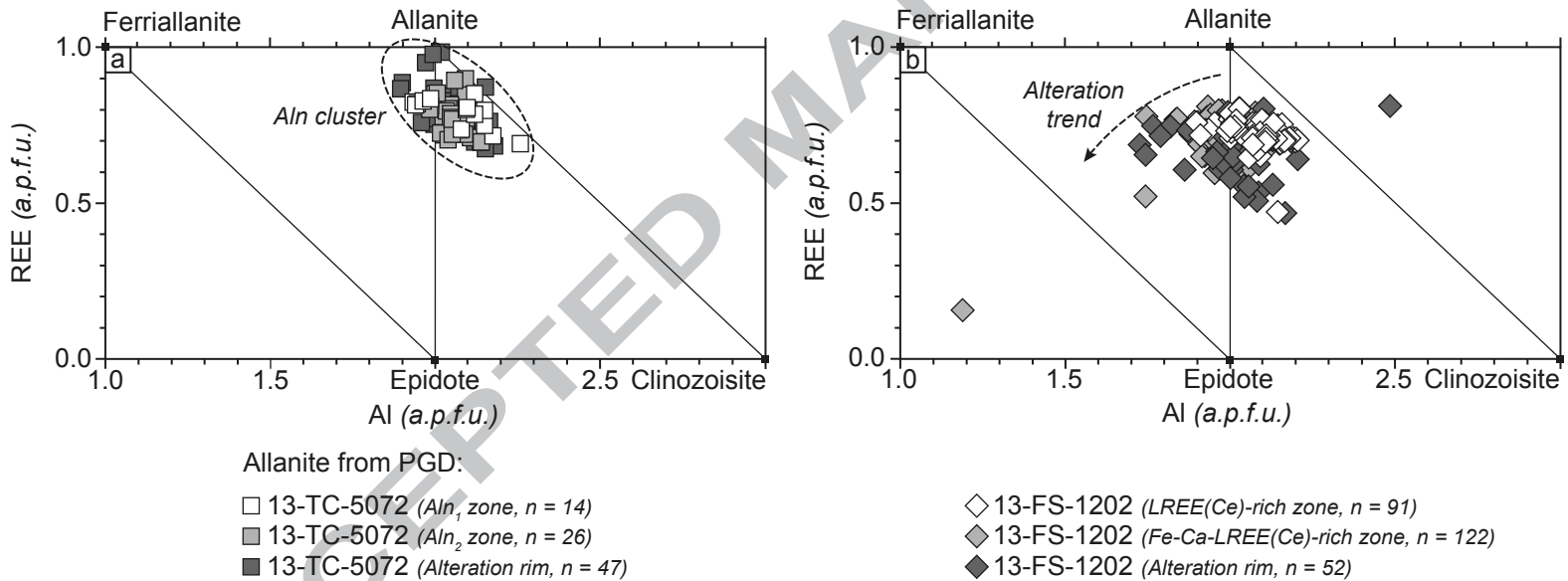


Figure 12 (black and white; 2 columns fitting)



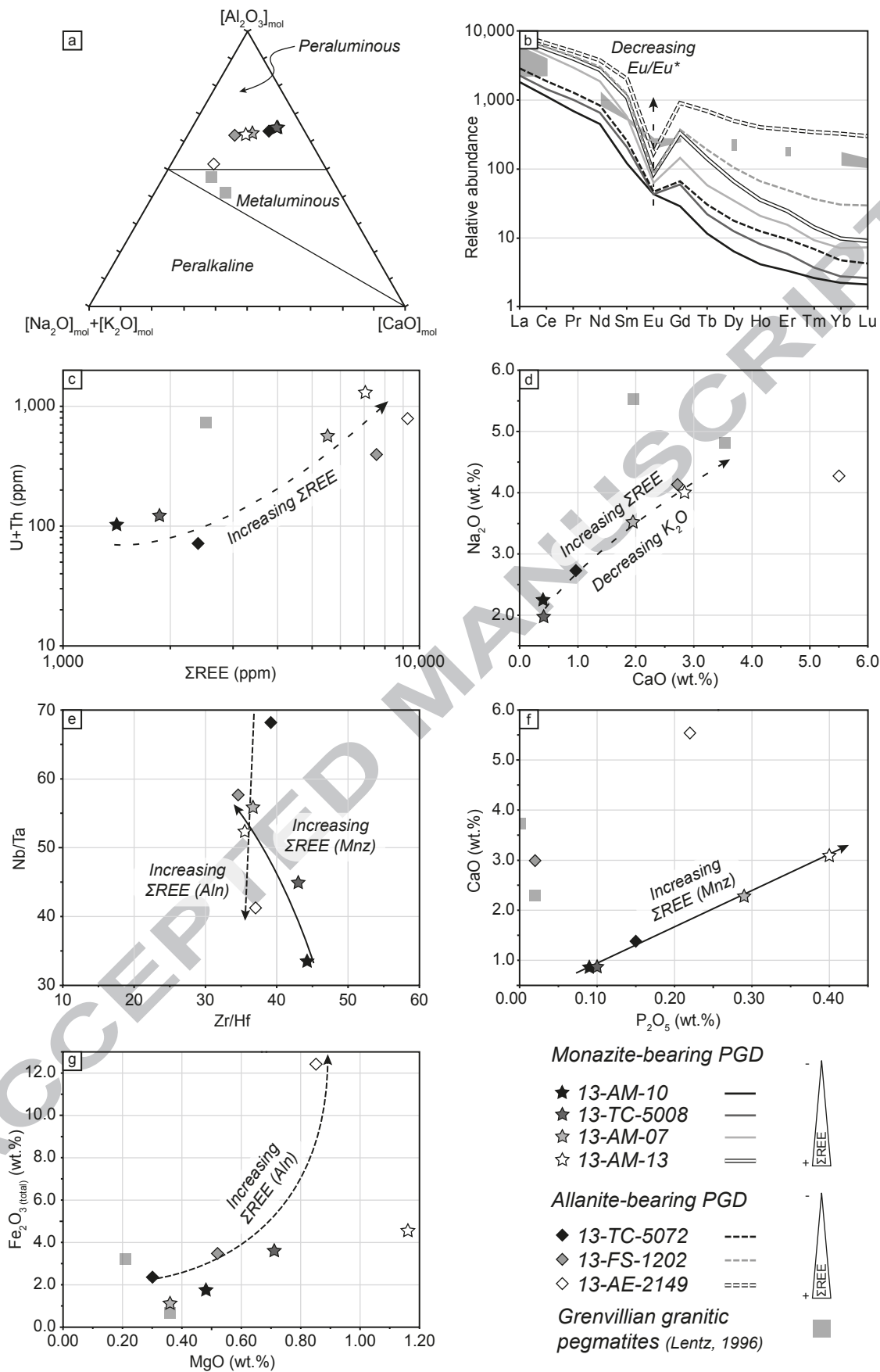
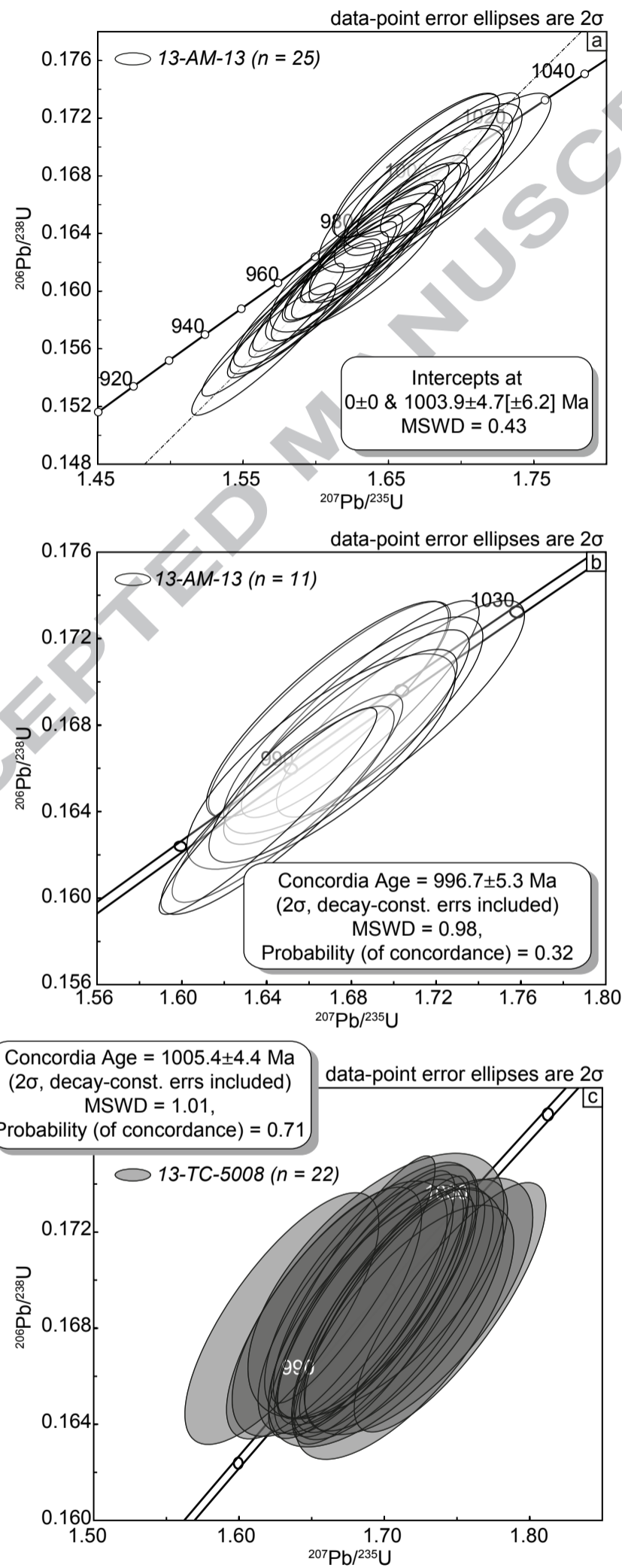
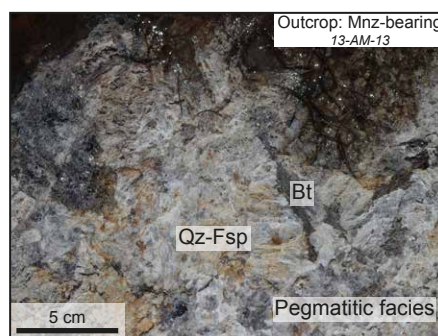
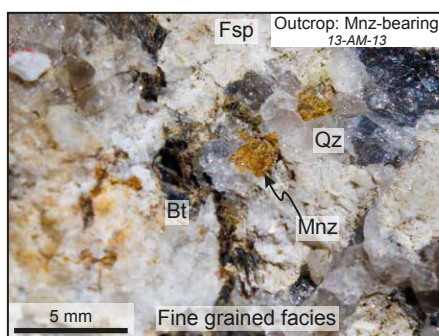
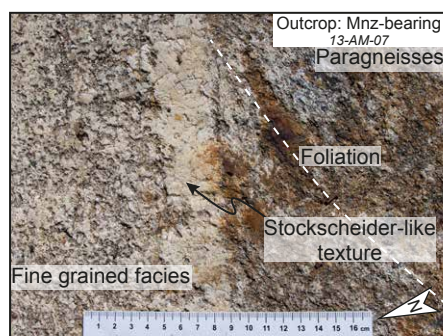


Figure 14 (black and white; 1 column fitting)

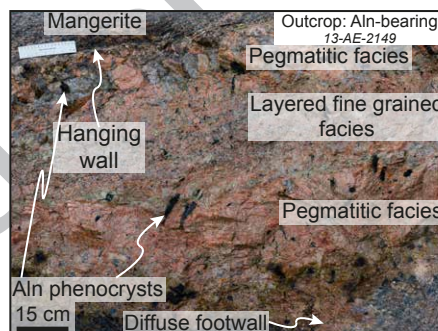
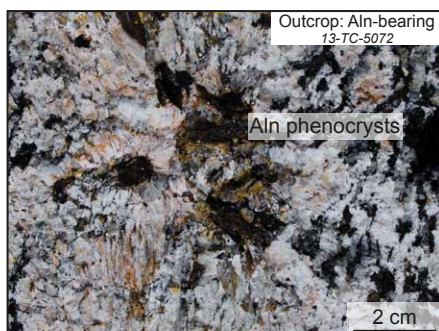
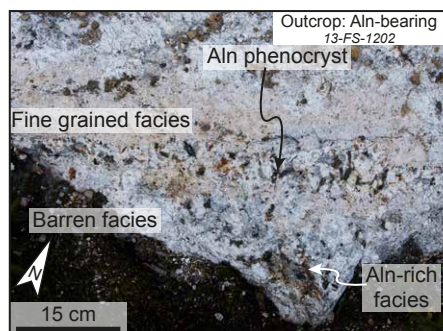


Two types of LREE-rich pegmatitic granite dykes (PGD): Monazite(Mnz)-bearing and Allanite(Aln)-bearing

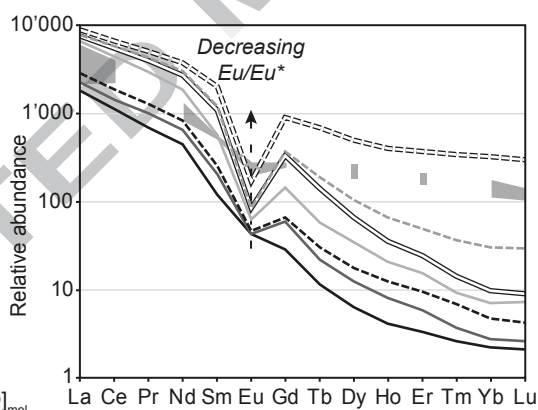
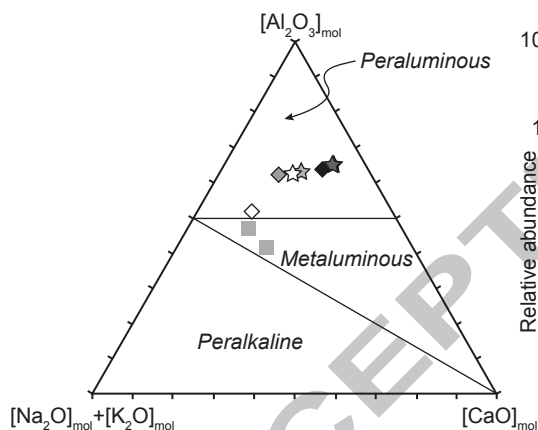
Mnz-bearing PGD



Aln-bearing PGD



Whole-rock geochemistry of the Mnz- and Aln-bearing PGD



Monazite-bearing PGD

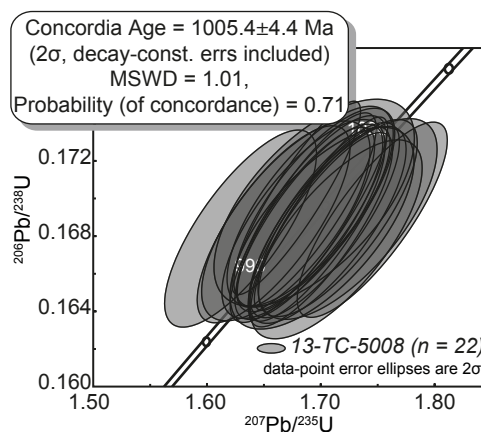
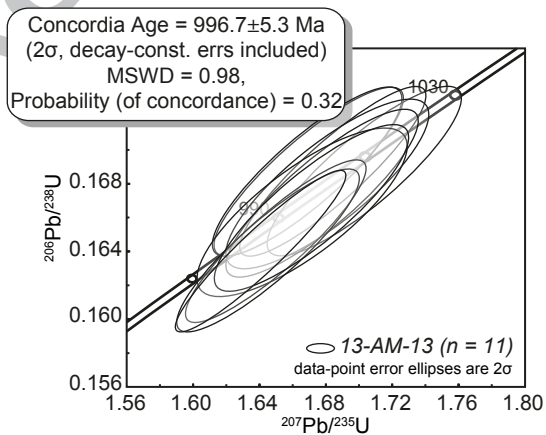
- ★ 13-AM-10
- ★ 13-TC-5008
- ☆ 13-AM-07
- ☆ 13-AM-13

Allanite-bearing PGD

- ◆ 13-TC-5072
- ◆ 13-FS-1202
- ◇ 13-AE-2149

Grenvillian granitic pegmatites (Lentz, 1996)

U-Pb dating of magmatic monazite (LA-ICP-MS)



594 **Research highlights:**

- 595 ✓ New LREE occurrences associated with peraluminous pegmatitic granite dykes in the
596 central Grenville
597 ✓ Unusual LREE mineralization hosted either in monazite (paragneiss-hosted pegmatitic
598 granite) or allanite (meta-igneous complexes-hosted pegmatitic granite)
599 ✓ A peraluminous character associated with a peralkaline behavior of trace elements and
600 in contrast with the formation of allanite
601 ✓ First evidence of monazite-only LREE mineralization in a pegmatitic granite in the
602 Grenville Province
603 ✓ A post-tectonic emplacement in the Allochthonous Belt associated with the initiation
604 of the crustal thickening of the underlying Parautochthonous Belt
605